Application of pH responsive hydrogel encapsulated bacteria for self-healing concrete

Gilles Trenson

Supervisors: Prof. dr. Nele De Belie, Dr. Sandra Van Vlierberghe
Counsellors: Dr. Jianyun Wang, Dr. ir. Arn Mignon

Master's dissertation submitted in order to obtain the academic degree of
Master of Science in Civil Engineering

Department of Structural Engineering
Chair: Prof. dr. ir. Luc Taerwe

Vakgroep Organische en Macromoleculaire Chemie
Chair: Prof. dr. José Martins

Faculty of Engineering and Architecture
Academic year 2016-2017

GHENT
UNIVERSITY

Preface

As a young man born in the nineties, I was raised with the awareness to reduce waste in order to protect our planet. The time has past to be part of a throw-away society. I want to be part of a future generation, who cares about our planet and all its beauty. To prevent further global warming and to protect against the consequences of climate change, we should join forces to work towards a brighter future.

To overcome resource depletion caused by usage and consumption of non-renewable resources, we should constantly be looking for new ways to exploit renewable resources. Furthermore, to reduce the ever-growing waste stream, progress in the recycling of packaging and other waste product is of utmost importance. All while keeping in mind to protect and reduce the usage of fresh water.

Growing up meant a constantly increasing urge to contribute to a sustainable future. I want to ensure future generation to live as comfortable as we do now, but then all of us, without having such a large impact on our planet.

I've chosen this resource topic because it lends itself to a more sustainable future. By increasing the durability of new concrete structures, less repair, less demolition and renewal is necessary. The application of bacteria for self-healing concrete sounds like a green solution to cope with the durability problems, mainly originated through crack formation in concrete. A significant amount of greenhouse gasses is produced by the building industry each year.

I'm extremely grateful to be part of a research with the aim to extend the lifetime of structures and indirectly contribute to a reduction in waste materials, resource mining and green gas emission. Aside the potential environmental benefits, which motivated my participation in this research topic, the increase of the durability of concrete structure is also aimed to be a cost effective measurement. However, this was not my main driving force.

This master's dissertation would not be what it was meant to be without the help and believe of my supervisors, counsellors, friends and family. Above all, I want to thank my counsellors Jianyun and Arn for having a lot of patience when I once again struggled to keep up with writing of my master's dissertation. Furthermore, I want to thank them for their advice;

for answering all my questions; for guiding me through an intense research schedule; for the many reviews and for their motivation. I'm extremely grateful for having the chance to be part of this diverse research topic, that fits both in Civil Engineering, Applied Microbiology and Organic Chemistry. Therefor, I want to thank my supervisors Prof. dr. Nele De Belie and Dr. Sandra Van Vlierberghe. Moreover, I want to thank them for letting me use all the equipment both in Magnel laboratory and in the Polymer Chemistry and Biomaterials Group.

I have to admit that it was not easy to cope with advice of both of my counsellors who have a different research background and field of study. From my background in Civil Engineering, it would be logical to focus especially on the self-healing of concrete with the use of pH responsive hydrogel encapsulated bacteria. Nevertheless, I attach great importance to the properties of the carrier and put a lot of effort into it as well.

Lastly, I want to thank all my friends and family for their support and for having patience when I complained about my master's dissertation. I would pay tribute to my girlfriend Bo as well for her strong support and trust. Thank you.

Gilles Trenson, August 2017

Copyright license

Application of pH responsive hydrogel encapsulated bacteria for self-healing concrete

Gilles Trenson

Supervisor(s): Prof. dr. Nele De Belie, Dr. Sandra Van Vlierberghe

Counsellor(s): Dr. Jianyun Wang, Dr. ir. Arn Mignon

Abstract— **The low tensile strength of cementitious materials make them vulnerable to cracking, and hence require repair upon crack formation to sustain its service lifetime. Self-healing strategies are regarded as a promising approach for sustainable infrastructure through reduction of maintenance and repair costs. Bacterial-based self-healing is recognised as a one of the promising self-healing approaches, though its efficiency depends on a continuous water supply and protection against the harsh environment and densification of the cementitious matrix. In the present work, the addition pH responsive hydrogel immobilised spores is proposed to take care of the aforementioned limitation. Furthermore, the pH responsive behaviour of the hydrogel is adapted to minimise the swelling upon addition to the cementitious matrix, in order to not impair its mechanical properties, and should substantially swell upon crack formation. Bacterial spores were encapsulated in various hydrogels and subsequently added to mortar specimens. Water flow measurements and the crack closure monitoring using optical microscopy were used to investigate the healing efficiency and revealed that this approach can attain a maximum completely closed crack width equal to about** $0.34\,\mathrm{mm}$ **and** $0.26\,\mathrm{mm}$ **under full immersion and wet/dry cycles, respectively. However, this was not a distinct improvement compared to the reference samples containing pure hydrogel with or without directly added bacterial spores. The development of the flow rate revealed that a reduction of 85.9% (10 weeks) is possible by addition of hydrogel immobilised spores, whereas the maximum sealing efficiency of the reference specimens was limited to 72.3%. In addition, bacterial spores, whether or not immobilised in hydrogels, promote crack healing of larger crack width when incubated under full immersion.**

Keywords— **Self-healing, self-sealing, mortar specimens, bacteria, pH responsive hydrogel, crack closure**

I. Introduction

CONCRETE is the second most consumed material after water worldwide [1] and has the inherent property to form cracks due to its limited tensile strength. Small cracks, not necessarily causing a risk of collapse of the structure, will accelerate the degradation by allowing harmful chemicals to enter the cementitious matrix [2, 3]. Maintenance and repair will become inevitable to restore or extend the service lifetime of civil infrastructures. However, convention repair techniques are often slow, expensive and inconvenient when the structure is in continuous service [4]. Self-healing strategies are regarded as a promising approach towards more sustainable infrastructures requiring less repair and maintenance. Moreover, they can be applied in civil infrastructures inaccessible for conventional repair methods, e.g., tunnels and submerged structures [5]. Mechanical damages are being healed or repaired by internal mitigation treatments who either promote the inborn capacity of cementitious materials (autogenous) or rely on an alternative path way (autonomous) to repair damages [2]. In the present study, the bacterial-based self-healing approach is proposed as an alternative mechanism to the intrinsic autogenous healing of cementitious materials. Spores of *Bacillus sphaericus*, an ureolytic alkali-tolerant strain, are used for their high productivity of calcium carbonate ($CaCO_3$) precipitation [6]. Bacterial spores, a dormant state of viable cells, have a survival time from several to hundreds of years under extreme environmental changes [7, 8]. Their long-term survivability makes them very suitable regarding a robust self-healing approach [5]. However, spores only break and germinate under favourable environmental conditions, and hence require water and nutrients to be available in their vicinity. Moreover, during mixing and densification of the cementitious matrix due to ongoing hydration, they might get damaged and hence, encapsulation of the bacterial spores is preferred [9, 10]. These encapsulation techniques should be biocompatible and should not impair the mechanical properties of the cementitious materials. In previous research, porous aggregates [10], glass capillaries [11], diatomaceous earth [12] and hydrogels [13] were proposed and evaluated as a potential carrier for carbonate precipitating bacteria. Hydrogel immobilised spores showed a distinct self-healing superiority with a maximum healed crack width

G. Trenson is with the Magnel Laboratory for Concrete Research, Faculty of Civil Engineering and Architecture, Ghent University (UGent), Ghent, Belgium.

of 0.5 mm [13]. Sufficient water supply is an essential element for bacterial activity. However, a robust self-healing approach should be versatile and should enhance the self-healing ability under exposure to a variety of environments, some continuously dry, others continuously wet, and still others exposed to an alternating cycle of dry and wet periods [5]. Since hydrogels possesses the ability to retain water, they can extend the period of water being available and hence make themselves suitable to be applied in two latter environments. Furthermore, they have the ability to seal cracks and limited to flow of potentially harmful agents to the matrix. However, their addition is accompanied by a mechanical strength reduction of the cementitious material and this limits their practical application [14]. In order to overcome this issue, Mignon et al. (2016) suggested and investigated the use of pH-sensitive hydrogels for their application in concrete. In the particular research, hydrogels of a lower swelling at high pH levels were synthesised in order to prevent the formation of macro-pores in the cementitious matrix [15]. Thus in this research, the combined use of pH responsive hydrogels and microbial $CaCO_3$ will be investigated. The hydrogel is used as a carrier for the protection of the bacterial spores and possesses the ability to retain and slowly release water after a wet period, hence promoting spore germination and bacterial activity which in itself facilitate the precipitation of $CaCO_3$ [9].

In the present study, the application of pH responsive hydrogel encapsulated bacterial spores will be evaluated. Based on the research by Mignon et al. (2016), several hydrogels were selected, synthesised, characterised and evaluated for their application in mortar specimens. Those hydrogels include methacrylated alginate (AlgMOD) and chitosan (ChiMOD) covalently cross-linked with acrylic monomers, i.e. acrylic acid (AA) and/or acrylamide (AM), and 2-(dimethylamino)ethyl methacrylate (DMAEMA), respectively. A fourth hydrogel, synthetic in nature, consists of N-N'-methylene bisacrylamide (MBA) covalently cross-linked with DMAEMA [15]. Subsequently, the encapsulation method and biocompatibility of the hydrogels is evaluated, followed by the application of hydrogel immobilised bacteria in mortar specimens. The self-healing efficiency was evaluated by means of water transport and crack closure measurements.

II. Materials and methods

A. Materials

Acetic acid (AcOH), ammonium persulfate (APS), chitosan (Chi), DMAEMA, hydrogen chloride (HCl), methacrylic anhydride (MAAH), sodium alginate (Alg), sodium hydroxide (NaOH) and Millipore syringe filter of pore size 0.22 µm were purchased from Sigma-Aldrich (Bornem, Belgium). Acrylic acid (AA) and N,N,N',N'-tetramethylethylene-diamine (TEMED) were purchased from Acros Organics (Geel, Belgium). Acrylamide (AM) was obtained from Janssen Chimica (Geel, Belgium). All materials were used as supplied, unless otherwise specified. Dialysis membranes Spectra/Por® 4, MWCO 12,000-14,000 Da were supplied by Polylab (Antwerp, Belgium). The paper filters of retention 8 - 12 µm and 12 - 15 µm were purchased from VWR filters (Leuven, Belgium). The studied mortar mixtures were composed of CEM I 52.5 N cement (510 kg/m^3; Holcim, Belgium), CEN-standard sand according EN 196-1 (1530 kg/m^3; Beckum, Germany) and tap water. *Bacillus sphaericus LMG 22557* (Belgian Coordinated Collection of Microorganisms, Ghent).

B. Bacterial strain

B. sphaericus strains were cultivated in a sterile growth medium (YU medium) consisting of yeast extract (20 g/l) and urea (20 g/l). The viable cells were sporulated according the method described by [9]. The spores were harvested by centrifuging the culture at 7000 rpm for 7 minutes and were subsequently resuspended in a 8.5 g/l NaCl sterile solution. The spores suspension (about 10^9 spores/ml) was stored in a fridge at 4 °C.

C. Synthesis of hydrogels

The hydrogels used were developed by the Polymer Chemistry and Biomaterials Group of Ghent University (PBM-UGent). Both alginate and chitosan were methacrylated by MAAH to provide the monomer with double bonds on its backbone, increasing its reactivity during consecutive covalently cross-linking. The methacrylation process involves either reacting 2 m/v sodium alginate dissolved in demineralised water or chitosan dissolved in a 2 m/v acetic acid solution, with MAAH. The solution was stirred at room temperature for 24H. The MAAH was added dropwise to the solution and the pH was monitored and adjusted to 8 for alginate, respectively 5 for chitosan, with a 5 M NaOH solution. Afterwards, dialysis was performed during 72 hours while changing the dialyses water 3 times a day. The methacrylated alginate (AlgMOD) and methacrylated chitosan (ChiMOD) were subsequently subjected to freeze drying via lyophilisation (Christ freeze-dryer alpha 2-4-LSC at −85 °C and 0.37 mbar).

TABLE I: poly(algMOD_AA/AM) hydrogel composition

Solvent	*T*	*AlgMOD*	*AA+AM*	*AA/AM*	*TEMED*	*APS*
	[°C]	[m/v%]	[m/v%]	[mol%]	[v/v%]	[m/v%]
H_2O	50	1	7	100/0	$8.08e^{-2}$	0.16
H_2O	50	1	7	75/25	$8.08e^{-2}$	0.16

Cross-linking of AlgMOD with acrylic monomers is carried out in the quantities as listed in table I using a free radical polymerisation in solution. All substances, with the exception of APS, were dissolved in an aqueous solution. The mixture was brought under a nitrogen N_2 environment by vacuuming cycles alternated by flushing through the addition of N_2 to remove all oxygen, which can inhibit the proper polymerisation reaction. Subsequently, the radical initiator APS is dissolved in a 10 m/v% aqueous solution and added to the mixture through a septa by a syringe. The same procedure is followed for the cross-linking of both MBA and ChiMOD with DMAEMA (or shorter EMA), as described in table II and III. However, the later is synthesised in a slightly acidic medium (6 v% aqueous AcOH solution) to improve the solubility of ChiMOD.

TABLE II: poly(MBA_DMAEMA) hydrogel composition

Solvent	*T* [°C]	*MBA+EMA* [m/v%]	*MBA/EMA* [mol%/mol%]	*TEMED* [v/v%]	*APS* [m/v%]
H_2O	45	25	98.04/1.96	0.252	0.499

TABLE III: poly(chiMOD_DMAEMA) hydrogel composition

Solvent	*T* [°C]	*ChiMOD* [m/v%]	*DMAEMA* [m/v%]	*TEMED* [v/v%]	*APS* [m/v%]
6 v% aq. AcOH	35	2	14	0.96	0.64

After 24 hours, unless otherwise specified, the synthesised hydrogel is removed from the three-neck flask and broken into smaller particles. Those particles are subjected to dialyses over 24 hours and thereafter, the consecutive steps of freezing, freeze-drying via lyophilisation and grinding are performed before obtaining the final product.

Encapsulation of bacteria - Before addition to the free radical polymerisation in solution, spores of *B. sphaericus* were harvested as described in section II-B and resuspended in sterile Milli-Q water of equal volume to the removed saline solution. During synthesis of the hydrogel, spores were added once a stable N_2 atmosphere was set up and followed by one last flushing cycle before addition of the radical initiator APS.

D. Hydrogel characterisation methods

Gel fraction quantification - Gel fraction quantification is used to reveal the production capacity of the synthesised hydrogels. The mass of a dry hydrogel particle prior and after subjection to dialyses is compared.

Degree of methacrylation - To determine the efficiency of the modification, i.e. methacrylation, of alginate, the polysaccharide is analysed by nuclear magnetic resonance ^{1}H NMR spectroscopy. The degree of substitution (DS) is calculated by evaluation of the intensity of the characteristic peaks of the methacrylate group compared to those peaks of alginate.

Swelling capacity by filtration method - The swelling capacity is measured for hydrogel particles exposed to aqueous solution of varying pH and cement filtrate solution of pH 12.5. NaOH or HCl where added to the aqueous solution in order to obtain respectively an acidic and alkaline environment. The cement filtrate solution was made by filtration of a 10 m/v% CEM I 52.5 N suspension in Milli-Q water that was left stirring over a period of 3 hours. A small amount (0.20 g) of hydrogel particles were added to a cup filled by about 100 ml of solution. Subsequently, the cup was sealed and left untouched for 24 hours. Then, the swollen hydrogel particles were removed by filtration and the leaked liquid was weighed.

$$S\,[\%] = \frac{(m_0 - m_f)}{m_{hydrogel}} \cdot 100\% \tag{1}$$

Structure confirmation via ATR-IR - The hydrogel structure was confirmed and analysed by attenuated total reflectance-infrared (ATR-IR) spectroscopy using a PerkinElmer Frontier FT-IR (midIR) combined with a MKII Golden Gate set-up with a diamond crystal from Specac. ATR-IR spectroscopy is regarded as a reliable fingerprinting technique. Characteristic peak were indicated and clarified. Where peaks change in relative intensity compared to their neighbours after exposure to a certain solution, the behaviour could be explained by hydrolysis of certain functionalities on the hydrogels backbone.

E. Influence hydrogel incorporation on mortar strength

The mortar specimens are composed out of the materials listed in section II-A and are made in accordance with the standard mortar mixture procedure, as described in EN 191-1. A reference specimen consists of 450 g CEM I 52.5 N, 1350 g silica sand and 225 ml tap water (W/C ratio equal to 0.5). In addition to those components, 0.5, 1.0 or 2.0 m% hydrogel relative to the mass of cement was added to form hydrogel incorporated mixtures. Samples were moulded ($160 \times 40 \times 40\,mm^3$) and stored in a climate room of relative humidity of $95 \pm 5\%$ and a temperature of $20 \pm 2\,°C$ for 28 days. Demoulding of the specimens took place after 24 hours, unless otherwise specified.

After curing over 28 days, the mechanical properties, i.e., flexural and compressive strength, were determined by means of a three-point-bending test followed by a compression test using a Walter + Bai ag servo-hydraulic testing apparatus, as described in NBN EN 196-1.

F. Ureolytic activity of hydrogel immobilised spores

The viability of the encapsulated spores is evaluated based on the ureolytic activity of viable cells after germination. A series of hydrogels were made and before each consecutive step towards the final hydrogel powders, a small sample was taken in order to investigate the potential process which impair the viability of the cells. Those samples are added to an YU medium containing 20 g/l urea. Bacterial urease activity decomposes urea to NH_4^+, which can be measured by the method of Nessler, producing a colour shift depending on the concentration of NH_4^+ molecules. This technique is also known as the total ammonium nitrogen (TAN) method. The TAN concentration itself is measured colorimetrically (Biochrom WPA Lightwave UV/Visible Spectrophotometer) and is back-calculated to the amount of urea decomposed in the original medium, which in case is the parameter used to evaluate the viability of encapsulated spores.

G. Performance measurement of self-healing capacity

Different series of mortar specimens were prepared using the components listed in section II-A. All specimens consists of 450 g CEM I 52.5 N, 1350 g silica sand and 225 ml tap water (W/C ratio equal to 0.5), with or without the addition of bio-reagents, spores, hydrogel or hydrogel immobilised spores as listed in table IV. After curing for 28 days in a climate room ($95 \pm 5\%$ RH; $20 \pm 2\,°C$), testing was started.

TABLE IV: Composition of mortar specimens for water flow evaluation

Type	*YE* [g]	*Urea* [g]	*Ca-nitrate* [g]	*S* [ml]	*H* [g]	*HS* [g]
R	0	0	0	0	0	0
N	3.84	18	36	0	0	0
N+S	3.84	18	36	4.5	0	0
N+CD	3.84	18	36	0	4.5	0
N+CD+S	3.84	18	36	4.5	4.5	0
N+CDS	3.84	18	36	0	0	4.5
N+AA	3.84	18	36	0	4.5	0
N+AA+S	3.84	18	36	4.5	4.5	0
N+AAS3H	3.84	18	36	0	0	4.5
N+AAS20H30	3.84	18	36	0	0	4.5

Sealing efficiency evaluation - The water permeability through the crack is evaluated over time. In figure 1, the time schedule used for the water flow experiment is presented. Prior to water flow tests, the sample was pre-cracked. The mortar specimens ($160 \times 40 \times 40$) possesses a cavity through which water could flow. The cavity was sealed at one end and a push-to-connect fitting was glued at the other edge, allowing a water flow to enter the specimen and flow out at the crack. The water flow rate is determined by continuously monitoring the mass of the leaked water. The sealing efficiency (SE) represents the relative decrease of the water flow over time. During the testing period, the specimen were incubated under full immersion in demineralised water.

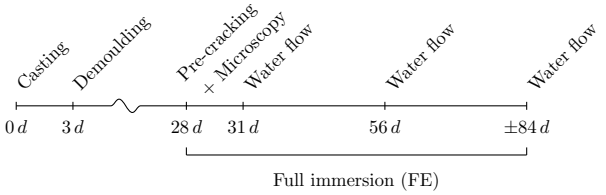

Fig. 1: Timeline regarding the water flow measurements

Crack closure evaluation - Long mortar prisms ($360 \times 30 \times 30$ mm) are pre-cracked under stroke control. The average crack width aimed for is equal to 250 µm. Each side of the specimen is marked by a number, as well as 4 cracks. For each crack, 5 images are taken using optical microcopy (Leica S8 APO, DFC295 camera) and subsequently crack widths are measured using software (Fiji). The healing ratio (HR) represents the relative decrease of the crack width over time. The different series are incubated both under full immersion and under wet/dry cycles consisting of a wet period of 2 hours alternated by a dry period of 4 hours (RH = 60%).

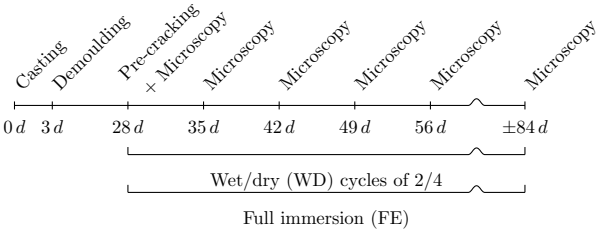

Fig. 2: Timeline regarding the crack-closure measurements

H. Statistical analysis

Where applicable, results were analysed and supported by a univariate ANOVA test and a Levene's test to accept the assumption of homogeneity of variances. If the assumption of equal variances was not violated, the test was continued by a Tukey post-hoc test, whereas a Brown-Forsythe and Dunnett's T3 post-hoc test were performed if the assumption was violated. Potential significant differences ($p < 0.05$) were identified using the statistical program SPSS.

III. Results and discussion

A. Hydrogel characterisation methods

Gel fraction quantification - A lower gel fraction corresponds to a higher mass loss after dialysis due to an increased amount of unwanted impurities that were removed. Thus, it represents the production efficiency of the hydrogel. The hydrogels were synthesised with a high production capacity, similar to that of Mignon et al. (2016). AlgMOD covalently cross-linked with AA (AlgMOD/AA) and both AA and AM (AlgMOD/AA+AM) had a gel fraction equal to 92.4 and 82.1% respectively. ChiMOD/DMAEMA had a low gel fraction equal to 68.3% which is in accordance with the results from Vermeulen (2016). This lower gel fraction can possibly be explained the presence of AcOH during synthesis which is not incorporated during polymerisation. The synthetic hydrogel MBA/DMAEMA had a gel fraction of 83.2%.

Degree of methacrylation - Methacrylated or modified alginate (AlgMOD) had a high degree of substitution (DS). The DS per hydroxyl group was equal to 29.6%, a substantial increase compared to the DS of AlgMOD (18.6%) of the same composition that was synthesised by Vermeulen (2016). Thus, more reactive double bond are available on the polysaccharides backbone, and hence a denser network is expected after cross-linking. The direct consequence was a slightly lower swelling capacity compared to the results of Vermeulen (2016).

Swelling capacity by filtration method - Swelling test were performed both in aqueous solutions of varying pH and a cement filtrate solution. Above pH 3.38, carboxylic acid functionalities of AlgMOD/AA and AlgMOD/AA+AM get deprotonated, resulting in a gradually increase of swelling capacity with increasing pH and reaching a maximum at pH 12.5 equal to 88.9 and 58.1 $g_{water}/g_{hydrogel}$ respectively. However, the swelling capacity is limited under exposure to a cement filtrate solution due to the presence of mono- and multivalent cations which shield off functionalities of the hydrogels backbone. Swelling capacity studies of ChiMOD/DMAEMA revealed that the material was less sensitive to pH variations. A stable value of about 40.8 $g_{water}/g_{hydrogel}$ was reached in between pH 7 and 11. However, DMAEMA possesses a pK_a of 8.4 and hence electrostatic interaction between charged functionalities will diminish above pH 8.4. From pH 9 onwards, a slight reduction in swelling is observed in ChiMOD/DMAEMA and followed by a significant reduction at pH 12.5, equal to 12.4 $g_{water}/g_{hydrogel}$. The swelling in a cement filtrate solution is not significantly different (12.8) compared to the swelling in a pH 12.5 aqueous solution. Thus, the material showed a desirable trend for its application in cementitious materials. A similar swelling trend is observed for MBA/DMAEMA, though its swelling capacity increases at a much higher pace at low pH and is significantly larger, reaching a swelling of 96.2 $g_{water}/g_{hydrogel}$ at pH 3. However, a tremendous increase in swelling capacity (112.4 $g_{water}/g_{hydrogel}$) was noticed at pH 9 and could

TABLE V: Swelling capacity for synthesised hydrogels both in aqueous solutions (pH 3 to 12.5) and in cement filtrate solution (CF)

Hydrogel	*pH 3*	*pH 7*	*pH 8*	*pH 9*	*pH 10*	*pH 11*	*pH 12.5*	*CF*
p(algMOD_AA)	27.2 ± 0.5	39.4 ± 0.2	43.6 ± 0.8	42.0 ± 1.1	43.8 ± 1.0	76.7 ± 7.9	88.9 ± 3.5	12.4 ± 1.4
p(algMOD_AA/AM)	19.0 ± 0.3	39.8 ± 2.2	37.4 ± 0.8	36.7 ± 1.6	—	54.1 ± 4.0	58.1 ± 0.1	11.4 ± 0.8
p(chiMOD_DMAEMA)	28.9 ± 0.5	35.8 ± 5.4	42.5 ± 0.7	42.9 ± 1.5	39.6 ± 1.1	38.5 ± 0.5	12.4 ± 0.3	12.8 ± 1.0
p(MBA_DMAEMA)	96.2 ± 9.8	47.0 ± 2.8	37.7 ± 1.8	112.4 ± 2.5	—	25.2 ± 1.9	17.6 ± 1.9	15.8 ± 1.0

be attributed to batch variation. A slight change is cross-linking concentration of MBA has a high influence on the swelling behaviour, as was evaluated by Mignon et al. (2016). Thus, the higher swelling than anticipated might be related to a lower cross-linked MBA concentration compared to DMAEMA.

Structure confirmation and degradation evaluation via ATR-IR - Attenuated total reflectance-infrared (ATR-IR) spectroscopy was used to verify the chemical composition of the hydrogels. The characteristic peaks of the spectra revealed a successful cross-linking of all hydrogels. Some hydrogels are vulnerable to degradation which was revealed by ATR-IR spectroscopy. The structural integrity of hydrogels containing AlgMOD is endangered when subjected to alkaline solution above pH 11. Carboxylic acid functionalities on the hydrogels backbone will gradually start to hydrolyse, leading to a more open network. ChiMOD/DMAEMA and MBA/DMAEMA are less prone to degradation.

B. Influence hydrogel incorporation on mortar strength

The mechanical properties, i.e. flexural (figure 3 and compressive strength, of hydrogel incorporated mortar specimens under varying quantities were compared with those of a control sample. The series MBA/DMAEMA had a poor performance and makes practical application impossible due to a severe strength reduction. It can be related to a substantial swelling during mixing of the mortar specimens resulting in the formation of macro-pores in the cementitious matrix during hardening. Even after addition of 1m% hydrogel relative to the mass of cement, the flexural and compressive strength decrease remained within the range of 12.4-17.4% and 4.7-12.8% for the other hydrogels. In order to promote the self-sealing and -healing ability of cracks, the largest possible amount of hydrogels should be added to the cementitious material without compromising the mechanical properties. Hence the addition of 1m% hydrogel is chosen to be further used in this research.

C. Degradation study of hydrogels

In addition to the swelling test and ATR-IR spectroscopy analyses for samples exposed to an aqueous and cement filtrate solution over 1 day, a long term evaluation (at 7, 28, 90 and 180 days) is conducted. Both the hydrogel as the bacterial spores should possess a shelf life as long as the service life of the infrastructure, as was included as one of the six robustness criteria by Li and Herbert (2012) to evaluate the robustness of a self-healing approach. The swelling studies were performed in triplicate. Over time, the swelling studies became less reliable and more variation in swelling capacity between the replicates was observed, though no significant difference of their ATR-IR spectra was noticed. The swelling of AlgMOD/AA increases over time, reaching a maximum swelling capacity for 90 and 180 days. However, this swelling behaviour is not related to degradation as was confirmed by ATR-IR spectra analysis. The same conclusion holds for AlgMOD/AA+AM since no significant degradation was evaluated, though an increase in swelling over time is noticed in a cement filtrate solution. However, the consistency of the swelling property over time of AlgMOD/AA+AM is doubtful, and hence, its use would suggest a lack of reliability of the self-healing approach. The swelling properties of ChiMOD/DMAEMA over time do not differ significantly. In an aqueous solution, MBA/DMAEMA tends to increase significantly over time, reaching

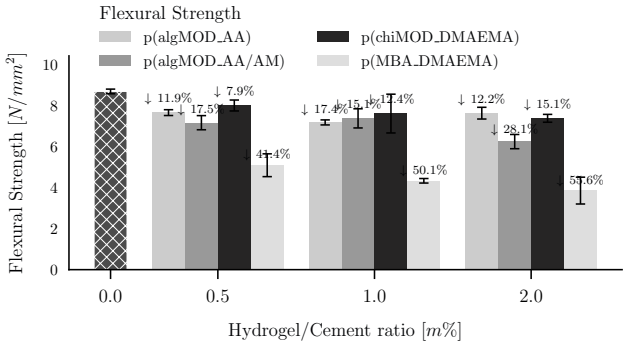

Fig. 3: Flexural strength of the reference mortar specimen (hatched) and mortar specimens with addition of the synthesised hydrogels

a maximum of 107.1 $g_{water}/g_{hydrogel}$ after 180 days, more than twice as much as the initial swelling capacity (47.0). Despite severe degradation was expected, it could not be confirmed by ATR-IR spectroscopy. The swelling properties over time become unreliable and unpredictable and consequently, the results cannot be substantiated by statistically evidence.

D. Ureolytic activity of hydrogel immobilised spores

The final batches of series ChiMOD/DMAEMA and AlgMOD/AA, to be applied in mortar specimens, showed bacterial activity within 3 and 7 days, respectively. However, the bacterial activity of AlgMOD/AA was similar to that in its reference specimen, and hence no conclusion regarding the viability of the immobilised spores could be drawn. It is suggested to further investigate the use of the free radical polymerisation in solution technique to encapsulate bacterial spores. In this research, the author suggested a reduction of the synthesis period and temperature to improve the survivability of bacterial spores. However, a reduction of the temperature caused failure of the synthesis process. It was observed that AlgMOD/AA and AlgMOD/AA+AM induces a significant drop in pH of the growth medium, related to the high amount of carboxylic acid moieties available on the hydrogel's backbone. The addition of a 5M NaOH solution to adjust the pH to ±9 promotes the germination and consequently ureolytic activity of the bacterial spores. In case of AlgMOD/AA immobilised spores synthesised over 3 hours (3H) and 20 hours 30 minutes (20H30), no statistically significant reduction in ureolytic activity is observed. ChiMOD/DMAEMA immobilised spores synthesised over 1 hour were able to completely decompose the urea of the growth medium within 3 days, whereas a different batch synthesised over 24 hours showed no activity after 25 days.

E. Performance measurement of self-healing capacity

Based on the viability tests and evaluation of the influence on the mechanical properties of mortar specimens, ChiMOD/DMAEMA and AlgMOD/AA were selected as the most promising hydrogel immobilised materials and their self-healing capacity was evaluated by means of a water flow test and crack closure measurements.

Sealing efficiency evaluation - Overall, specimens containing ChiMOD/DMAEMA were observed to have the highest and most consistent sealing efficiency (SE). The sealing efficiency for series incorporating ChiMOD-/DMAEMA, whether or not in the presence of bacterial spores, varied between 73.6 and 85.9%. The latter value is

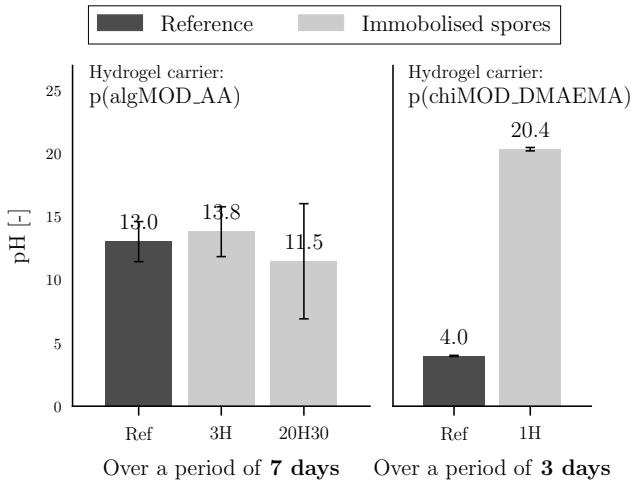

Fig. 4: Urea decomposed in a growth medium with the addition of p(algMOD_AA) and p(chiMOD_DMAEMA) with and without bacterial spores evaluated over respectively 7 and 3 days. After 3 days, the pH of the samples containing p(algMOD_AA) were adjusted to ±9 by a 5M NaOH solution in order to promote the germination and consequently the ureolytic activity of the bacterial spores.

related to specimens containing ChiMOD/DMAEMA immobilised spores. When specimen incorporating hydrogel immobilised spores are compared, the results reveal that the ratio between the sealing efficiency and the healing ratio of the ChiMOD/DMAEMA series is relatively larger than those of the AlgMOD/AA series. AlgMOD/AA is prone to degradation and the results suggest that the hydrogel might escape over time from the crack during incubation under full immersion. This suggestion was confirmed by analysing the development of the sealing efficiency over time. The increase in sealing efficiency stagnated and moreover, some specimens encountered a higher flow rate after 10 weeks than after 4 weeks. Because of its high sealing efficiency and reliable SE development over time, ChiMOD/DMAEMA was selected for crack closures measurements.

Crack closure evaluation - Specimens were either subjected under full immersion or under wet/dry cycles, 2 hours under submersion alternated by a dry period of 4 hours (RH = 60%). On average, specimens under full immersion can close cracks up completely to about 0.3 mm within 10 weeks. The bottom face of the specimen experiences the best crack closure efficiency and could often not be tested up to its full potential because of the lack of wider cracks. The amount of completely closed cracks for specimens containing ChiMOD/DMAEMA immobilised spores and directly added spores equals to 51.3 and 66.9% respectively, whereas that of the other specimens varies between

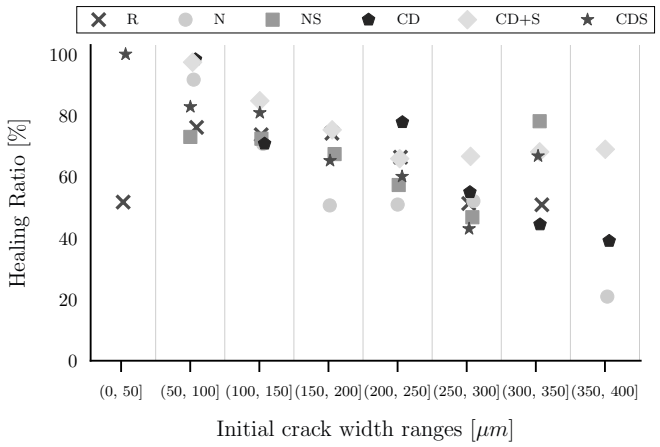

Fig. 5: Average crack healing ratio in different ranges of crack widths of specimens under full immersion over a period of 10 weeks

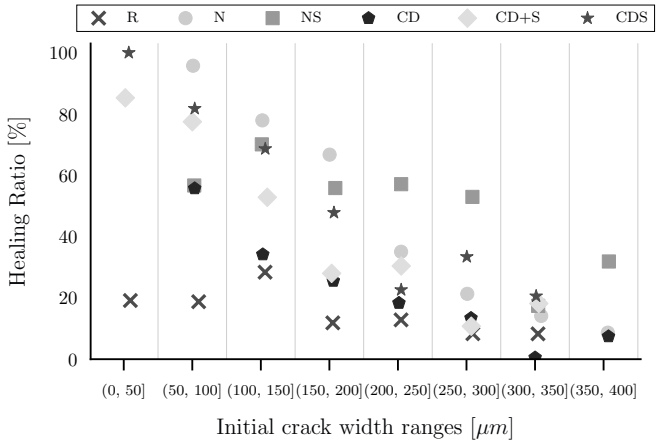

Fig. 6: Average crack healing ratio in different ranges of crack widths of specimens under full immersion over a period of 10 weeks

34.3 and 46.6%. Furthermore, the average healing ratio above 0.25 mm was higher for specimens containing bacterial spores, whether or not immobilised in the hydrogel, than for the specimens without bacteria, though no significant improvement of hydrogel immobilised spores is observed compared to directly added spores.

On the other hand, optical microscopy of specimens under wet/dry cycles reveals an improved crack closure efficiency of specimens containing hydrogel immobilised spores. Complete crack closure for 31.9% of the measured cracks was observed, whereas the other specimens containing ChiMOD/DMAEMA experienced a limited crack closure equal to 12.3 and 5.6%, respectively with and without directly added spores. However, microscopic evaluation of specimens containing solely nutrients or both nutrients and directly added spores reveal a relatively high amount of completely closed crack as well, equal to 29.7 and 21.2% respectively, though the maximum completely closed crack and healing ratio for large cracks ($> 250\,\mu m$) is higher in specimens containing bacterial spores.

IV. Conclusion

The application of pH responsive hydrogels in combination with bacterial spores lead to an improved crack closure when incubated under full immersion. Bacterial spores, whether or not immobilised, promote crack closure of wider cracks. On the other hand, pH responsive hydrogels can improve the sealing efficiency of cracks, minimise the strength reduction of mortar specimens and are found to be biocompatible. However, the biocompatibility is closely related to the polymerisation technique and more research is required to further optimise this technique.

When specimens are subjected to wet/dry cycles, the hydrogel immobilised spores series closed significantly more cracks than those specimens including hydrogels with or without directly added spores. However, the overall crack closure efficiency is closely related to the initial crack widths distribution on each side of the specimen.

V. Acknowledgement

The author would like to thank Dr. Jianyun Wang and Dr. Ir. Arn Mignon for their assistance and support during this master's dissertation. Furthermore, the author would like to thank the staff from Magnel Laboratory for Concrete Research and Polymer Chemistry and Biomaterials Group of Ghent University for their help.

References

[1] *The Cement Sustainability Initiative - Recycling Concrete*, Geneva. World Business Council for Sustainable Developments, wbcsdcement.org.

[2] COST Association. Memorandum of Understanding for the implementation of the COST Action "Self-healing As preventive Repair of Concrete Structures" (SARCOS) CA15202. *COST Association*, pages 1–19, March 2016.

[3] BASF. Repairing Concrete: Solutions to Re-Establish Structural Integrity. pages 1–19, December 2013.

[4] Tomoya Nishiwaki, Marina Koda, Makoto Yamada, Hirozo Mihashi, and Takatsune Kikuta. Experimental Study on Self-Healing Capability of FRCC Using Different Types of Synthetic Fibers. *Journal of Advanced Concrete Technology*, 10(6):195–206, 2012. doi: 10.3151/jact.10.195.

[5] Victor C Li and Emily Herbert. Robust Self-Healing Concrete for Sustainable Infrastructure. *Journal of Advanced Concrete Technology*, 10(6):207–218, 2012. doi: 10.3151/jact.10.207.

[6] Jan Dick, Wim De Windt, Bernard De Graef, Hans Saveyn, Paul Van der Meeren, Nele De Belie, and Willy Verstraete. Biodeposition of a calcium carbonate layer on degraded limestone by Bacillus species. *Biodegradation*, 17(4):357–367, February 2006. doi: 10.1007/s10532-005-9006-x.

[7] P Setlow. Mechanisms which contribute to the long-term survival of spores of Bacillus species. *Journal of Applied Bacte-*

riology, 76(S23):49S–60S, June 1994. doi: 10.1111/j.1365-2672.1994.tb04357.x.

[8] Peter Setlow. Resistance of Bacterial Spores. In *Bacterial Stress Responses, Second Edition*, pages 319–332. American Society of Microbiology, January 2011. ISBN 9781555816216. doi: 10.1128/9781555816841.ch18.

[9] Jianyun Wang. *Self-Healing Concreteby Means of Immobilized Carbonate Precipitating Bacteria* . PhD thesis, February 2013.

[10] Henk M Jonkers, Arjan Thijssen, Gerard Muyzer, Oguzhan Copuroglu, and Erik Schlangen. Application of bacteria as self-healing agent for the development of sustainable concrete. *Ecological Engineering*, 36(2):230–235, February 2010. doi: 10.1016/j.ecoleng.2008.12.036.

[11] Jianyun Wang, Kim Van Tittelboom, Nele De Belie, and Willy Verstraete. Use of silica gel or polyurethane immobilized bacteria for self-healing concrete. *CONSTRUCTION & BUILDING MATERIALS*, 26(1):532–540, January 2012. doi: 10.1016/j.conbuildmat.2011.06.054.

[12] J Y Wang, N De Belie, and W Verstraete. Diatomaceous earth as a protective vehicle for bacteria applied for self-healing concrete. *Journal of Industrial Microbiology & Biotechnology*, 39(4):567–577, September 2011. doi: 10.1007/s10295-011-1037-1.

[13] J Y Wang, D Snoeck, S Van Vlierberghe, W Verstraete, and N De Belie. Application of hydrogel encapsulated carbonate precipitating bacteria for approaching a realistic self-healing in concrete. *CONSTRUCTION & BUILDING MATERIALS*, 68:110–119, October 2014. doi: 10.1016/j.conbuildmat.2014.06.018.

[14] H X D Lee, H S Wong, and N R Buenfeld. Self-sealing of cracks in concrete using superabsorbent polymers. *Cement and Concrete Research*, 79:194–208, January 2016. doi: 10.1016/j.cemconres.2015.09.008.

[15] Arn Mignon, Nele De Belie, and Sandra Van Vlierberghe. Effect of pH-responsive superabsorbent polymers on the self-sealing and self-healing of cracks in concrete . Technical report, September 2016.

[16] Jolien Vermeulen. *Self-Healing Concrete with Algae and Seaweed. Science or Fiction?* . PhD thesis, Ghent, June 2016.

Contents

Abbreviations and symbols

AA	acrylic acid
AAS	alkali-activated slag
AcOH	acetic acid
algMOD	methacrylated alginate
AM	acrylamide
ANOVA	analysis of variance
APS	ammonium persulfate
ASR	alkali-silica reaction
ATR-IR	attenuated total reflectance infrared
$\mathbf{Ca^{2+}}$	calcium ion
$\mathbf{CaCO_3}$	calcium carbonate
$\mathbf{Ca(OH)_2}$	calcium hydroxide
CF	cement filtrate
CFRP	carbon fibre reinforced polymer
chiMOD	methacrylated chitosan
CHT	cementitious hollow tube
$\mathbf{CO_2}$	carbon dioxide
$\mathbf{CO_3^{2-}}$	carbonates
CSH	calcium silicate hydrate
DIC	dissolved inorganic carbon
DMAEMA	2-(dimethylamino)ethyl methacrylate
DMSO	dimethylsulfoxide
DS	degree of substitution [%]
EC	expanded clay
ECC	engineered cementitious composite
EP	expanded perlite
EVOH	ethylene vinyl alcohol
HCl	hydrochloric acid
$\mathbf{HCO_3^-}$	bicarbonates
LWA	lightweight aggregates

MAAH	methacrylic anhycride
MICP	microbiologically induced carbonate precipitation
MBA	N,N'-methylene bisacrylamide
N_2	nitrogen gas
Na^+	sodium cation
NaOH	sodium hydroxide
NB	nutrient broth
NDT	non destructive testing
NH_3	ammonia
PE	polyethylene
POM	polyacetal
PP	polypropylene
PSD	particle-size distribution
PU	polyurethane
PVA	polyvinyl alcohol
RH	relative humidity [%]
SAP	superabsorbent polymer
SMA	shape-memory alloys
SRA	shrinkage-reducing admixtures
TEMED	N,N,N',N'-tetramethylethylene-diamine
W/C	water to cement ratio
YE	yeast extract

Chapter 1

Introduction

1.1 Durability problems of concrete

1.1.1 Concrete as a building material

Concrete is the second most consumed material after water worldwide [1]. The global production of concrete is estimated between 38.3 and 57.5 billion tonnes in 2015. This estimation is based on the cement production, a major component of concrete where it's used for 8 up to 12% of its weight [1, 2]. The total world cement production in 2016 is estimated at 4.6 billion tonnes [3]. If properly designed and mixed, the material has excellent mechanical and durability properties. It has a high compression strength, is relatively low in price, is moldable, is generally available and has a good fire resistance [4]. Buildings made out of concrete are endorsed as long-lasting and energy-efficient [1].

The disadvantage of concrete is its relatively low tensile strength. The material tends to crack under a tensile force that could be caused by stress mechanisms like thermal stress, shrinkage and expansive chemical reactions. Reinforcement is used to carry the tensile forces after the concrete has cracked. Small cracks, not necessarily causing a risk of collapse of the structure, will accelerate the degradation of the structure and will diminish the service life and sustainability [5]. They allow harmful chemicals to enter the concrete with the deterioration of the matrix and reinforcement steel as a consequence [6].

The production of cement is one of the most carbondioxide (CO_2) producing industries. The industrial manufacturing of cement clinker and the fuel combustion emission of CO_2 related to its production are responsible for 8% of the global CO_2 production [7, 8]. To reduce the environmental load, fly-ashes and other constituents have been used as a partial replacement of Portland cement. A study by the World Business Council for Sustainable Developments (2009) has shown that the share of blended cement considerably increased in most countries compared to Ordinary Portland Cement. The current average clinker-to-cement ratio over all

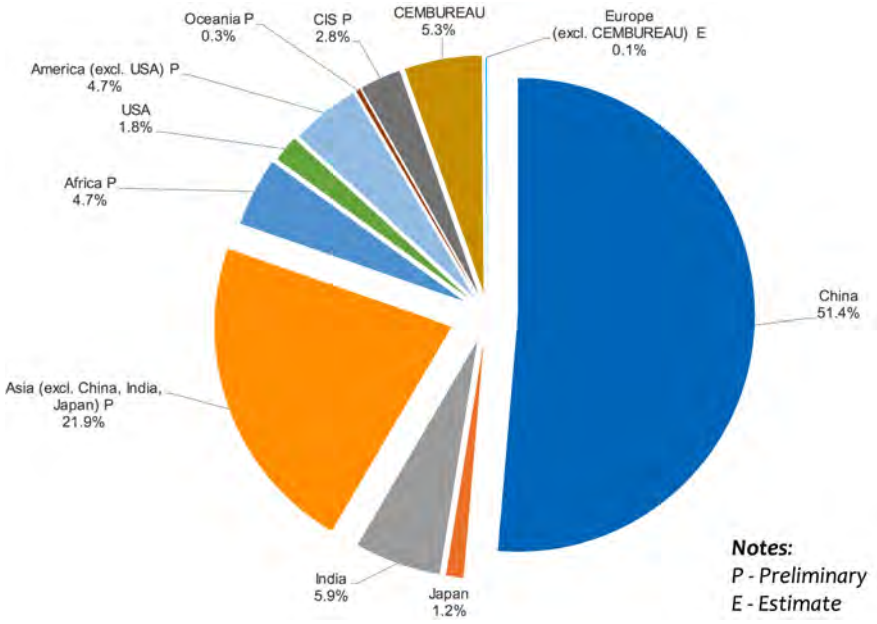

Figure 1.1: World cement production 2015, by region and main countries, % of 4.6 billion tonnes [3]

cement types in the EU27 is 73.7% [10].

By extending the service lifetime of the infrastructure, the environmental impact is reduced in an indirect way. Either the loss of strength and stiffness of the concrete structure or the loss of aesthetics require the structure to be repaired. Conventional repair methods (e.g., epoxy injection, spraying of high molecular weight methacrylate, etc) require labour work, are often slow and/or expensive [11]. By increasing the durability, concrete structures need less repair and maintenance. The formation and propagation of cracks foster the deterioration mechanisms that harm the concrete and its reinforcement. The improvement of concrete crack-healing contributes to the reduction of deterioration, extension of the service life, reduction of repair frequency and a cost reduction over the service life of the concrete infrastructure. These benefits imply a reduction of necessary repairs and replacements, lower raw material usage and consequently a reduction in energy consumption and pollutant emission due to production and transportation. That is, self-healing concrete could be a key development towards sustainable civil infrastructure [12].

1.1.2 Cracking of concrete

Concrete deteriorates over time due to various time-dependent mechanisms, e.g., thermal stresses, shrinkage, differential settlements, expansive chemical reactions, carbonation-induced corrosion and freeze/thaw cycles [13, 14]. Cracking of concrete is inevitable, although measures can be taken to minimise early age cracking and to control crack formation [14].

1.1.2.1 Early-age cracking

Creep and shrinkage deformation of concrete under restrained conditions during the first days after casting are a severe problem for concrete. Rapid and complex volume changes cause tensile stresses in the concrete when the strength is still relatively low. During the first days, the development of tensile forces and gain of strength are still evolving with time. When the strength of the young concrete is not sufficient to take up the tensile forces, early-age cracks will form. Even though it may not affect the structural integrity, this early age deterioration leads to durability problems and restraints the service life of the concrete structure [15, 16].

In the first hours after casting, the expansion/shrinkage ratio depends on which mechanism is most dominant, either thermal effect or drying. After that period, shrinkage of the concrete occurs at a rapid rate which is attributed to both autogenous and drying shrinkage. The latter is the result of shrinkage due to evaporation of excess water. Restraint of shrinkage, provided by the reinforcement or an adjacent structural component, causes tensile stresses to develop in the hardened concrete [14, 15]. Autogenous shrinkage on the other hand is the phenomena of concrete shrinking by itself, without any change in mass or temperature. It gained attention when high strength concrete became feasible because the cracking of high strength concrete could not be explained solely by thermal stresses or drying shrinkage [17]. According Altoubat and Lange (2001), tensile stress is not the only governing factor in the cracking mechanism of restrained concrete. The other important factor that must be considered is the stress history of the concrete, particularly at very early age. They further state that the key to prevent early age microcracking is to prevent the built-up stress from exceeding 50 % of the tensile strength at every point in time.

Despite being inevitable, early-age cracking of normal strength concrete can be limited through proper curing. To minimise surface cracks due to shrinkage, measures are taken to prevent rapid water loss from the concrete surface, i.e., fog nozzles, plastic sheeting, windbreaks, or sunshades [14, 17]. Regarding high performance concrete, the small amount of water used for mixing is rapidly consumed by early-age hydration of cement. The central part of the specimen is subjected to self-desiccation (i.e. consumption of capillary water in progress of cement hydration; without water supply from the surrounding environment), forming a dense microstructure and making the penetration of external curing water impossible. Consequently, a large amount of autogenous shrinkage is observed in high performance concrete [17, 18].

1.1.2.2 Time-dependent cracking

The material limitations and severe exposure conditions can cause time-dependent cracking which may result in functional, structural or aesthetic problems. Corrosion of reinforcing steel is recognised as the leading cause of deterioration in concrete [14]. Corroded steel occupies

a greater volume than the original material, creating tensile stresses in the mass concrete, which can cause cracking, spalling or even delimitation [14, 19]. The corrosion rate is increased when the alkalinity of the concrete is reduced or when the chloride concentration in concrete is increased to a certain level. The former phenomena can be induced by carbonation of the concrete, i.e. formation of carbonates when carbon dioxide (CO_2) from the air penetrates the concrete and reacts with hydroxides such as calcium hydroxide ($Ca(OH)_2$).

$$Ca(OH)_{2(aq)} + CO_{2g} \longrightarrow CaCO_{3s} + H_2O_l \tag{1.1}$$

The thin oxide layer formed on the steel at high pH is no longer stable because of the reduction of pH due to the above reaction. In combination with an increase in water content in the carbonated mortar spores or the addition of $CaCl_2$, this leads to an increased corrosion rate [14, 20].

Water-soluble chlorides, present in deicing salts and seawater, foster corrosion. The mechanism by which chlorides promote corrosion is not completely understood [14]. Multiple mechanisms are suggested, e.g, local acidification at the anode, which is corrosion rate determining according Gonzalez et al. (2013); and penetration of the protective oxide layer leaving the steel vulnerable to corrosion [14, 20, 21].

Figure 1.2: Cracking of concrete: (1) restraint to drying shrinkage, (2) cracking of pavement caused by freeze-thaw deterioration, (3) map cracking and spalled concrete surface due to alkali-silica reactivity [14]

Another source of crack formation is the expansion of ice crystals during the formation of ice. The expansion of the ice crystals produces pressure in the capillary boundaries and pores of the concrete, which will dilate and rupture when the tensile strength is exceeded. The main parameters that influence this mechanism are closely related to the pore system, i.e. total porosity and pore size distribution, which can be altered by for example the usage of an air-entrainer [14, 22].

Some aggregates react with alkali hydroxides in concrete, causing expansion and cracking over time. Two forms of alkali-aggregate reactivity are distinguished, i.e., alkali-silica reactions (ASR) and alkali-carbonate reaction (ACR), the former of greater concern [14]. Measures taken to control ASR include a reduction of internal relative humidity of concrete; the use of

certain mineral admixtures like silica fume, fly ash and ground blast furnace slag which have significantly reduced alkali-silica reactivity [14, 23–25].

1.1.3 The danger of cracking

Cracks in concrete structures reduce overall durability by allowing the penetration of water and harmful chemical agents, thereby accelerating the concrete deterioration [26]. As aforementioned, a variety of deterioration mechanisms related to material limitation, design and construction practices (e.g. differential settlements) and severe exposure conditions, may result in aesthetic, functional or structural problems. Concrete damage is often the result of a combination of deterioration mechanisms [14].

Cracks within a specific crack range are allowed in reinforced concrete according the present codes of practice. They facilitate the ingress of harmful chemical agents like chloride ions. The chloride penetration generally increases with crack density. The chloride diffusivity increases significantly with increasing crack width [27, 28]. According Li and Herbert (2012), sealing of the cracks by improved concrete self-healing is an effective measure to reduce the diffusion coefficient of chloride ion transport. The initiation of corrosion takes longer and translates into an extended service life before repair is required [12].

1.2 Crack mitigation methods

The strategies involving the mitigation of cracks can be divided in autogenous strategies and non-autogenous strategies. The former concerns the concrete mixture properties while the later involves all other strategies [18].

1.2.1 Autogenous strategy

The addition and saturation of fine lightweight aggregates (LWA), who act as internal water reservoirs, enhances internal curing of concrete; reducing the drying shrinkage and self-desiccation shrinkage by consequence [18, 29]. Possible problems related to this technique are the reduction in strength, rheological inconsistency and reduction of elastic modulus of the concrete [18].

Changes in concrete mix design (alkali-activated slag (AAS) binder [30], silica fume, gypsum [31], aggregate content, blast-furnace slag (BFS) [32], etc.) will alter autogenous shrinkage. Higher autogenous shrinkage is observed in concrete made with BFS, which may be due to greater chemical shrinkage and the formation of a finer pore structure than ordinary concrete [32]. The addition of gypsum on the other hand reduces both autogenous and drying shrinkage thanks to the formation of expansive products such as ettringite [31]. It has also been noted that the use of coarser cement, creating larger pores, produces less autogenous shrinkage.

Thus engineering the particle-size distribution may be one of the methods to mitigate early age cracking of high-performance concrete [33].

1.2.2 Non-autogenous strategy

Cracks caused by volume changes are often created in combination with external restraints. Restraints may be imposed by adjacent members, formwork or reinforcement. Cracking due to restraint movement imposed by adjacent members can be controlled by applying construction joints [18]. The restraining effect from reinforcement is not necessarily bad. It may facilitate the formation of more evenly spaced cracks instead of a few wide cracks, making reinforcement a measure to provide crack control [18, 34].

The contribution of fibres in the scenario of early-age cracking is to reduce the rate of stress evolution by improving relaxation characteristics and redistributing the internal stresses. Microstructure damage can lead to cracking sooner than predicted by a simple strength criterion [15]. The addition of fibres adds a self-controlling mechanism for tight crack width which reduces the chloride diffusivity [27, 28], autogenous shrinkage [35] and improves the intrinsic healing capacity of the concrete [12].

Proper curing is required to prevent extensive autogenous shrinkage and drying shrinkage of early-age concrete [14, 15, 36]. Rapid water loss from the concrete surface can be prevented by using fog nozzles, plastic sheeting, windbreaks or sunshades [14, 17, 18]. Water exchange between the environment and the mass concrete on the other hand depends to some extent on the element's thickness [18]. The addition of internal water is required to benefit from the effects of internal curing, including further hydration and strength development, reduced autogenous shrinkage and cracking, reduced permeability and increase durability [36]. In a new approach, saturated superabsorbent polymer (SAP) particles are added to the concrete mixture to provide additional internal water and foster internal curing [37, 38].

1.3 Crack repair methods: traditional methods and new technologies

1.3.1 Traditional repair methods

The performance of traditional repair depends on the inspection, diagnosis of the problem, design of the repair and quality of workmanship [39, 40]. Most commonly, the assessment of repair is based on visual examination. In some cases, non destructive testing (NDT) is used, which includes measurement of electrode potential, cover thickness, pull-off strength (to check adhesion of patches to the substrate), chloride content and carbonation depth [39]. Incorrect diagnosis, i.e., failure to identify the root cause of the concrete cracking, is reported

to be one of the causes of repair failures. Furthermore, poor workmanship and the use of incorrect repair materials are two more causes, which originate from the pressure imposed by the working conditions and contractor. To meet the demand of competition, costs have to be minimised, which endangers the performance of the repair. To reduce the social cost, structures should be kept operational at all cost [39].

Commonly applied repair methods include patching, coating and crack injection or a combination of these. The former requires defective concrete to be removed and cleaned before applying the patch, which can be strictly cementitious based or which can contain polymers as an admixture [39–41]. By injection or gravity filling of cracks with a low-viscosity epoxy resin, the structural integrity of the concrete can be restored to some extend [40]. Other methods of restoring strength included: external bonding of steel or CFRP plates, adding external prestress and adding concrete [39, 40]. Coatings are usually applied in combination with the aforementioned repair methods. They reduce the water penetration, vapour and gas diffusivity and can exhibit better chemical resistance than concrete does [40].

The main problem related to conventional repair methods is its disappointing performance. The expectation of repair varies according to the type of the structure and requirements of its owner. In many cases, to minimise the social impact of taking the structure out of service, a hurried repair is applied, which is likely to have a short life [39]. Furthermore, it is difficult to repair cracks which are not accessible, as in underground or submerged concrete structures [42].

Throughout the last decade, the potential of using internal and active mitigation treatments over external, passive and expensive treatments is recognised. Mechanical damages are being healed or repaired by internal mitigation treatments, also referred to as self-healing processes, restoring (partially) the mechanical properties of the damaged concrete [43]. In what follows, we discuss concrete as a self-healing material.

1.3.2 Self-healing concrete

A new concept for repair in construction industry is the use of self-healing cement-based construction materials. Self-healing materials fit in the mindset of the industrialised countries, whom see sustainable development as a key priority of the ruling governments [5, 43]. They are an innovative solution that could fulfil challenges such as minimising the consumption of natural resources and raw materials by guaranteeing durability performance, hence reducing the investment on maintenance and/or intensive repair works [5].

Self-healing cement-based materials have an inborn capacity to repair damages. The autogenous self-healing is improved by incorporating “healing promoter additives”. There are two main approaches for self-healing in concrete: autogenous healing and autonomous healing.

Autogenous healing is a natural process. It relies on the hydration of unreacted cement particles and carbonate precipitation, which are intrinsic mechanisms of concrete. Autonomous healing on the other hand is an engineered mechanism to improve the self-healing properties of concrete.

To assure robustness of self-healing concrete, Li and Herbert (2012) suggested six criteria that should be met and that can be used to evaluate the advantages and limitations of different self-healing approaches in concrete infrastructure. They are: *Shelf life, Pervasiveness, Quality, Reliability, Versatility, and Repeatability* [12]. The success of the self-healing approach and consequently the ability to reverse the damage development once, several or even multiple times ('damage management' [43]) is closely related to the performance on aforementioned criteria. If self-healing of damage can significantly increase the service lifetime and reliability of structures, life-cycle cost could be drastically cut down as shown in figure 1.3 [12, 44].

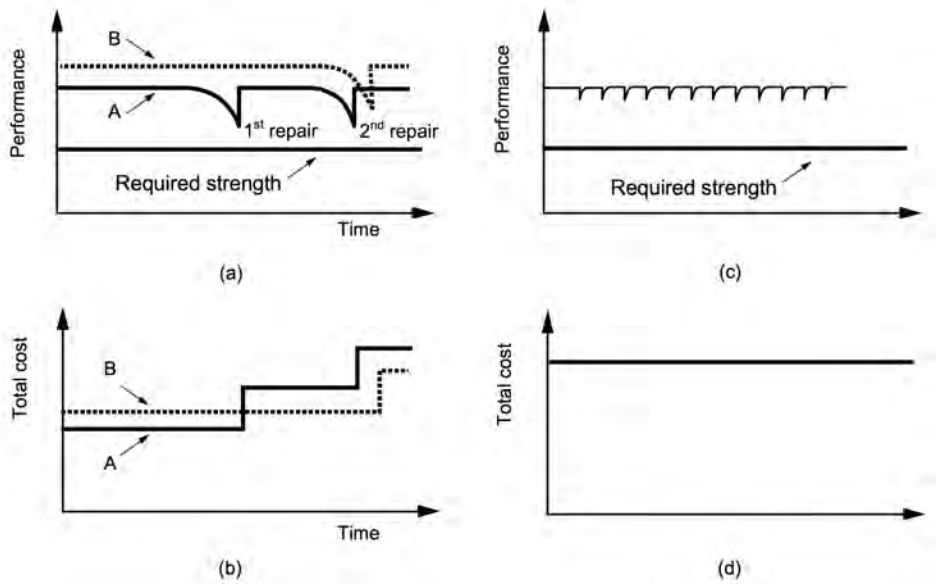

Figure 1.3: (a) and (b): Performance and cost with the elapse of time for concrete structures requiring traditional repair; The dotted line represents a concrete B of higher performance compared to concrete A; (c) and (d): Performance and cost with the elapse of time for structures which include self-healing mechanisms [44]

1.3.2.1 Autogenous healing of concrete

Autogenous healing as an inherent property of concrete

Concrete has an intrinsic ability to precipitate non-soluble products inside cracks. This property is mainly caused by continuous hydration of unreacted cement particles and by the calcium carbonate ($CaCO_3$) precipitation [5]. Other possible causes are illustrated in figure 1.4 on the next page [45]. Still, the physico-chemical process of the autogenous healing is

not completely understood [46].

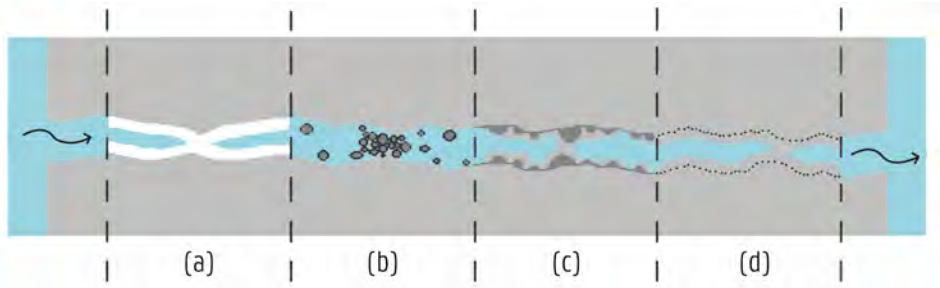

Figure 1.4: Possible causes of autogenous healing in cementitious materials: (a) formation of $CaCO_3$ or $Ca(OH)_2$, (b) clogging by pollutants and loose concrete fragments from spalling, (c) hydration of unreacted cement particles, (d) expansive reaction (e.g. ettringite formation) of hydrated cementitious matrix [45]

The primary mechanism and reaction products formed in cracks remain a matter of debate [46]. To better understand the physico-chemical process and the potential of autogenous self-healing in different cement pastes, an investigation for each of them is required [46]. The autogenous self-healing due to continued hydration is expected to diminish for ageing concrete [47]. The deposition of $CaCO_3$ on the crack edges becomes the dominant mechanism at later age. The chemical reaction process 1.2 outlines the formation of $Ca(OH)_2$ and $CaCO_3$ at the crack edges [48].

$$H_2O + CO_2 \rightleftarrows H_2CO_3 \rightleftarrows H^+ + HCO_3^- \rightleftarrows 2\,H^+ + {CO_3}^{2-} \tag{1.2}$$

$${Ca}^{2+} + {CO_3}^{2-} \overset{\mathrm{pH_{water}} > 8}{\rightleftarrows} CaCO_3 \tag{1.3}$$

$${Ca}^{2+} + HCO_3^- \overset{7.5 < \mathrm{pH_{water}} < 8}{\rightleftarrows} CaCO_3 + H^+ \tag{1.4}$$

The width of the crack closure depends on the concrete composition, cement particle size and the surrounding conditions. The diffusion of ions from the bulk paste into the concrete matrix is essential for the formation of reaction products in the crack. The use of a coarser cement is one of the measures to promote the potential autogenous self-healing since more cement particles will be available for ongoing hydration after crack initiation [46]. Furthermore, presence of water in the surrounding environment is essential to promote self-healing [49, 50]. Decreasing the diffusivity of ions after autogenous healing results in a slower ingress of harmful chemical agents into the bulk paste, but despite of this advantage, continuation of autogenous healing is hampered by the fallback of diffusivity of ions from the bulk to the crack [46]. For this reason, autogenous healing is not sufficient for full crack repair in case of larger cracks [48]. Therefore, the crack width should be controlled to below 150 µm for partially healing and to 50 µm to engage complete self-healing behaviour [50].

Improved autogenous healing

To improve autogenous healing, three different approaches may be used, namely crack width control, supply of additives, and ensuring a moist environmental condition [51]. They offer a solution to one or more of the aforementioned shortcomings of the intrinsic autogenous self-healing.

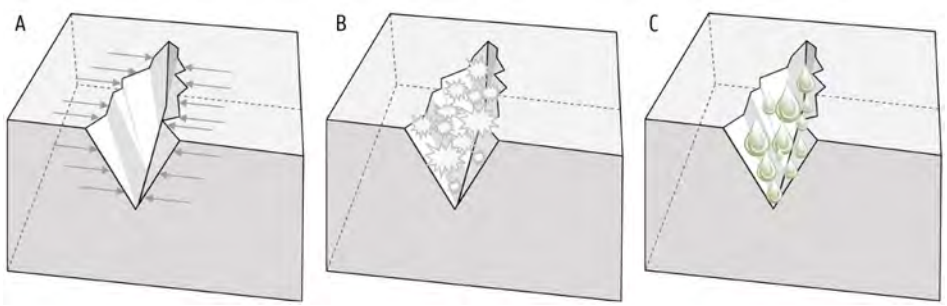

Figure 1.5: Improved autogenous healing by crack width control (A); supply of additives (B); or ensuring a humid environment (C) [51]

Crack width control

Steel reinforcement has not attained adequate reliability for controlling the crack width in concrete structures for a robust self-healing approach. Therefore, Yang et al. (2009) proposed the use of engineered cementitious composite (ECC) with polyethylene (PE) and polyvinyl alcohol (PVA) fibres to restrict the crack width. The maximum crack width remained below 60 µm [50]. Homma et al. (2009) compared the self-healing performance of fibre reinforced cementitious composites (FRCC) containing polyethylene (PE) fibre, steel cord (SC) fibre or a hybrid fibre composite containing both. The latter showed the most significant recovered tensile strength while self-healing by $CaCO_3$ precipitation of the other fibres was also confirmed [52]. Nishiwaki et al. (2012) evaluated the self-healing capability of FRCC for ethylene vinyl alcohol (EVOH), polyoxymethylene (POM), polypropylene (PP), and PVA fibres and found that PVA fibres induced the highest healing efficiency. The synthetic fibre has a high polarity, which enhances its property as a precipitation site for self-healing products. Furthermore, the PVA fibre contributes to optimal geometrical properties of the crack surface, necessary to improve the capability of self-healing [53]. Kuang and Ou (2008) took advantage of the self-restoration characteristics of shape-memory alloys (SMA) to minimise the crack width, thus promoting the autogenous self-healing of concrete. In the particular application, Kuang and Ou (2008) used low viscosity epoxy adhesive-filled brittle fibres as the sealing/repairing chemicals, which is recognised as an autonomous self-healing approach. Unfortunately, the economics of SMA still need to be analysed for practical applications [54, 55].

Supply of additives

Mineral admixtures can be added inside concrete during mixing with the purpose of increasing the capability of autogenous self-healing. Changes in concrete mix design will alter the type and amount of main reaction products formed in cracks. The main reaction products of a Portland (CEM I) cement paste and a slag (CEM III) cement paste were compared by Huang (2014). The main mineral formed in the Portland cement paste is $Ca(OH)_2$ while reaction of unreacted slag (forming CSH) and recrystallisation of dissolved ettringite of the bulk paste are the main mechanisms of autogenous self-healing of cracks in the slag cement paste [46]. Other researchers incorporated expansive additives and swelling materials, e.g., geo-materials composed out of silicon dioxide SiO_2 to improve crack-sealing potential [56]. Kishi et al. (2007) found an increased self-healing ability after addition of carbonates such as $NaHCO_3$, Na_2CO_3 and Li_2CO_3 in combination with $Ca_4Al_6(SO_4)O_{12}$, which form ettringite after hydration. Sisomphon and Copuroglu (2011) added a calcium sulfoaluminate based expansive additive (CSA) and crystalline additive (CA) and concluded that their usage is beneficial for crack closing. However, microcracks were noticed on the interfacial transition zone between matrix and aggregates [58].

Water supply

The presence of water is essential for autogenous self-healing [49, 59]. To provide and retain additional water, the possibility of mixing super absorbent polymers (SAP), a hydrogel that can absorb and retain an extremely large amounts of a liquid relative to its own mass, into cementitious material is investigated. Snoeck and De Belie (2016) stated that the addition of SAP particles proved to be an effective measure to promote self-healing, resulting in more visual crack closure and more regain in mechanical properties [59]. The initial swelling of the SAP particles during concrete mixing alter the microstructure, i.e. causes formation of macropores and the reduction of strength. To solve this problem, the use of pH responsive SAPs is proposed. In the vicinity of the crack, the pH is reduced and more swelling of the SAP particles is observed, sealing the crack temporary and promoting autogenous healing by providing additional water through release of their water content during dry periods [60]. In another approach, water is encapsulated in a paraffin shell and distributed throughout the concrete matrix. Upon cracking, the water reservoir splits and releases its content into the crack in order to improve the formation of new hydration products. However, the capsules lost their water in a short period [61].

1.3.2.2 Autonomous healing of concrete

The design of an autonomous self-healing method can be approached in two different ways. The self-healing ability can either be achieved by improving the autogenous healing ability (see *Improved autogenous healing* in paragraph 1.3.2.1) of concrete and/or by providing alter-

native healing mechanisms. In this subsection, alternative healing mechanisms to the intrinsic autogenous healing (subsection 1.3.2.1 on page 8) are discussed. The main challenges of engineering an autonomous self-healing mechanism are the protection of the healing agent inside the concrete and the ability to be only activated when necessary [5]. Several encapsulation techniques are still being actively developed [62–65]. Those healing agent protections should resist mixing and casting of concrete, a highly alkaline environment and other type of damages, like change of the pH in the vicinity of cracks. Ideally, a healing agent should be capable of fully restoring the transport and mechanical properties of the damaged concrete. Hence, the percentage of recovery can be an indicator for the quality. Furthermore, it must posses a shelf life equal to the long service life of the civil infrastructure. Cracks should be healed regardless their position and direction and this implies the self-healing agent to be pervasive in the structure. The versatility of the self-healing concrete is evaluated through their wide application in different environments. Even after cracks occurred and sealed, new cracks can develop and should repeatably be healed by the self-healing agent during the service life of the concrete infrastructure [5, 12].

Healing agent nature	*Introduction Method*		
	Without encapsulation	*Dispersed encapsulation*	*Localized encapsulation*
Cement	Autogenous healing	Encapsulation of water by superabsorbent polymers or by porous fibers	
Chemical agent	Admixtures such as: crystalline admixtures	(Micro-) capsules, impregnated porous aggregates or fibers containing the chemical or bacterial solution	Porous networks, encapsulating vessels containing the chemical or bacterial solution
Biological agent	Bacteria		

Table 1.1: Autonomous healing methods categorized by healing agent nature and introduction method [5].

In what follows, the healing agent nature is divided according the introduction method in concrete, based on the categorisation by the COST Association (2016).

Non-encapsulated healing agent

The autonomous self-healing approach relies on the existence of a new pathway to improve the self-healing properties of concrete elements [5]. One approach uses bacteria that can induce calcium carbonate ($CaCO_3$) precipitation. Bacterial spores, a dormant life form of bacteria, nutrients such as urea and yeast extract; and a mineral precursor compound like

calcium lactate [66, 67] are mixed in the concrete. The addition of spores and nutrients in concrete has a direct influence on the initial and final setting time [66, 68]. Furthermore, the addition of bacteria-based additives may result in an unwanted strength loss in early curing age, while a less significant influence is found in 28 days of curing [67, 68]. The bacterial spores can remain dormant for over two centuries [69] before activation through water ingress [67]. After germination, carbonate precipitation is induced by the vegetative bacterial cells. For different bacteria, different precipitation pathways exist, each largely dependent on the environmental conditions [70, 71]. Despite the long survival of dormant cells, the high alkalinity of concrete and the densification of the matrix during hardening of the concrete limits the lifespan of the bacterial spores that were directly added to the cement paste mixture [62, 67]. A possible solution to prevent crushing of the bacterial spores in aged specimens could be the encapsulation of spores in a protective matrix prior to addition to the concrete mixture or the addition of an air-entraining agent to create isolated micropores [67].

Encapsulated healing agent

Micro- and macro-capsules containing healing agent are added inside concrete and repair mortars to provide autonomous self-healing properties. The activation of the healing mechanism relies on release of the healing agent from the capsules upon crack formation or after an environmental trigger [5, 72]. Several encapsulation techniques are developed for both bacterial [62, 66] and chemical healing agent [73].

Chemical healing agent

The chemical agents used to seal cracks and connect both crack faces can either be a one-component, two-component or even a multi-component agent. The hardening process varies and in some approaches an additional additive is necessary to activate the healing mechanism [74]. For instance, Perez et al. (2015) embedded epoxy-containing silica microcapsules and amine-functionalized nanosilica in cement paste specimens with silica fume. After the microcapsules were broken, a chemical reaction took place between the epoxy and the amine groups of the amine functionalised cementitious matrix. Through scanning electron microscopy (SEM) analysis, it was confirmed that microcapsules remain intact during mixing and hydration of the specimens. A decrease of compressive strength of the cement paste specimens after addition of microcapsules was reported by Perez et al. (2015) and other researchers [75, 76]. It was proven by capillary water absorption test that this approach is effective to regain material tightness after cracking to a nominal width of 150 µm [74].

Glass tubing macrocapsules that include repair chemicals like polyurethane are carefully positioned inside the concrete matrix and are not pervasive. The repair chemicals are released when a concrete crack intersect the glass tube and cause it to fracture. The glass tubes should be oriented perpendicular to the anticipated cracks. This technique could not be repeated

after a first crack healing since only a limited amount of macrocapsules are available [12]. Qureshi et al. (2016) encapsulated various expansive materials (MgO, bentonite and quicklime) and water in double tube glass macrocapsules and proofed their ability to restore the mechanical and transport properties of the undamaged concrete. The glass macrocapsule system is found to be very effective in closing very large cracks (∼400 µm) because of the large amount of healing agent available [77].

The most severe limitation of this technique is the lack of repeatability. Once the micro- or macrocapsules break and are emptied, they cannot be used in the next cycle of damage. The use of microcapsules sized on the scale of cement particles could solve this limitation since the capsules are widely available and uniformly dispersed inside the matrix, but then under crack formation, it is believed that only a limited amount of healing agent will be available [12]. If the healing product has a higher mechanical strength than the surrounding concrete matrix, cracks might emerge on new locations and this problem can be overcome. Furthermore, capsules have to survive concrete mixing and impact during casting.

Biological healing agent

In bacteria based self-healing concrete, bacteria are used for their ability to produce calcium carbonate $CaCO_3$ in a high calcium environment. The bacteria should withstand the high alkalinity of cement and the high pressure as a result of the densification of the microstructure caused by cement hydration. Therefore, a protection mechanism should be provided to guarantee their life and metabolic activity inside concrete [62, 66, 78]. Furthermore, bacteria need sufficient water to germinate and therefore the applicability may be limited to civil structures with a constant water supply [12]. By using a carrier that can absorb, retain and supply water to the bacterial spores, this limitation can be overcome [62, 79]. Researchers used various solutions to protect the bacteria, including immobilisation in silica gel [80], polyurethane (PU) [80, 81], hydrogel [79], diatomaceous earth [82], expanded clay [83], metakaolin and zeolite [66]. Furthermore, Ersan et al. (2015) suggested to encapsulate the nutrients who feed the ureolytic activity, i.e., carbonate precipitating metabolism, as well [66]. Microbial $CaCO_3$ precipitation is regarded as an economical and environmentally friendly material [84]. The application of ureolytic bacteria is found to effectively heal cracks and increase the durability properties of cementitous materials. Further research into the use and encapsulation of biological healing agents is needed in order to exploit the full potential of this autonomous healing method.

Vascular system containing healing agent

In another autonomous approach, the healing agent is added through a vascular system of tubes running through the structure and connected to the exterior. Thus, the healing agent is introduced manually into the vascular system by means of gravitational forces. The tubes

can be made of glass, which probably cannot withstand concrete impact during casting, an acrylonitrile butadiene styrene 3D-printed material, a cementitious hollow tube (CHT) or an inorganic phosphate cement (IPC) material [85]. Sodium silicate [86], polyurethene (PU) [85] and a saturated $Ca(OH)_2$ solution [87] were selected as healing agents in previous research. Huang et al. (2014) noticed an improved self-healing efficiency of the vascular system compared to capsules supplied with a saturated $Ca(OH)_2$ solution because of the higher dosage of supplied healing-agent [87].

1.4 Bacteria-based self-healing system

Although different approaches have been proposed by research groups all over the world, it is still difficult to compare their healing efficiency because no standard test methods are defined. Autogenous healing is restricted to small cracks and depends on the composition of the matrix, determining the feasibility of the healing method. Thus, autonomous healing methods are designed to go beyond those boundaries. Researchers suggest the use of capsule based self-healing methods which release their healing agents upon crack formation. According Van Tittelboom and De Belie (2013), those healing agents are preferred to be activated by a second component present in the cementitious matrix or provided by additional capsules [51]. The addition of encapsulated microorganisms to the cementitious matrix is considered to meet the previously mentioned general opinion about effective healing approaches.

Microbial calcium carbonate ($CaCO_3$) precipitation is regarded as an economical and environmentally friendly material [84]. The phenomenon, which involves the activity of the enzyme urease, is also known as microbiologically induced calcite precipitation (MICP) [84]. Research was conducted into the use of MICP to consolidate sand columns [88, 89], reduce water absorption and increase strength of bricks [90], and to repair concrete structures [84]. $CaCO_3$ precipitation is a chemical process governed by four parameters: (1) the calcium ion concentration, (2) the dissolved inorganic carbon concentration, (3) the pH level and (4) the availability of nucleation sites [91]. Those parameters can be altered by the microorganisms [92].

The self-healing efficiency of carbonate precipitating bacteria in concrete depends on the type of bacteria, the viability in an alkaline environment, type of encapsulation and the activation of the bacteria [93]. The bacteria should withstand the harsh alkaline environment, a high pressure and ideally, they should consume oxygen when active to reduce corrosion of the reinforcement steel [67, 94, 95]. Crack healing is evaluated through different criteria, including: crack width measurements, permeability, visual inspection, regain of compression strength, SEM images and X-ray diffraction scan to evaluate the nature of healing compound which are produced [51, 93]. It is also important to test the healing within the time domain of 28 days when the strength gain is of great importance.

Calcium carbonate crystals are formed in 3 particular formations: calcite, argonite and vaterite. Calcite is the most stable form [93]. The process of calcium carbonate $CaCO_3$ formation in bacteria incorporated concrete (via calcium lactate $CaC_6H_{10}O_6$ catalysis) differs strongly from the process in the reference concrete samples (carbonation of calcium hydroxide $Ca(OH)_2$). But portlandite ($Ca(OH)_2$) is soluble in water and can leave the concrete so less reagentia is available to convert in $CaCO_3$. The process of carbonate precipitating produces CO_2 which react with the $Ca(OH)_2$ on the spot and won't let it waste.

1.4.1 Bacterial strains

Different bacterial strains have been examined for their use in the precipitation reaction of calcium carbonate. Both bacteria of autotrophic and heterotrophic nature have been used [92]. The latter requires food, chemical energy stored in organic molecules, to be available while the former can synthesise food by itself using light (photosynthesis) for example. In this master's thesis dissertation, heterotrophic bacterial strains inducing $CaCO_3$ precipitation by urease activity (microbial process part of the nitrogen cycle) are discussed.

Urease activity

Urease is an enzyme that catalyses the hydrolyses of urea to yield ammonia and carbamate, an organic compound derived from a carbamic acid (NH_2COOH). Carbamate spontaneously degrades to an carbonic acid and ammonia molecule [96, 97].

$$H_2N{-}CO{-}NH_2 + H_2O \xrightarrow{\text{Urease}} NH_3 + H_2N{-}CO{-}OH \tag{1.5}$$

$$H_2N{-}CO{-}OH + H_2O \longrightarrow NH_3 + H_2CO_3 \tag{1.6}$$

Microbial urease is known to have K_m-values, concentration of the substrate urea ($CO(NH_2)_2$) which permits the enzyme to achieve half the maximum rate of reaction v_{max}, ranging from 9.2 to 230 mM [98–100]. At physiological pH, the carbonic acid proton dissociates and the ammonia molecule get protonated, resulting in a net increase in pH [97]. In an alkaline solution, the hydroxide ion and bicarbonate (HCO_3^-) form a carbonate ion [88].

$$H_2CO_3 \longrightarrow H^+ + HCO_3^- \tag{1.7}$$

$$2\,NH_3 + 2\,H_2O \longrightarrow 2\,NH_4^+ + 2\,OH^- \tag{1.8}$$

$$HCO_3^- + OH^- \rightleftharpoons CO_3^{2-} + H_2O \tag{1.9}$$

Both the carbonate CO_3^{2-} and bicarbonate HCO_3^- function as a buffer, slowing down the pH increase from urease activity. The overall equilibrium reaction in the calcium carbonate precipitation is [88]

$$Ca^{2+} + CO_3^{2-} \rightleftharpoons CaCO_3\downarrow \tag{1.10}$$

To summarise, urease catalyses the hydrolysis of urea to carbonate and ammonia, resulting in an increase of the pH and carbonate concentration in the vicinity of the bacteria [88].

1.4.1.1 Bacillus Pasteurii

In early research on the repair of concrete using micro-organisms, the alkalophilic endospore-forming soil micro-organism, *Bacillus pasteurii* were used to induce calcium carbonate ($CaCO_3$) precipitation. The pH value is a key factor in the $CaCO_3$ precipitation [91], thus the ability to generate an alkaline environment is of vital importance [92]. Stocks-Fischer et al. evaluated the kinetics of microbiological $CaCO_3$ precipitation at different pH values and found that from pH 9 onwards, the initial Ca^{2+} concentration was almost completely precipitated. According to Stocks-Fischer et al., the urease activity in a cell free extract of *B. pasteurii* peaked at pH around 8. Still, a substantial amount of urease activity remained at pH 9. The optimum pH for both growth of *B. pasteurii* and microbiologically $CaCO_3$ precipitation is around pH 9 [84, 88]. To survive the highly alkaline pH of concrete, the endospore, a dormant form of the cell, of *B. pasteurri* is added to the concrete instead of viable cells [84].

Ramachandran (2001) examined the stiffness values and compressive strength of Portland cement mortar beams containing $3.8 \cdot 10^9$ *B. pasteurri* spores per cm^3 cured in a Urea-$CaCl_2$ medium for 28 days. The presence of the bacteria showed an effective remediation of shallow cracks. A maximum increase of stiffness by 9.4 % and compressive strength by 61 % compared to that of the control specimens are observed in his research [84]. The author expected and proved by SEM examination that microbial remediation is in general more effective in shallow cracks because *B. pasteurri* prefer the presence of oxygen, though being facultatively anaerobic. Furthermore, Ramachandran (2001) found that due to the extremely alkaline environment, the bacterial activity of *B. pasteurri* remains absent. The increase of the overall strength of the mortar specimens when mixed with micro-organisms resulted from the microbial biomass acting as organic fibres rather than the presence of calcite induced by microbial activity. On the other hand, MICP is effective in crack repair and moreover in shallow cracks primarily because the bacteria grow more actively in the presence of oxygen [84].

1.4.1.2 Bacillus Subtilis

Park et al. (2012) were the first researchers to apply *B. Subtilis* for its ability to improve the durability of concrete by $CaCO_3$ precipitation. The weight growth of the cement paste treated with *B. Subtilis* showed a higher rate compared with that of treatments with *E. Coli* and *B. Cereus*, suggesting their use as nucleation site for the growth of $CaCO_3$ crystals is effective. Furthermore, after immersion in a B4 precipitation medium, mortar specimens treated with *B. Subtilis* closed cracks up to 300 µm within 5 days of full immersion [101]. Reddy et al. (2012) performed durability tests by exposing *B. Subtilis* incorporated concrete

(10^5 cells per ml of mixing water) specimens to a 5% HCl and 5% H_2SO_4 medium and revealed that concrete treated with *B. Subtilis* suffered from less weight and strength loss than their reference. The author concluded that *B. Subtilis*, which is readily available in soil, might be safe, non pathogenic and cost effective [102]. This conclusion is supported by Manikandan and Padmavathi (2015), who confirmed $CaCO_3$ precipitation by *B. Subtilis* to be an effective measure for crack remediation by SEM analysis [103]. Furthermore, several researchers observed a gain in compressive strength after 28 days of hardening after direct incorporation of *B. Subtilis*, varying between a 19.5 and 23% increase compared to that of the control specimens [101, 102, 104]. In a more recently conducted research by Khaliq and Ehsan (2016), *B. Subtilis* was incorporated in concrete through LWA and graphite nano platelets. The former showed consistency in crack healing of concrete irrespective of crack initiation at early or later age, while the encapsulation in graphite nano platelets presented a significant decrease in healing efficiency of cracks at later age. Thus, the encapsulation of *B. Subtilis* by LWA is regarded as a more robust approach [93].

1.4.1.3 Bacillus Sphaericus

Dick et al. (2006) proposed two parameters to be evaluated to support the choice of bacterial strain prior to the addition in concrete, i.e., ζ-potential and ureolytic activity. The former parameter indicates the potential of the bacterial strain cell wall to attract calcium ions, resulting in a higher adhesion of precipitated $CaCO_3$ on the cell surface. A high ureolytic activity results in a vast amount of $CaCO_3$ being precipitated. Based on those parameters, *B. Sphaericus* strains with a very negative ζ-potential and high initial urea degradation are suitable for coherent $CaCO_3$ production [105]. Burbank et al. (2012) compared the ureolytic activity of ten different bacterial strains grown in a nutrient broth (NB) alone and a NB supplemented with 100 mmol $(NH_4)_2SO_4$ (NH4). The urease specific activity of *B. Sphaericus* was similar compared to that of *B. Pasteurii* in a NH4 medium, but outperformed the specific activity in a NB medium since no growth of *B. Pasteurri* was observed [106]. Van Tittelboom et al. (2009) selected *B. Sphaericus* based upon the work done by Dick et al. (2006). In her research, bacterial strains were immobilised in silica gel and brought into the cracks by means of a syringe. The greater part of the sealing of the cracks is related to the crack filling by the silica gel matrix, but the presence of $CaCO_3$ crystals, absent for control specimen, emphasises the microbial activity which may enhance the durability of the repair [13]. It was shown, based on experimental results from light microscopy and water permeability tests, that specimens with melamine based micro-encapsulated *B. Sphaericus* strains (10^9 cells/g microcapsules) had a much higher crack healing ratio (48%-80%) compared to control specimens (18%-50%). Despite the gain in crack healing efficiency, the addition of microcapsules showed a distinct decrease of compressive strength, varying from 22% to 47% [107].

1.4.2 Encapsulating methods

In previous subsection, the application of different bacterial strains to improve self-healing concrete were discussed. In earlier research, crack repair by plugging or injecting of bacteria who have the ability to precipitate $CaCO_3$ was evaluated [13, 84]. Even than, encapsulation of the bacteria was necessary to protect the bacteria from the high pH in concrete to substantially increase their growth and efficiency. More recently, the potential of microbial $CaCO_3$ precipitation after direct introduction in concrete has been evaluated [108]. However, protection of the bacteria is necessary to optimise their microbial metabolic activity which is dramatically influenced by the high pH and dry condition of concrete. Furthermore, the densification of the matrix make bacteria vulnerable to death [67, 83]. Numerous encapsulation techniques have been proposed and analysed for the immobilisation of bacterial spores for their application in cementitious materials [42, 79, 80, 82, 107].

Graphite nano platelets

According to Khaliq and Ehsan (2016), the small size of *Graphite nano platelets* (GNP) assures a uniform distribution throughout the mixture which allow bacteria to become readily available at the crack site. However, GNP are not capable to protect the bacteria from multi axial loading. This means the older the concrete gets, the denser the microstructure and the greater the pressure on the carrier. The bacteria are no longer well protected and the viability decreases for increasing age of the concrete. *Light weight aggregates* (LWA) serve better to provide a lasting high self-healing efficiency [93].

Light weight aggregates

Khaliq and Ehsan (2016) observed that specimens incorporated with *Light weight aggregates* showed a consistent crack healing efficiency for pre-cracking at 3, 7, 14 and 28 days. Maximum crack healing of 0.61 mm was observed in the specimens comprising of LWA, while direct introduction of bacteria showed healing of 0.37 mm [93]. Wiktor and Jonkers (2011) impregnated LWA (expanded clay) with both calcium lactate, yeast extract and a bacterial spore suspension containing endospore-forming *B. alkalinitrilicus* strains. After 100 days of immersion in tap water, cracks up to 0.46 mm were completely healed in bacteria-based specimens compared to 0.18 mm at of the control specimens, proving the effectiveness of the carrier [83]. Zhang et al. (2017) proposed the use of expanded perlite (EP) as a cost effective LWA and compared the crack closure with that of expanded clay (EC). The maximum value for complete crack closure was 0.79 mm and 0.45 mm in respectively EP and EC specimens [78]. However, the decrease in compressive strength which is reported by both Khaliq and Ehsan (2016) and Tziviloglou et al. (2016) might limit the application of LWA as a carrier for bacteria in cementitious materials [110].

Polymeric material

Wang et al. (2014) used a melamine based microcapsule to immobilise the bacterial spores. Yeast extract, urea and calcium nitrate were incorporated together with the microcapsules during mixing. The healing ratio of the specimens with bacteria compared to that of the control specimens was much higher: 48%-80% compared to 18%-50%. After addition of microcapsules of dosage 3% and higher, a significant reduction of the compressive strength of the concrete was observed. Moreover, the combined effect of the addition of nutrients and microcapsules showed an even higher decrease, around 33% to 47%, making this approach not suitable for practical applications [107]. The use of polyurethane for the immobilisation of bacteria has been tested and compared to silica immobilised bacteria by Wang et al. (2012). Despite a higher microbial metabolic activity was exhibited by silica immobilised bacteria, more self-healing efficiency was obtained from specimens with incorporated polyurethane immobilised bacteria. However, the aforementioned immobilised bacteria were incorporated in glass tubes and carefully positioned and glued inside the specimens prior to concrete casting [80]. Thus, the most severe limitation of this approach is the difficulty to meet the repeatability criteria suggested by Li and Herbert (2012) for qualifying the feasibility of a self-healing approach.

Hydrogels

Wang et al. (2014) proposed and discussed the feasibility of using hydrogels as the carrier for the protection of bacterial spores. During synthesis of the hydrogel, the bacterial spores together with nutrients and deposition agents (urea and calcium nitrate) were encapsulated by UV irradiation. Experimental results showed that spores were still viable after encapsulation and that they precipitate $CaCO_3$ in/on the hydrogel matrix. The encapsulation of *B. sphaericus* spores into hydrogels for self-healing is demonstrated to be effective. The maximum crack width that was closed was about 0.5 mm compared to $0 - 0.3$ mm for control specimens. Moreover, the self-healing was evaluated after 4 weeks of incubation under wet-dry cycles (1 hour immersed in water and 11 hours exposed to air) to mimic the application in practical cases [111], which put the feasibility of other self-healing mechanisms in perspective. In another study by Wang et al. (2015), an alginate-based hydrogel was investigated. A good biocompatibility was confirmed based on decomposed urea and precipitation of $CaCO_3$. However, the addition of the alginate-based hydrogel in mortar specimens had a negative effect on its compressive strength, decreasing the strength by 23.4% with addition of 1m% hydrogel relative to the cement mass. By means of an oxygen consumption test, it was validated that hydrogel encapsulated *B. sphaericus* spores became active on the damaged surface while the non-encapsulated spores showed no activity [79]. Despite the reduction of the mechanical properties of cementitious materials after addition of hydrogels, the combined use of hydrogel and microbial $CaCO_3$ for self-healing concrete is promising because of two benefits: (1) the use of hydrogels as a carrier for the protection of bacterial spores has been proven; (2)

the hydrogel serves as a water reservoir, providing water in dry periods to promote spores germination and bacterial activity, and hence, facilitate the precipitation of $CaCO_3$ [111].

1.5 Superabsorbent Polymers

Superabsorbent polymer hydrogels (SAPs) are hydrophilic polymers with a low cross-linking density that are able to absorb, swell and retain aqueous solutions up to hundreds of times their own weight [112–114]. These materials originated as water retention agents in agriculture [115] and were developed in Japan in the mid 1970s in hygienic products such as disposable diapers [116, 117], sanitary napkins and surgical pads [113].

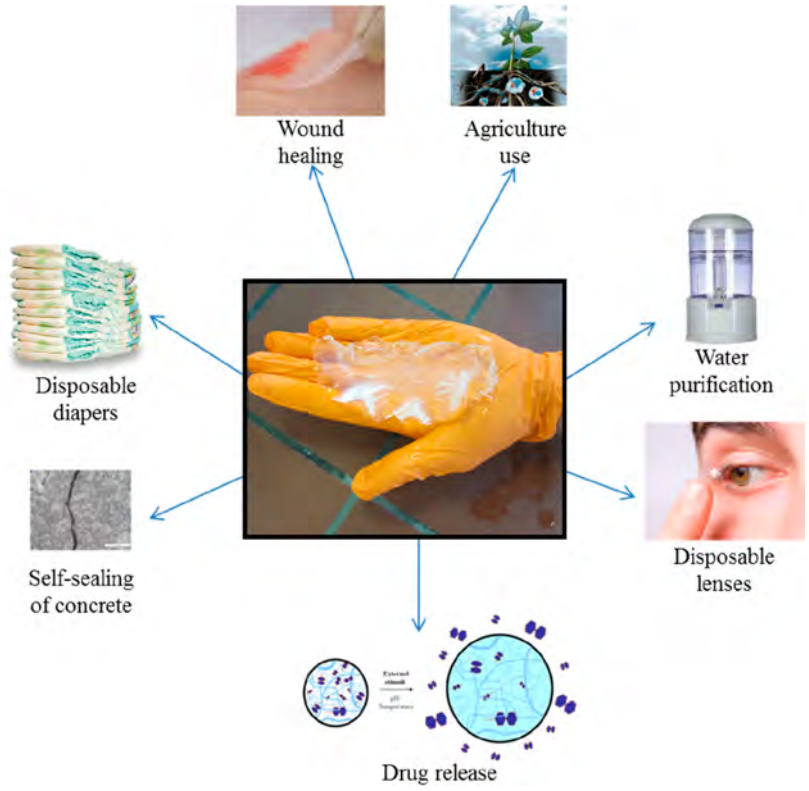

Figure 1.6: Overview of several applications of SAPs including wound healing, agricultural use (e.g., as soil conditioner, nutrient carrier [118] and water reservoir [119]), water purification, disposable lenses, drug release, disposable diapers and self-sealing of concrete [114].

Water absorption in SAP materials relies on a physical process. Physical absorbers imbibe water through changes in their crystal structure, by physically entrapping water via capillary forces and/or by hydration of functional groups. They should not be confused with chemical absorbers, who bind water via chemical reaction converting their entire nature [120].

The swelling of the polymers is related to the affinity of the macromolecules with the aqueous solvent and their elasticity, which is limited by the presence of crosslinks. The equilibrium swelling is controlled by the balance of osmotic forces [121]. The swelling properties of the polymers are also influenced by the presence of charges, obtained by incorporating ionogenic groups to the polymer chains [115].

1.5.1 Classification of SAPs

SAPs can be classified in different categories based on the absence or presence of electrical charges, morphological appearance, mechanism of water absorption either via physical bonds or strong covalent bonds, but most importantly by chemical composition [114, 117].

1.5.1.1 Classification based on electrical charges

There are four different categories based on the presence or absence of electrical charges to which a SAP may belong [120]. (1) non-ionic - polymers with no anionic or cationic moieties; (2) ionic - polymers which possess either anionic or cationic moieties; (3) ampholytic - amphoteric electrolyte containing both acidic and basic groups; (4) zwitter-ionic - containing both anionic and cationic groups in each repeating unit, with a net charge of zero. The majority of commercial SAPs have anionic moieties [117].

1.5.1.2 Classification based on morphological appearance

SAPs can be subdivided in several morphological categories. Depending on the synthesis and the intended application, SAPs are produced in the form of powders, emulsion, fibres [122], granules and membranes [122]. The SAP particle shape has to be preserved after swelling and release. Therefore, the SAP should have sufficient strength to prevent a loosening, mushy or slimy state [117].

1.5.1.3 Classification based on cross-linking

The network stability in swollen state is closely related to the type of cross-linked structure being present. Cross-linking can be achieved through two main pathways, either physically or chemically. On physical cross-linked SAPs, the polymeric chains hold together by physical interactions, such as hydrogen bonds, Van der Waals forces, electrostatic interactions and molecule entanglement. Though, physical cross-linking bonds are reversible and the matrix can be destroyed by modified physical conditions or applied stresses [123]. On the other hand, chemically crosslinked SAPs form irreversible covalent bonds among the polymeric chains [124, 125].

1.5.1.4 Classification based on environmental sensing

The ability of water absorption of SAPs can be promoted by environmental changes. A distinct set of environmental changes influencing the swelling capacity of SAP were studied, including changes in pH of the absorbed medium [126–128], light intensity [127, 129], pressure [127, 130] and temperature [127, 131].

1.5.1.5 Classification based on chemical composition

SAPs are mainly divided according to their chemical composition. Originally, SAPs were divided into two main classes; i.e., synthetic (petrochemical based) and natural (e.g. polysaccharides and polypeptides) SAPs [117]. A third category involves combining a natural polymer with a synthetic polymer and is referred to as semi-synthetic polymers [132, 133]. The most conventional type of SAPs are anionic acrylates made up of a copolymeric network based on acrylic acid (AA) or acrylamide (AM) [117].

1.5.2 Polymerisation techniques to produce SAPs

The majority of SAPs are synthesised through free-radical polymerisation technique [117]. This technique can be performed according different polymerisation methods, i.e. bulk, solution, inverse-suspension and inverse-emulsion [117, 125]. Some additional treatments like drying of the polymer and fine-tuning the SAP morphology are necessary depending on the used method.

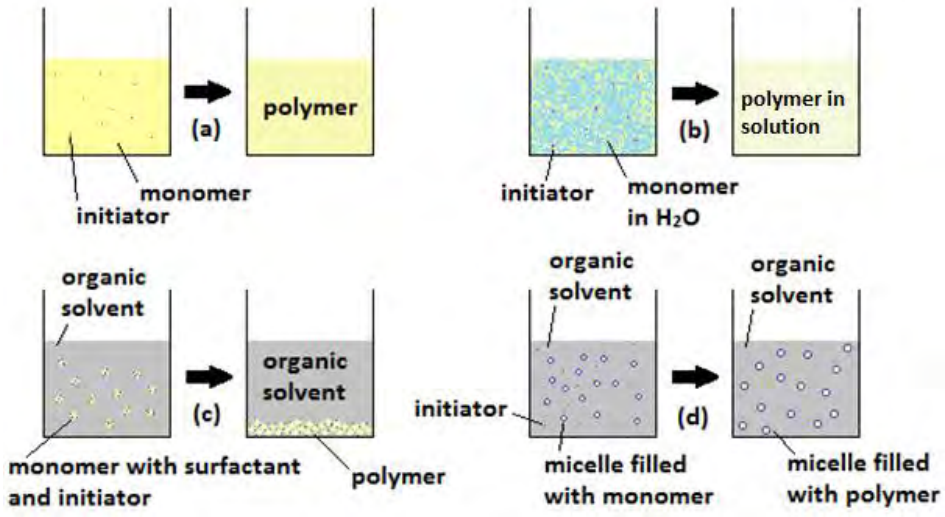

Figure 1.7: Schematic representation of different types of free radical polymerization methods: (a) bulk, (b) solution, (c) inverse, and (d) inverse emulsion polymerisation [134]

Bulk polymerisation

Bulk polymerisation is the most straightforward polymerisation technique, requiring only monomers and a monomer-soluble initiator. Due to a high monomer concentration, a high polymerisation rate is obtained [135]. The structure of polymer chains is easy to control but an additional step of grinding the material is necessary before addition in cement-based materials. The absence of a solvent, restricting this method for liquid monomers only, could be seen as a downside of this technique.

Solution polymerisation

Solution polymerisation makes use of a solvent which requires both monomer and initiator to be soluble. The increased mobility of the monomer compared to bulk polymerisation results in a higher polymerisation degree. Furthermore, the solvent serves as a heat sink to control the significant heat generation during gel formation. A disadvantage of solution polymerisation is the removal of the solvent before obtaining the final state of the polymer [135].

Inverse suspension and inverse emulsion polymerisation

Inverse suspension and inverse emulsion polymerisation are the other two polymerisation methods. They have the advantage that the products are obtained as powder or microspheres (beads), and thus grinding is unnecessary [117]. The monomers and initiator are dispersed in a continuous water-in-oil, hydrophobic phase by mechanical stirring. The viscosity of the monomer solution, stirring speed and dispersant type mainly influence the SAP particle shape and size [113]. Inverse-suspension process has some advantages over solution polymerisation, including a better control of the reaction heat removal and possibilities for adjusting the SAP particle morphology [136]. On the other hand, the solvent and surfactant still need to be removed [135].

1.5.3 Applications of SAPs in cement-based materials

Superabsorbent polymers (SAPs) were introduced as a novel admixture for the prevention of self-desiccation in high-performance concrete [137]. Self-dessiccation is defined by Persson (1998) as "the reduction in internal relative humidity of a sealed system when empty pores are generated". Chemical shrinkage takes place through the matrix at a stage where it has formed a self-supportive skeleton. Moreover, chemical shrinkage is larger than the autogenous [138]. The use of finer cements and a much lower w/b ratio in high-performance concrete led to a significant reduction of the capillary pore diameters, and often resulted in a concrete where the effects of self-desiccation are visible as early-age cracking [138]. A strategy to prevent self-desiccation in hardening cement-based materials is the use of fine SAP particles added as an admixture to conceive as an internal curing agent [38, 137]. Other applications of SAPs inside cement-based materials includes controlling the rheological properties of concrete

[139], reduction of the thermal expansion coefficient [140], reduction of fire-spalling in high-performance concrete [141] and contribution to self-sealing and self-healing [60, 134, 142–144].

For the intended application in concrete, the SAP is required to protect the bacteria from the high alkaline environment and to prevent crushing them in aged concrete specimens [67]. After crack initiation, the SAP absorbs and blocks fluids containing possible harmfully chemicals to further enter the crack during wet periods, while in dry periods they tend to slowly release the fluid and improve the autogenous and autonomous healing [111, 145]. Furthermore, the particle size and shape [146] of the SAPs, initial swelling behaviour during mixing, degradation in the matrix, good strength of the swollen gel [112], compatibility with micro-organisms and swelling upon crack formation are other parameters which are of great importance [62, 114].

1.5.4 Chemical composition of SAPs

The most important classification system applied to SAPs is the classification based on chemical composition. As mentioned in subsection 1.5.1.5 on page 23, SAPs are subdivided in three main distinct categories: natural, synthetic and semi-synthetic SAPs [132, 133].

Synthetic SAPs

Synthetic SAPs contain petrochemical compounds such as acrylic monomers like acrylic acid (AA) and acrylamide (AM), i.e., two of the most often used monomers in the industrial production of SAPs. A number of other monomers are used such as methacrylic acid (MAA), dimethylaminoethyl methacrylate (DMAEMA), dimethylaminopropyl methacrylamide (DMAPMA) and 2-acrylamido-2-methylpropane sulphonic acid (APMS) [60]. Two general pathways can be followed to prepare acrylic SAP networks; either through simultaneous polymerisation and cross-linking by a polyvinylic cross-linker, or cross-linking of a water-soluble prepolymer by a polyfunctional cross-linker [117].

Natural SAPs

Natural polymers are further subdivided in two distinct groups; the polysaccharides and polypeptides (proteins) [117]. Polysaccharides are found and retrieved from biosynthesis in plants and animals. In a new approach, polysaccharides are produced by microbial activity in bacterial hyaluronan, gellan or xanthan [147]. Polysaccharidic superabsorbents received great attention in a number of studies because of their biodegradability, biocompatibility, renewability and non-toxicity [148–151]. Fewer work has been reported on natural SAPs comprising polypeptides (proteins) as the main part of their structure [117].

Even though a variety of natural polymers such as alginate [147, 152–154], chitosan [132, 154–157], agar [158], carrageenan [159], dextrin [160], cellulose [161], starch [162], gellan gum [163] and proteins [164, 165] are used for the basis of natural biopolymers, only a few are selected

as the basis for SAP production in this master's dissertation.

Based on previous research by Mignon et al. (2016) suitable monomers; i.e. monomers that have ionisable functional groups that protonate or deprotonate under environmental changes in pH, are selected as a basis for the SAP production. Those are the polysaccharides alginate and chitosan, and the synthetic compounds, N,N'-dimethylaminoethylmethacrylate (DMAEMA), acrylic acid (AA) and acrylamide (AM). Only polysaccharides and synthetic monomers are selected. Nevertheless, polypeptides like EDTAD-modified soy protein SAPs are reported to also be highly pH sensitive [164, 165].

pH-sensitive SAPs are constructed by incorporating reactive groups in the polymeric backbone, which will form ions at specific pH-ranges, hence repelling or attracting one another depending on their charge. As a consequence, the water absorption capacity will increase or decrease, respectively [126, 137].

1.5.4.1 Alginate

Alginates, mainly obtained from brown algae (*Phaeophyceae*), are linear anionic polysaccharides comprised of (1, 4)-linked α-L-guluronic (GG, pKa of 3.38) and β-D-mannuronic (MM, pKa of 3.65) acid blocks [166, 167]. Alginate has extensively been investigated and used for many biomedical applications, due to its biocompatibility, low toxicity and relatively low cost [166]. The typically extraction method consist of treating brown algae with aqueous alkali solution, typically with NaOH [168]. Next, one of two processing methods is applied to precipitate alginate; either by addition of sodium (*acid precipitation method*) or calcium chloride (*calcium precipitation method*) to the filtrated extract [169]. The chemical composition of seaweed-derived alginate can vary with the source, harvest location, season and part of the seaweed that is used [147], while the chemical structure and physical properties of bacterial biosynthesised alginate can be better controlled [170]. Functional carboxylic acid groups are present in alginate and become negatively charged in aqueous solutions with a pH above the pKa values of the monosaccharide units. The total production of alginate is estimated to be roughly 40000 t per year [147].

1.5.4.2 Chitosan

Chitosan is a polymer obtained by deacetylation, removal of an acetyl group by reaction, of N-acetylamino groups in chitin, a polysaccharide which is a major constituent of the exoskeleton of arthropods (e.g. crabs and shrimps) and the cell walls of fungi. The chemical structure, see figure 1.8 on the next page, is comprised of randomly distributed β-(1-4)-linked D-glucosamine and N-acetyl-D-glucosamine units. Whereas chitin is practically insoluble, chitosan will eventually dissolve after formation of a carboxylate salt, yielding to a viscous solution [155, 157]. Chitosan derived SAPs belongs to the polycationic superabsorbent ma-

terials, who generally have an optimum water uptake capacity at mildly acidic rather than basic pH [157]. This could be explained with chitosan having little or no charge above pH6, i.e, pKa of ∼6.3, limiting its ability to form ionic complexes, and subsequently, reducing its use under physiological conditions [155].

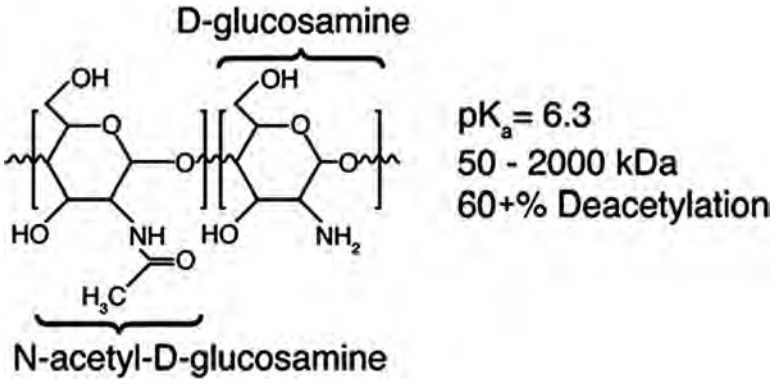

Figure 1.8: Chemical structure of chitosan [155]

1.6 Master's thesis objectives

In previous research, the combined effect of using hydrogel and microbial $CaCO_3$ was recognised as an effective and promosing technique towards an improved self-sealing and self-healing of cementitious materials [79, 111]. Hydrogel encapsulated bacteria perform well on the six robustness criteria proposed by Li and Herbert (2012) [12]. Regarding their shelf life, bacterial spores, a dormant form of the bacteria are added to increase the survival in harsh concrete conditions from several years to hundreds of years [171, 172]. However, to withstand the high alkalinity of cementitious materials and the internal compressive pressure by densification of the microstructure, protection is required [12]. Moreover, nutrients and water favours growth conditions which allow bacterial spores to germinate and form vegetative cells [171, 173]. Thus, the supply of water is essential to obtain a good self-healing since the bacterial activity relies on its availability [111]. Civil infrastructures are exposed to a variety of environment, some continuously wet, others continuously dry and some periodically dry and wet. To minimise the influence of environmental changes, the self-healing approach should be versatile and therefore water retention for self-healing cementitious materials relying on microbial $CaCO_3$ precipitation should be encouraged [12]. Thus, hydrogels are particularly suitable as a carrier for bacterial spores. Swollen particles act like water reservoirs for spore germination and bacterial metabolic activity when cracks appear, and hence promoting the microbial $CaCO_3$ precipitation [111].

To tackle the disadvantage influence on the mechanical properties of cementitious materials after addition of hydrogels, the use of pH-responsive hydrogels was suggested by Mignon

et al. (2016). Those hydrogels are sensitive to the difference in pH-value of the surrounding fluid by forming ions, depending on the pKa-value of the available functional groups on the polymer's backbone, and hence, altering the water uptake capacity of the hydrogel [60]. For the intended use in cementitious materials, the swelling at pH-values around 12.5∼13.0 should be limited whereas it should increase drastically at pH-values around 9, in the vicinity of cracks. Mignon et al. (2016) developed different hydrogels who had a negligible effect on the compressive strength of the cementitious materials, fulfilling the aforementioned criteria [60]. To benefit from the combined effect of hydrogels and microbial $CaCO_3$, the hydrogels should be biocompatible (e.g. low of toxic components), exhibit a strong moisture uptake in the vicinity of cracks to completely block them, promote precipitation of $CaCO_3$ and be non-degradable upon incubation in cementitious materials [60, 62].

The design of the aforementioned self-healing approach involves the investigation into the properties of different pH-responsive hydrogel candidates based on the research performed by Mignon et al. (2016). Furthermore, their influence on the mechanical properties after direct incorporation without bacteria in mortar specimens will be evaluated. Thereafter, the viability of incorporating bacteria spores during free radical polymerisation in solution will be evaluated by decomposition of urea. Next, the two most suitable hydrogel encapsulated bacteria solution are selected and their crack-sealing efficiency is evaluated by water permeability tests. At last, crack closure is measured for the most promising self-healing material.

Chapter 2

Materials and methods

2.1 Overview of applied materials

Acetic acid, Sigma-Aldrich (Bornem, Belgium)

Acetone, Univar (Anderlecht, Belgium)

Acrylamide (AM), Janssen Chimica (Geel, Belgium)

Acrylic acid (AA), Acros Organics (Geel, Belgium)

Ammonium persulfate (APS), Sigma-Aldrich (Bornem, Belgium)

Chitosan (Chi), Sigma-Aldrich (Bornem, Belgium)

Dialysis membranes (Spectra/Por® 4, MWCO 12,000-14,000 Da), Polylab (Antwerp, Belgium)

Dimethylaminoethyl methacrylate (DMAEMA), Sigma-Aldrich (Bornem, Belgium)

Dimethyl sulfoxide (DMSO), Acros Organics (Geel, Belgium)

Hydrochloric acid (HCl), Sigma-Aldrich (Bornem, Belgium) **Methacrylic anhydride** (MAAH), Sigma-Aldrich (Bornem, Belgium)

N,N'-methylene bisacrylamide (MBA), Merck (Nottingham, UK)

Millipore syringe filter (pore size of 0.22 µm), Sigma-Aldrich (Bornem, Belgium)

Paper filters (retention of 8 - 12 µm), VWR filters (Leuven, Belgium)

Paper filters (retention of 12 - 15 µm), VWR filters (Leuven, Belgium)

Sodium hydroxide (NaOH), Sigma-Aldrich (Bornem, Belgium)

Sodium alginate (Alg), Sigma-Aldrich (Bornem, Belgium)

N,N,N',N'-tetramethylethylene-diamine (TEMED), Acros Organics (Geel, Belgium)

All materials were used as supplied, unless stated otherwise.

The reference mortar samples used for both mechanical strength, water flow and crack-closure experiments consisted of CEM I 52.5 N (510 kg/m^3; Holcim, Belgium), CEN-standard silica sand according to EN 196-1 [174] (1530 kg/m^3; Beckum, Germany) and tap water. Next to these reference mortar specimens, specimens including nutrients, hydrogels, bacterial spores or a combination of all three are added on top of the aforementioned components.

2.2 Development and properties of hydrogels

2.2.1 Methacrylation of polysaccharides

2.2.1.1 Modification of alginate with methacrylic anhydride

Alginate or alginic acid is a component found in marine algae, more specifically brown algea (Phaeophyceae), which are known to be linear unbranched polysaccharide that contains the repeating units of 1,4-linked β-*D*-man- nuronic acid and α-*L*-guluronic acid [**?**]. Modification by methacrylic anhydride (MAAH) is a possibility to introduce double bonds on the polysaccharide backbones of the alginate. The modification involves the replacement of the secondary alcohol groups with methacrylate groups on the alginate. The methacrylates incorporated on the polysaccharide backbone enables network formation during polymerisation reaction.

The methacrylated alginate was prepared by reacting 2 m/v sodium alginate dissolved in demineralised water with methacrylic anhydride (MAAH). The solution was stirred using a mechanical stirrer on room temperature for 24 hours. MAAH was added dropwise to the solution. During the reaction, methacrylic acid was released which dropped the pH. The pH was compensated and adjusted to 8 with a 5 M sodium hydroxide (NaOH) solution in order to improve reactivity. After addition of MAAH, the mixture was stirred for 24 hours. Afterwards, dialysis was performed during 72 hours while changing the dialysis water 3 times a day to remove unreacted reagents. The methacrylated or modified alginate was frozen and dried via lyophilisation using a Christ freeze-dryer alpha 2-4-LSC at −85 °C and 0.37 mbar. In what follows, the term modified alginate (algMOD) is preferred to refer to the methacrylated alginate.

2.2.1.2 Modification of chitosan with methacrylic anhydride

Similar to alginate, chitosan was modified by methacrylic anhydride (MAAH) to introduce double bonds on the polysaccharide backbones, enabling the possibility to form strong covalent bonds during cross-linking of the modified polysaccharide with acrylic monomers [60]. The method is described by Devisscher (2015) [134].

The methacrylated chitosan was prepared in a round-bottom flask containing an aqueous solution of 2 m/v acetic acid. Chitosan was dissolved under mechanical stirring on room

temperature. Acetic acid was added in order to make chitosan more soluble by protonating the amine ($-NH_2$) functionalities to $-NH_3^+$ on the chitosan backbone. After dissolving, the pH was adjusted to 5 by adding a 5 M sodium hydroxide (NaOH) solution and kept constant during addition of MAAH. 0.8 equivalents MAAH, with respect to the amine functionalities of chitosan, were added dropwise in the solution whitin a timespan of 3 hours. The mass MAAH per g chitosan amounts to 0.589 g. After termination, the dialysis was performed during 72 hours while changing the dialysis water 3 times a day to remove unreacted reagents. Subsequently, the methacrylated or modified chitosan was frozen and dried via lyophilisation. Hereinafter, the term methacrylated chitosan is referred to as modified chitosan (chiMOD).

2.2.2 Synthesis of hydrogels

2.2.2.1 Synthesis of poly(algMOD_AA/AM) hydrogel

A three-neck flask filled with Milli-Q water was kept at a constant temperature of 50 °C using an oil bath while constantly stirring by a magnetic stirring bar. Modified alginate (algMOD; 1 m/v%) was dissolved in the aqueous solution and subsequently, acrylic monomers (acrylic acid (AA) and acrylamide (AM); 7 m/v% in total) were added in two different molar ratios, namely 100/0 and 75/25 [mol%/mol%]. The activator TEMED was supplied to the solution in the same volume as the theoretically necessary volume of APS (density of 1.98 g/cm^3; 0.16 m/v%). An overview of the hydrogel compositions is given in table 2.1. After the addition of TEMED, the three-neck flask was closed from the atmosphere. The closed system was emptied by a vacuum pump in a cycle consisting of three minutes under vacuum followed by a supply of nitrogen gas (N_2) from a balloon. This cycle was repeated for three times while simultaneously preparing a 10 m% solution of the radical initiator APS in Milli-Q water. Next, the dissolved APS, which is sensitive to the presence of oxygen, was added through a septum by means of a syringe to the closed nitrogen environment, followed by repeating one more flushing cycle to remove the oxygen that may be injected through the septum as well. Thirty minutes after addition of APS, gelation was noticed. The mixture was left stirring under a nitrogen atmosphere for 24 hours, after which dialysis was performed during another 24 hours. Finally, the material was filtered, frozen, dried via lyophilisation and grinded to fine particles.

Table 2.1: poly(algMOD_AA/AM) hydrogel composition

Solvent	*Temperature* [°C]	*AlgMOD* [m/v%]	*AA+AM* [m/v%]	*AA/AM* [mol%/mol%]	*TEMED* [v/v%]	*APS* [m/v%]
H_2O	50	1	7	100/0	$8.08e^{-2}$	0.16
H_2O	50	1	7	75/25	$8.08e^{-2}$	0.16

2.2.2.2 Synthesis of poly(chiMOD_DMAEMA) hydrogel

A three-neck flask was filled with an 6 v% aqueous acetic acid AcOH solution while stirring by a magnetic stirring bar at constant temperature of 35 °C. Modified chitosan (chiMOD; 2 m/v%) was dissolved in the 6 v% aqueous AcOH solution and subsequently, the acrylic monomer DMAEMA (density of 0.933 g/cm^3; 14 m/v%) and the activator TEMED (0.96 v/v%) were added. Next, a nitrogen atmosphere was set up by emptying the sealed flask three times for three minutes by means of a vacuum pump, each time alternated by a supply of nitrogen gas by means of a N_2-filled balloon. Simultaneously, a 10 m% solution of the radical initiator APS (0.64 m/v%) in Milli-Q water was prepared. This solution was added through a septum by means of a syringe to the closed nitrogen environment, followed by repeating one more flushing cycle. After a few minutes, polymerisation was noticed and finally stirring stopped because of complete gelation. The mixture was kept at temperature and under a nitrogen atmosphere for 24 hours. Afterwards, the hydrogel was removed from the flask, cut in small pieces and added to a dialysis bath consisting of Milli-Q water for another 24 hours. After freezing, drying by lyophilisation and grinding, the final hydrogel powder is obtained.

Table 2.2: poly(chiMOD_DMAEMA) hydrogel composition

Solvent	*Temperature* [°C]	*ChiMOD* [m/v%]	*DMAEMA* [m/v%]	*TEMED* [v/v%]	*APS* [m/v%]
6 v% aq. AcOH	35	2	14	0.96	0.64

2.2.2.3 Synthesis of poly(MBA_DMAEMA) hydrogel

2-(dimethylamino)ethyl methacrylate (DMAEMA; 0.933 g/ml; 157.21 g/mol) was cross-linked with N,N'-methylene bisacrylamide (MBA; 1.235 g/cm^3; 154.17 g/mol) in a molar fraction of 2 mol% as a function of added DMAEMA. The polymerisation was performed in a three-neck flask filled with Milli-Q water (250 g of monomers and cross-linker/L) at constant temperature of 45 °C under nitrogen (N_2) atmosphere. First, the monomer DMAEMA and cross-linker MBA were added to the aqueous solution, followed by the addition of TEMED (1/1 vol% with respect to APS). Subsequently, the flask was closed from its surrounding environment and flushed three times for three minutes by a vacuum pump, alternated by a supply of nitrogen gas by means of a N_2-filled balloon. Meanwhile, an APS solution (10 m/v%) was prepared and the tenfold of the required dry mass of APS (1.98 g/cm^3; 228.18 g/mol; 1.4 mol% as a function of added DMAEMA) was injected in the closed environment through a septum by means of a syringe. The system was flushed one more time to avoid inhibition of oxygen. The mixture was kept at temperature of 45 °C and under a nitrogen atmosphere for 24 hours. Finally, the hydrogel was removed from the flask, cut in small pieces and added to a dialysis

bath for another 24 hours, frozen, dried via lyophilisation and grinded, before obtaining the final hydrogel powder.

Table 2.3: poly(MBA_DMAEMA) hydrogel composition

Solvent	*Temperature* [°C]	*MBA+DMAEMA* [m/v%]	*MBA/DMAEMA* [mol%/mol%]	*TEMED* [v/v%]	*APS* [m/v%]
H_2O	45	25	98.04/1.96	0.252	0.499

2.2.2.4 Encapsulation of bacteria

The spores of *B. sphaericus* were resuspended in a 8.5 g/l NaCl saline solution. Before addition to the free radical polymerisation in solution, the culture was centrifuged for 8 min at 7000 RPM to harvest the spores. The spores were washed once with sterile Milli-Q water. The final spores were suspended in sterile Milli-Q water to make a total volume equal to the original saline solution.

The spores were added to the solution after the three initial flushing cycles in the aforementioned synthesis methods. For each gram hydrogel, 0.5 ml of a bacterial culture suspended in Milli-Q water (10^9 cells/ml) was added to the solution. After addition, the flask was flushed for 30 seconds before adding the radical initiator APS.

2.2.3 Characterisation of hydrogels

2.2.3.1 Gel fraction

Before dialysis of synthesised hydrogel, a sample was taken and freeze dried. The sample consisted of 3 small particles of about 1 cm^3. The dry product of those 3 particles was weighted and unreacted particles out of the synthesis were removed via dialyses in approximate 40 mL for 24 hours. After dialysis, the sample was freeze dried and the dry weights were measured again. The gel fraction is expressed as the ratio of the dry weight before and after removal of unreacted particles [60].

$$G\,(\%) = W/W_0 \cdot 100\% \tag{2.1}$$

2.2.3.2 Freeze drying

The hydrogel was freeze-dried, i.e., process of lyophilisation, using a Christ freeze-dryer alpha 2-4-LSC at −85 °C and 0.37 mbar.

2.2.3.3 Swelling test

The swelling capacity (S) of the hydrogels were measured using a backwards method. In 100 g Milli-Q water, 0.2 g of grinded hydrogel powder was added. After 24 h, the sample was filtered through a pre-saturated filter in which the swollen hydrogel particles were gathered, whereas the filtered liquid (m_f) was collected into a cup of known weight. By subtracting the filtered liquid from the initial added Milli-Q water (m_0), the swelling capacity per unit weight can be calculated. Each measurement was performed in triplicate.

$$S\,(\%) = \frac{(m_0 - m_f)}{m_{hydrogel}} \cdot 100\% \tag{2.2}$$

Aqueous solution with varying pH

The swelling capacity has been tested under aqueous solutions of different pH. NaOH or HCl were added to the aqueous solution in order to obtain respectively an acidic and alkaline environment. For the intended application in cementitious materials, hydrogel behaviour in an alkaline environment is of great importance, hence, the swelling capacity in a pH range from 8-13 was the primary region of interest.

Cement filtrate solution

Furthermore, the swelling capacity was also tested in a cement slurry filtrate. Ordinary Portland Cement (CEM I 52.5 N, 10 m/v%) was added to Milli-Q water. The mixture was stirred for three hours with a mechanical stirrer, followed by filtration to remove the solid cement particles. The resulting cement filtrate (CF) solution had a pH of 12.6.

2.2.3.4 Degree of substitution calculation for algMOD

To determine the efficiency of the modification of alginate, the methacrylated polysaccharide was analysed by nuclear magnetic resonance ^{1}H NMR spectroscopy. A sample was sent to Hasselt University to analyse the spectrum of algMOD. To calculate the degree of substitution, the characteristic peaks of the methacrylate group at 5.73 (H_b) and 6.16 (H_a) ppm, belonging to the vinyl protons were compared with the characteristic peak of alginate at 4.97 (H_G) ppm. This peak corresponds to the proton on the anomeric carbon, i.e. stereocenter of a cyclic carbohydrate [175], of the α-L-guluronate (G) blocks. The G-block content can be calculated by comparing the peak at 4.97 ppm with the peak of the proton on the anomeric carbon of the β-D-mannuronate (M) block at 4.58 (H_M) ppm using equation 2.3.

$$[G]\,(\%) = \frac{H_G}{H_M + H_G} = \frac{I_{4.97\,ppm}}{I_{4.58ppm} + I_{4.97\,ppm}} \cdot 100\% \tag{2.3}$$

Once the G-block content is calculated, the degree of substitution (DS) is determined. A correction factor 1/2 is added because each G-block has two hydroxyl groups.

$$DS\,(\%) = [G] \cdot \frac{H_a + H_b}{4 \cdot H_G} = \frac{I_{5.73\,ppm} + I_{6.16\,ppm}}{4 \cdot I_{4.97\,ppm}} \tag{2.4}$$

2.2.3.5 Structure confirmation via ATR-IR spectroscopy

The hydrogel powder was characterised by attenuated total reflectance Fourier transform infrared (ATR-IR) spectroscopy. The setup consisted of a PerkinElmer Frontier FT-IR (midIR) combined with a MKII Golden Gate set-up with a diamond crystal from Specac. An infrared beam is reflected on the surface of the material and the change of the internally reflected infrared beam is measured by a detector. To be more precise, the internal reflectance creates an evanescent wave, which penetrates the sample within a range of $0.5 - 5\,\mu m$ and whose energy gets absorbed by the sample. The attenuated energy of the evanescent wave is then passed to the infrared beam, which is measured by the detector in the IR spectrometer. The method is recognised as a reliable fingerprinting technique [**?**]. The spectra were measured within a wavenumber window between 4000 and 600 cm^{-1}. The sample wass firmly clamped against the ATR crystal and a background scan wass performed to avoid interference of trapped air. After each sample, the crystal was cleaned with ethanol. The results were analysed with the PerkinElmer Spectrum Analysis software. ATR-IR spectroscopy was used as a tool to characterise the hydrogels and to perform a degradation study on the long-term submersion of the hydrogel in physiological Milli-Q and cement filtrate solution.

2.2.4 Influence of hydrogel incorporation on mortar strength

2.2.4.1 Preparing mortar specimens

Mortar specimens were made out of the materials listed in section 2.1 on page 29 using a standard mortar mixer. The mechanical properties of cementitious materials was influenced by the addition of hydrogels. For each hydrogel, mortar specimens were made containing 0.5, 1.0 and 2.0 m% hydrogel relative to the mass of cement. One reference specimen was made without any addition. The mortar specimens were made according a standard mortar mixing procedure, as described in EN 196-1. To start with, the mixing bowl was cleaned with tap water and dried until the wall felt slightly wet. Next, 450 g Portland cement and the required amount of hydrogel (0.5, 1.0 or 2.0 m% hydrogel relative to the mass of cement; 2.25, 4.5 or 9.0 g respectively) were added to the mixing bowl. The hydrogel was mixed in the cement by the beater for 30 seconds. Then, 225 ml tap water (W/C = 0.5) was added to the dry mixture and mixed at 140 rpm for 30 s. Subsequently, 1350 g sand was added to the mixer by a filling hopper installed on top of apparatus while mixing continued for another 30 s. The mixer was brought to 285 rpm and mixing was stopped after another 30 s. A spatula was used to scrape off the mixture from the bowl's edge during for 30 s and was followed by a resting

period of 60 s. Finally, the mixing was continued for another 60 s at 285 rpm. The samples were then molded ($160 \times 40 \times 40\,mm^3$) and stored in a climate room with a relative humidity of $95 \pm 5\%$ and a temperature of $20 \pm 2\,°C$ for 28 days. However, the samples were removed from the mold after 24 hours, unless otherwise specified.

2.2.4.2 Measurement of flexural and compressive strength of specimens

After a total curing time of 28 days, the mechanical properties, i.e., flexural and compressive strength, were determined by means of a three-point-bending test followed by a compression test on both sides of the broken sample. Consequently, the flexural strength was measured in triplicate, whereas the compressive strength was measured in sextuple. The mechanical performance tests were carried out with a servo-hydraulic testing machine Walter + Bai ag. The test was run and saved using Proteus® 10.1 test program "CEM 250/15kN" conforming standard EN 196. The flexural strength was tested at incrementing force of 0.05 kN/s, whereas the compressive strength was tested at an incrementing force of 2.4 kN/s.

2.3 Production and properties of *B. sphaericus*

2.3.1 Germination of spores

The spores of *B. sphaericus* were added to a growth medium containing yeast extract (20 g/l) and urea (20 g/l). Before addition, the growth medium was autoclaved and during the process of autoclaving, about 1 g/l urea was decomposed, leading to the formation of 0.6 g/l $NH_4{}^+$. By consequence, the pH of the medium was increased to 9∼9.2. The solution was kept on a stirring table at 27 °C.

2.3.2 Cultivation of *Bacillus sphaericus*

Bacillus sphaericus used in this study were grown aseptically under batch cultivation conditions. All media used to cultivate the bacteria were sterilised by autoclaving at 120 °C for 20 min, unless stated otherwise. The morphology of the bacterial cells were observed under an upright light microscope (ZEISS Axioskop2 Plus). The formation of spores was observed through phase-contrast microscopy, therefore a special lens (ZEISS) was used. The cultivation of vegetative cells of *Bacillus sphaericus* LMG 22557 (Belgian Coordinated Collection of Microorganisms, Ghent) was done according the method described by Wang (2013). The cultivation took place in a growth medium containing yeast extract and urea. The yeast extract medium was autoclaved and since this could not be done for the urea solution, it was subjected to a filter sterilisation process through a sterile 0.22 µm Millipore filter. The concentration of both the yeast extract and the urea solution was 20 g/L. The pH of the medium was 7. The bacterial cultures were incubated at 28 °C with vigorous shaking at 100 rpm for 24 hours.

In order to cultivate spores of *B. sphaericus*, vegetative cells were added to a MBS liquid medium [176]: $MgSO_4 \cdot 7\,H_2O$ (0.3 g/l), $MnSO_4$ (0.02 g/l), $Fe_2(SO_4)_3$ (0.02 g/l), $ZnSO_4 \cdot 7\,H_2O$ (0.02 g/l), $CaCl_2$ (0.2 g/l), Tryptose (10 g/l), Yeast extract (2 g/l). Kalfon et al. (1984) stated that *B. sphaericus* sporulates only poorly in common media. The pH of the medium was adjusted to 7.4 with 1M HCl or NaOH. The cultures were incubated at 28 °C with vigorous shaking at 100 rpm for 14∼28 days till sporulation was finished for more than 90% of the vegetative cells. The spores were then harvested by centrifuging the culture medium at 7000 rpm for 7 min (Eppendorf, Centrifuge 5430, Hamburg, Germany). The centrifuged spores were resuspended in a sterile saline solution (NaCL, 8.5 g/L) [62]. In this master's dissertation, the spores were cultivated by my counsellor Wang (2013).

Before addition in mortar specimens and before encapsulation of the bacterial spores inside the hydrogels, the spores were harvested by centrifugation at 7000 rpm for 7 min and resuspended in a equal amount of Milli-Q water.

2.3.3 Leakage of spores from hydrogel

After encapsulating spores of *B. sphaericus*, the amount of spores coming out of the hydrogel during mortar mixing according EN 196-1 [177] was approached by a leakage test. The entire setup was handled in a sterile environment. Of the non-sterile dry hydrogel powder, 0.20 g was weighed and added inside a falcon tube containing 20 ml of an autoclaved physiological solution (8.5 g/l NaCL). Immediately after addition, the falcon tube containing the hydrogel powder was shaken for 2 min using a Vortex-Genie®[178] on speed 6.5 to mimic the mixing procedure during mortar mixing which according EN 196-1 [177] last 2 min as well. The falcon tube was stored at room temperature. At 5 min, 1 day and 3 days, samples were taken out of the falcon tube to analyse the amount of spores leaked from the hydrogel powder.

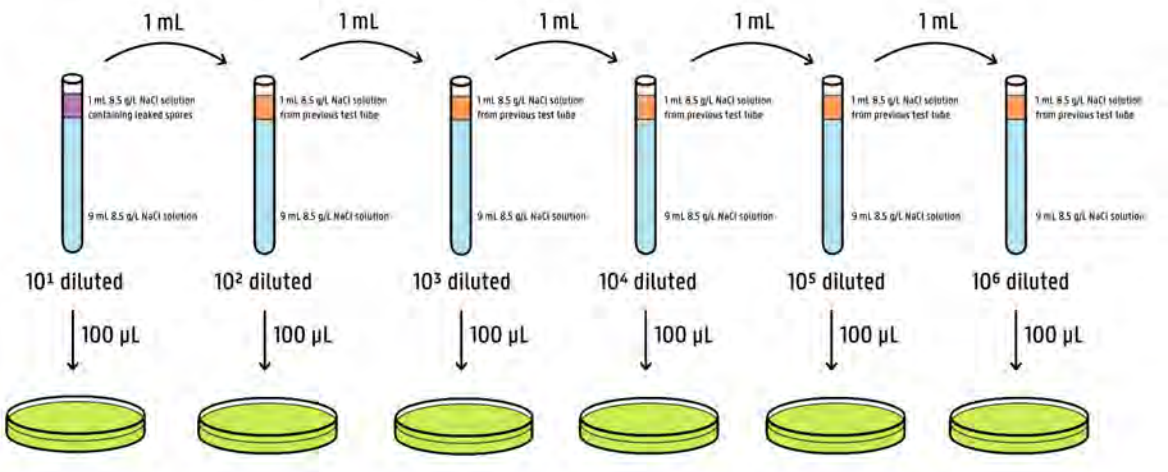

Figure 2.1: Preparing of agar plates with diluted spore solution [144]

Before analyses, 6 glass test tubes were filled with 9 ml of autoclaved physiological solution (8.5 g/l NaCL). The falcon tube was shaken for 5 s and 1 ml of the suspension was transferred to the first out of 6 tubes after the swollen hydrogel powder settled down. After shaking the first test tube for 5 s, 1 ml of the tube was transferred to the second test tube using a sterile syringe. This operation was repeated 6 times in total, creating 6 dilutions. Starting from the last and least concentrated dilution (10^{-6}), 100 µl was taken from the test tube and spread homogeneously on an agar plate (pH 9) using a Drigalski spatula. The operation was repeated for the dilution series of 10^{-2} to 10^{-6}. The 5 agar plates were stored upside down in an incubator held at 20 °C. After 48 hours, unless otherwise specified, the colonies formed on the agar plates were counted and the amount of spores leaked out could be calculated and is expressed as the leakage ratio (LR).

2.3.4 Ureolytic activity

The ureolytic or urease activity of *B. sphaericus* is used as an indicator of the possible microbial $CaCO_3$ precipitation. The total ammonium nitrogen method (TAN method) directly relates the ureolytic activity with the amount of $CaCO_3$ that can be formed. Ureolytic activity is measured in $\mathrm{mM\,min^{-1}}$. The total amount of urea decomposed is measured using the total ammonium nitrogen (TAN) method. As mentioned in section 1.5 on page 16, one mole urea produces 2 moles $NH_4{}^+$ and 1 mole $CO_3{}^{2-}$. Thus the amount of $NH_4{}^+$ indicates the amount of urea decomposed and the possible amount of $CaCO_3$ that could be formed microbiologically. The TAN concentration is measured colorimetrically (Biochrom WPA Lightwave UV/Visible Spectrophotometer at 425 nm) by the method of Nessler, i.e., addition of two chemicals (Nessler A and Nessler B), which are added to the solution, producing a colour shift depending on the amount of $NH_4{}^+$ [179].

$$\text{Specific ureolytic activity at } t_n = \frac{\text{Urea decomposed at } t_n}{Abs_{610} \text{ at } t_n} \tag{2.5}$$

The ureolytic activity of bacteria encapsulated in hydrogels was tested using the TAN method. The hydrogels contained 0.5 ml/g of a bacterial culture consisting of around 10^9 cells/ml suspended in Milli-Q water. The tests were performed in the "Laboratory for Microbial Ecology and Technology" (LabMET) of Ghent University.

The hydrogel (i.e. swollen hydrogel particles before/after dialysis, hydrogel chunks after lyophilisation and hydrogel powders) was added to 200 ml of a growth medium contained in an erlenmeyer flask in order to germinate spores (see section 2.3.1 on page 36). After 5 and 10 days, unless otherwise specified, the decomposed urea was measured. Of the solution, a small amount (∼1 ml) was withdrawn by a syringe equipped by a Millipore filter of pore size 0.22 µm and added to a test tube. Of this test tube, 25 µl or 50 µl was transferred to a flask which was then filled to 50 µl, respectively for samples containing bacteria or reference

samples. Thus, the dilution is 2000 or 1000 times, respectively. Next, 1 ml of Nessler A and 1 ml of Nessler B were added to the flasks which were sealed afterwards by Parafilm M. After shaking, the solution was left undisturbed for 10 minutes while the chemical reactions took place. Subsequently, approximately 3 ml of the solution was transferred to a cell that was inserted in the Biochron WPA lightwave II spectrophotometer [180]. This apparatus can measure the concentration of nitrogen, present in ammonium, based on the colour of the solution. The amount of urea decomposed in the original growth medium can be calculated based on the concentration of nitrogen (c_N) and the dilution (ω) of the solution.

$$A_{CO(NH_2)_2} = \frac{60 \cdot c_N \cdot 10^{-3}}{2 \cdot 14} \cdot \omega \tag{2.6}$$

Herein, $A_{CO(NH_2)_2}$ represents the amount of urea decomposed (g/L). The original growth medium contained 20 g/l urea. As stated in section 2.3.1 on page 36, a small amount of urea was decomposed prior to the addition of hydrogels, meaning the maximum amount of urea decomposed was 18 g/l [62].

2.4 Performance measurement of self-healing capacity

No standard methodology to evaluate the self-healing capacity of concrete has been designed until now. Different approaches toward the evaluation of the healing efficiency are used by each research group [51]. The test procedures to evaluate the healing efficiency can be divided into two groups. The tests are related to durability and focus on the measurement of crack closure, permeability and porosity changes, whereas a second group of evaluation methods is related to mechanical strength, usually comparing the load capacity recovery or the recovery of stiffness. In this master's dissertation, water flow tests and crack closure measurements were performed. They relate to the first group of evaluation methods.

2.4.1 Sealing efficiency evaluation of mortar specimens via water flow test

The sealing efficiency was evaluated by means of a water flow test, which gives an indication of the water permeability through the crack. In figure 2.2 on the following page, the time schedule used for the water flow experiment is presented.

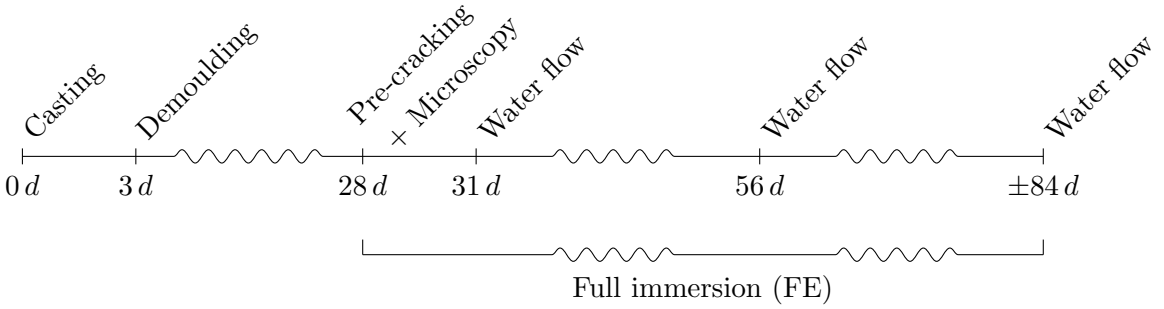

Figure 2.2: Timeline regarding the water flow measurements

2.4.1.1 Preparation of mortar specimens

Mortar specimens with dimensions $160 \times 40 \times 40$ were made in plastic moulds. For each series as listed in table 2.4 on the next page, samples were made in triplex. The preparation method confirms to both the method described in section 2.2.4.1 on page 35 and section 2.4.2.1 on page 42. The mould was provided with a notch to control pre-cracking and was pierced by two smooth copper bars ($\varnothing = 2\,\text{mm}$) and one smooth steel bar ($\varnothing = 5\,\text{mm}$). The latter was removed after demoulding the specimens, leaving a cavity behind at the location of the bar. One end of this cavity was closed by inserting a metal screw which was sealed by gluing with X60, a 2-component fast curing adhesive consisting of a liquid component (B) and a powder (component A) (Hottinger Baldwin Messtechnik HBM; Germany). On the other side of the cavity, a push-to-connect fitting was glued.

Table 2.4: Composition of mortar specimens for water flow evaluation

Type	*Cement* [g]	*Sand* [g]	*Water* [g]	*YE* [g]	*Urea* [g]	*Ca-nitrate* [g]	*S* [ml]	*H* [g]	*HS* [g]
R	450	1350	225	0	0	0	0	0	0
N	450	1350	225	3.84	18	36	0	0	0
N+S	450	1350	225	3.84	18	36	4.5	0	0
N+CD	450	1350	225	3.84	18	36	0	4.5	0
N+CD+S	450	1350	225	3.84	18	36	4.5	4.5	0
N+CDS	450	1350	225	3.84	18	36	0	0	4.5
N+AA	450	1350	225	3.84	18	36	0	4.5	0
N+AA+S	450	1350	225	3.84	18	36	4.5	4.5	0
N+AAS3H	450	1350	225	3.84	18	36	0	0	4.5
N+AAS20H	450	1350	225	3.84	18	36	0	0	4.5

2.4.1.2 Pre-cracking of mortar specimens

The mould was provided with a notch in the bottom centre of the specimen to promote cracking at that location. A displacement sensor was fitted into a holder which was glued at the side of the sample 15 mm above the bottom face. It was pressed against an L-shape metal plate, which was also glued to the specimen and tightly fixed with a plastic screw. The sensor was connected to Proteus® 10.1, which was also in control of the servo-hydraulic testing machine Walter + Bai ag used to pre-crack the specimen. A displacement-controlled test program was used to make cracks varying between 150 and 223 µm. Thereafter, the plastic holder and L-shaped metal plate were removed. Lastly, the specimens were stored in a container filled with 7 l demineralised water.

2.4.1.3 Evaluation of sealing efficiency using water flow test

The timeline for testing is shown in figure 2.2 on the preceding page. After pre-cracking, the initial width of the crack at the bottom face and 15 mm above it at the side were measured using optical microscopy.

A water flow test involves the measurement of the mass of leaked water out of the specimen when subjected to a constant pressure head of 0.5 mH_2O for 5 minutes. As such, the leaked water through the crack is registered in function of time. Water leaking from other locations

on the specimen are dipped dry to prevent interference of the results.

$$WF_x\,(g/min) = \frac{W_{x,j+1} - W_{x,j}}{\Delta t}\,(j = 1 \ldots m) \tag{2.7}$$

$$WF_{x,avg} = \frac{1}{m} \cdot \sum_{j=1}^{m} WF_{x,j} \tag{2.8}$$

Wherein x equals to 3 d, 28 d or final (f). The parameter m equals to the amount of measuring points. Finally, the sealing efficiency (SE) was calculated according equation 2.9.

$$SE\,(\%) = \frac{WF_{3\,\mathrm{d},avg} - WF_{f,avg}}{WF_{3\,\mathrm{d},avg}} \tag{2.9}$$

2.4.2 Crack closure evaluation by optical microscopy

Crack closure for mortar specimens was evaluated under optical microscopy. In figure 2.3, the time schedule used for the crack closure experiment is presented.

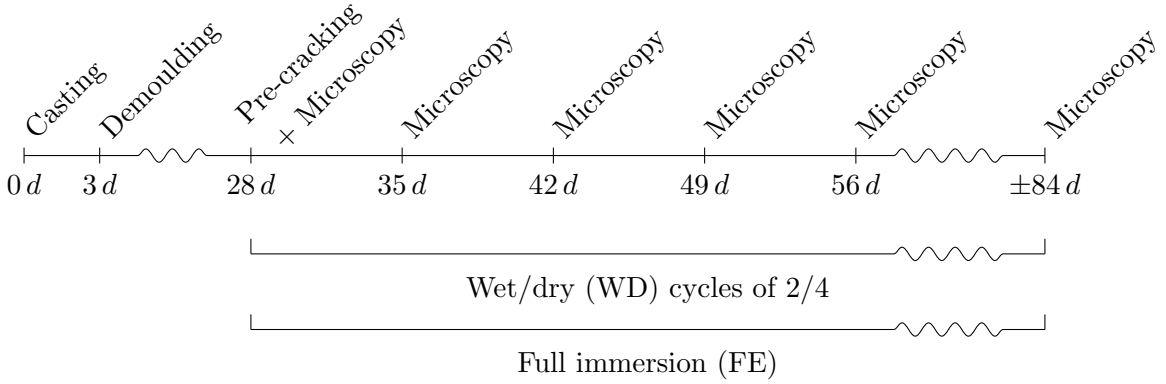

Figure 2.3: Timeline regarding the crack-closure measurements

2.4.2.1 Preparation of mortar specimens

Long mortar prisms with dimensions 360 × 30 × 30 mm were made according to the composition listed in table 2.5 on the next page. Of each composition, two long mortar prisms were made. The reference specimen (R) did not contain any additives, whereas the other specimens contain nutrients (yeast extract (YE), urea and Ca-nitrate ($Ca(NO_3)_2 \cdot 4\,H_2O$)) required for bio-precipitation in addition to non-encapsulated spores (N+S), non-encapsulated spores and a hydrogel (N+AA+S/N+CD+S), encapsulated spores (N+AAS3H/N+AAS20H/N+CDS) or none of these (N). The nutrients were dissolved in the required amount of tap water (W/C = 0.5; taking into account the amount of H_2O present in the nutrients) prior to the addition to the mortar mixer as described in subsection 2.2.4.1 on page 35. The required amount of

hydrogel added to the specimens is 1 m% relative to the mass of the cement. The specimens were cast in an oiled wooden mould protruded by a steel reinforcement bar ($\varnothing$= 6 mm) at the centroid.

Table 2.5: Composition of mortar specimens for crack closure evaluation

Type	*Cement* [g]	*Sand* [g]	*Water* [g]	*YE* [g]	*Urea* [g]	*Ca-nitrate* [g]	*S* [ml]	*H* [g]	*HS* [g]
R	450	1350	225	0	0	0	0	0	0
N	450	1350	225	3.84	18	36	0	0	0
N+S	450	1350	225	3.84	18	36	4.5	0	0
N+CD	450	1350	225	3.84	18	36	0	4.5	0
N+CD+S	450	1350	225	3.84	18	36	4.5	4.5	0
N+CDS	450	1350	225	3.84	18	36	0	0	4.5

2.4.2.2 Pre-cracking of mortar specimens

After curing for 28 days in a climate room ($95 \pm 5\%$ RH; $20 \pm 2\,^{\circ}$C), the specimens were pre-cracked. The protruding reinforcement bars were subjected to a tensile test (Amsler. 100, SZDU 230, Switzerland) under stroke control of a uniaxial load at speed of 0.01 mm/s. The loading was terminated when the load ($\pm$15 kN) remained stable over a stroke of length δ as determined by equation 2.10, in which b is the required average crack width (250 µm), n the number of cracks observed during loading, σ is the average yield strength of the reinforcement steel equal to 560 MPa, E is the Young's modulus of the reinforcement steel equal to 210 GPa, and L is the distance between the two clamps, installed at 50 mm from the prism edge [62].

$$\delta = b \cdot n + \frac{\sigma}{E} \cdot L = 0.25\,\text{mm} \cdot n + 1.23\,\text{mm} \tag{2.10}$$

$$L = L_{prism} + 2 \cdot d = 360 + 2 \cdot 50 = 460\,\text{mm} \tag{2.11}$$

After pre-cracking, the specimen was removed from the apparatus and the protruding steel bar was cut off. To prevent corrosion, an aluminium tape was used to cover the remaining visible reinforcement bar.

2.4.2.3 Preservation of mortar specimens

For the crack closure evaluation, two preservation methods were proposed. One involves full immersion of the mortar specimens in a container filled with 7 l demineralised water, whereas the second preservation method involves the exposure of the mortar specimens to a cycle

of 2 hours immersion in demineralised water alternated with a 4 hour period exposed to an environment of RH equal to 60%.

The test set-up of the wet-dry cycles consisted of two containers, connected via a pumping system. Periodically pumps were activated for 15 minutes to transfer the demineralised water from one to the other. In one of the containers, the long mortar prism was stored. To prevent the bottom face of the specimen to be in contact with a small amount of water that could not be removed by the pumps, the specimen is lifted up by a small inert element, e.g. plastic tube or aluminium profile.

Figure 2.4: Test set-up of the wet-dry cycles

2.4.2.4 Evaluation of crack closure by microscopy

The cracks were visualised using an optical microscope (Leica S8 APO, DFC295 camera). Each face of the sample was labeled (A, B, C and D) and subsequently, four cracks at each face were numbered from 1 to 4. For every labelled crack, five locations were selected and indicated by means of a pencil. At those locations, an image was taken at an optical zoom of 40x. At two locations on each image, the crack width was measured using Fiji (also called ImageJ), an image processing package which facilitated the crack measurements (see Appendix A on page 110 for futher information). In figure 2.3 on page 42, the six moments at which crack closure measurements were evaluated, are indicated. In total, approximately 11520 cracks were measured. The healing ratio (HR) was calculated for each crack measurement according the following equation.

$$HR\,(\%) = \frac{w_i - w_x}{w_i} \cdot 100 \tag{2.12}$$

Wherein w_i is the initial crack width after pre-cracking and w_x is the crack width after x days.

Chapter 3

Development and implementation of pH responsive hydrogels in mortar

3.1 Development and characterisation of hydrogels

The aim of this research is to find a suitable hydrogel for encapsulation of bacterial spores for the application in mortar, while limiting the detrimental effect on the mechanical properties of the mortar and improving the self-sealing and self-healing abilities of the cementitious material.

The present part of this chapter reports the development and characterisation of four different cross-linked copolymers. Three of them are semi-synthetic of nature, whereas the fourth one is a purely synthetic copolymer. The chemical structure of the synthesised hydrogels was analysed by ^{1}H NMR spectroscopy and attenuated total reflectance-infrared (ATR-IR) spectroscopy. The swelling capacity of the hydrogels was analysed in aqueous solutions of various pH and a cement filtrate solution. Based on these results, the hydrogels were compared with each other and with the hydrogels synthesised by both Mignon et al. (2016), Vermeulen (2016) and Devisscher (2015).

3.1.1 Methacrylation of hydrogels

Methacrylation of alginate

Alginate was modified by changing the hydroxyl groups on the monomer backbone to methacrylate functions, as explained in subsection 2.2.1 on page 30. It was performed in a slightly alkaline aqueous environment to increase the reactivity since more free hydroxyl groups on alginate are then deprotonated. The presence of methacrylate functions enables

the possibility of covalent linkages with acrylic monomers by means of a free radical polymerisation. After dialysis and freeze drying via lyophilisation, the methacrylated alginate, or simply modified alginate (AlgMOD), was obtained as a thin white sheet.

The degree of methacrylation or, more generally, degree of substitution (DS) was calculated as explained in subsection 2.2.3.4 on page 34. In terms of terminology, a low DS and high DS correspond to respectively one and two equivalents of MAAH per free hydroxyl group on the alginate chain that were added during methacrylation [60, 181]. Hence, 20 g of sodium alginate relates to 0.202 mol free hydroxyl groups based on the presence of two free hydroxyl groups per sodium alginate molecule ($(C_6H_7NaO_6)$n; 198.11 g/mol). In this research, AlgMOD with a high DS was synthesised. Proton nuclear magnetic resonance ^{1}H NMR spectroscopy was performed to determine the DS of the synthesised AlgMOD. The ^{1}H NMR spectrum was received from Gunter Reekmans (Institute for Materials Research (IMO), Hasselt University). The characteristic peaks are indicated on figure 3.1 and were used to calculate the DS, which gives an indication on the cross-linking efficiency during synthesis and is related to the elastic and swelling behaviour of the hydrogel.

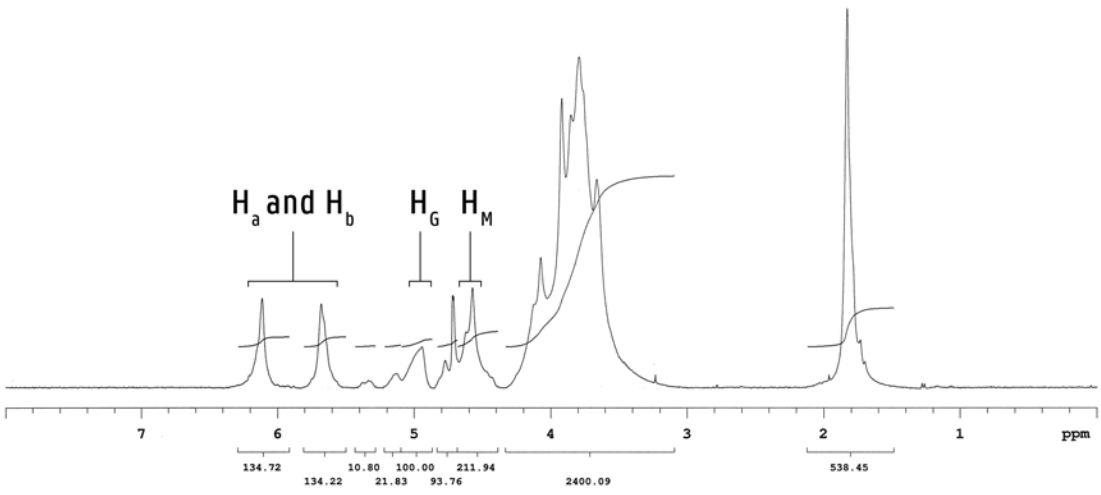

Figure 3.1: ^{1}H NMR spectrum of AlgMOD with a high degree of substitution (DS). The peaks correspond to different functional groups, namely vinyl protons (H_a and H_b), and anomeric carbon proton of the α-L-guluronate (H_G) and β-D-mannuronate (H_M) block.

The concentration of α-L-guluronate, i.e., G-block content, was calculated at 33.5% while its DS is equal to 29.6% per hydroxyl group for AlgMOD with a high DS. These results were compared to those out of the research of Vermeulen (2016). In her research, alginate was modified according the same method for an equal amount of MAAH per free hydroxyl group on the alginate chain. The G-block content was approximately the same, equal to 36.1%, whereas the DS per hydroxyl group (18.9%) differed considerably. The intensity of the vinyl

protons (H_a and H_b) in figure 3.1 on the previous page compared to the one of H_G was considerably higher than that of AlgMOD of a high DS out of the research by Vermeulen (2016). However, Vermeulen (2016) noted that nearby peaks in the spectrum could interfere with the reference peak, resulting in a less reliable DS determination [181].

Methacrylation of chitosan

Chitosan was dissolved in an acidic aqueous solution to increase its solubility. The methacrylation, or simply modification, of chitosan was performed as described in subsection 2.2.1 on page 30. 15 g of chitosan ($(C_6H_{13}NO_5)$n; 179.17 g/mol per repeating unit) equals to 0.167 mol of free hydroxyl groups because two free hydroxyl groups are available in each group of the chitosan chain. Consequently, 0.134 mol MAAH, or 19.9 ml, was added to the solution. After synthesis, dialysis and freeze-drying via lyophilisation a soft white sheet of methacrylated chitosan, or simply modified chitosan (ChiMOD), was obtained.

3.1.2 Development of hydrogels

Four different hydrogels were developed, consisting of anionic (alginate) and cationic (chitosan) polysaccharides, 2-(dimethylamino)ethyl methacrylate (DMAEMA), acrylic acid (AA) or acrylamide (AM). They were selected based on their properties evaluated in a previous research carried out by Mignon et al. (2016), who studied the effect of pH responsive superabsorbent polymers (SAPs) on self-sealing and self-healing of cracks in concrete [60]. Their pH responsive behaviour can be explained by the presence of different functional groups. Alginate is an anionic polysaccharide, containing hydroxyl and carboxylic acid functional groups, whereas chitosan is a cationic polysaccharide which possesses amine groups. DMAEMA is a basic monomer that doesn't swell substantially upon exposure to an aqueous solution of pH above its pKa, equal to 8.4 [182]. Lastly, acrylic acid (AA) becomes charged at pH above its pKa, equal to 4.25, while acrylamide (AM) is a hydrophilic monomer, which will not become charged in the pH range of interest.

Development of synthesised hydrogels

The hydrogels were synthesised according to the method described in subsection 2.2.2 on page 31. The cross-linker to monomer ratio for the three semi-synthetic hydrogels was 1/7, as displayed in table 3.1 on the following page. A horizontal line in the table makes the distinction between semi-synthetic hydrogels (p(algMOD_AA); p(algMOD_AA/AM); and p(chiMOD_DMAEMA)) and the synthetic hydrogel (p(MBA_DMAEMA)).

The gel fraction is determined as explained in subsection 2.2.3.1 on page 33. It's important to note that the samples were weighed immediately after lyophilisation because when they are exposed to an atmosphere, they can absorb some moisture depending on the relative humidity (RH). Their moisture uptake can be assessed by a dynamic vapour sorption (DVS)

Table 3.1: Overview of theoretical chemical composition and gel fraction of synthesised hydrogels

Sample	*Cross-linker*	*Monomer*	$\frac{\textit{Cross-linker}}{\textit{Monomer}}$	*Gel Fraction*
	[-]	[-]	[g/g]	[%]
p(algMOD_AA)	AlgMOD	Acrylic Acid (AA)	1/7	92.4 ± 1.1
p(algMOD_AA/AM)	AlgMOD	Acrylic Acid (AA) Acrylamide (AM)	1/7	82.1
p(chiMOD_DMAEMA)	ChiMOD	2-(dimethylamino)ethyl methacrylate (DMAEMA)	1/7	68.3 ± 6.2
p(MBA_DMAEMA)	N,N'-methylene bisacrylamide (MBA)	2-(dimethylamino)ethyl methacrylate (DMAEMA)	1/51	83.2 ± 9.5

test. However, no DVS tests were performed in this research because most of the materials were already extensively studied in previous research by Devisscher (2015), Vermeulen (2016) and Mignon et al. (2016). Nevertheless, during weighing of poly(MBA_DMAEMA), a weight increase of about $0.005\,\mathrm{g/g \cdot s}$ was observed based on visual interpretation of the weight increase on the balance display. In addition, when the material was removed from the vacuum applied during lyophilisation, it was brittle but quickly became more ductile, possibly due to water absorption. Mignon et al. (2016) measured a change in mass of about 6% before equilibrium of poly(MBA_DMAEMA) samples exposed to 60% RH, which could explain the rapid moisture uptake [60].

The gel fraction for the different synthesised hydrogels were compared to the ones of previous research. The gel fraction for p(algMOD_AA), or simply AlgAA, was higher than the one synthesised in previous research [60, 181], which was about 85%. However, the gel fraction for p(algMOD_AA/AM), or simply AlgAA/AM was less than the one synthesised by Vermeulen (2016) (92.7%). The gel fraction for AlgAA/AM was determined for a sample containing bacteria spores. This might caused the reduction in gel fraction since bacteria might leak out during dialysis. Furthermore, the gel fraction for the particular sample was not performed in triplicate, due to the limited amount of hydrogel that was made. The result of p(chiMOD_DMAEMA), or simply ChiMOD/DMAEMA, are similar [60, 181]. In figure 3.2 on the following page, the synthesised hydrogels before dialyses are shown. The semi-synthetic hydrogels (a-c) form a strong gel and absorb all fluid during synthesis, whereas the synthetic hydrogel (d) is a tough slimy material which did not absorb all fluid. After removal from the three-neck flask, the hydrogel was broken into pieces and added to a petri dish. Once this was done, it was observed that ChiMOD/DMAEMA, who was once a crystal clear colourless gel, tends to discolour pink. This may be caused by an oxidation reaction, but was not further

Figure 3.2: Development of hydrogels: (a) poly(algMOD_AA), (b) poly(algMOD_AA/AM), (c) poly(chiMOD_DMAEMA), and (d) poly(MBA_DMAEMA)

investigated.

3.1.3 Chemical structure elucidation using ATR-IR spectroscopy

The chemical structure of the synthesised hydrogels was characterised by using attenuated total reflectance infrared spectroscopy (ATR-IR), as explained in subsection 2.2.3.5 on page 35. The most relevant characteristic peaks of all hydrogels are indicated on figure 3.3 and 3.4 on page 53 and can be found in table 3.2 on the next page.

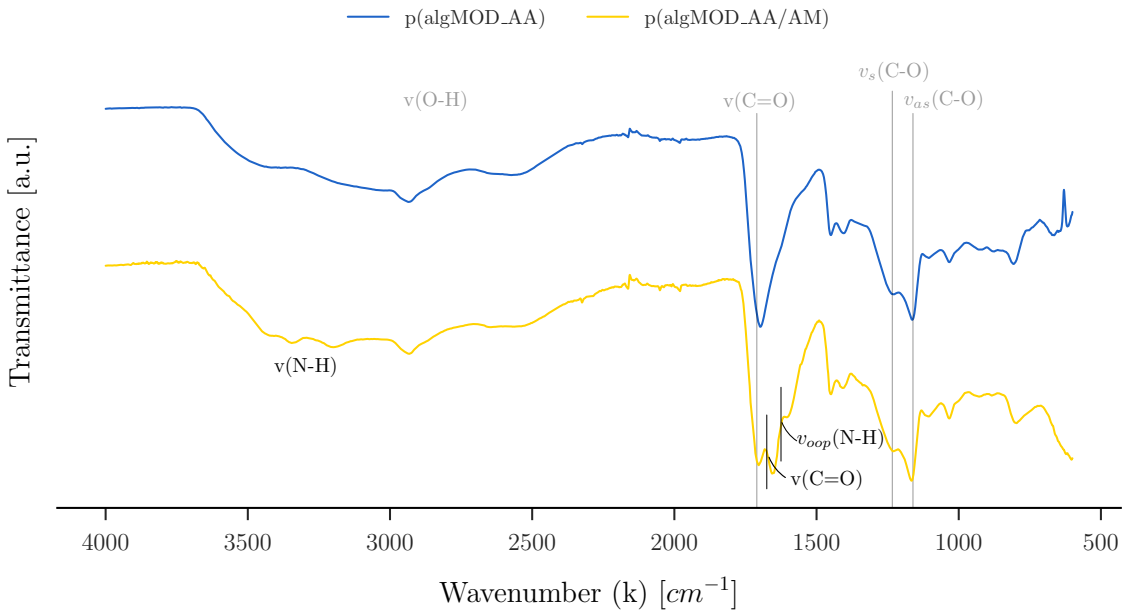

Figure 3.3: ATR-IR spectra of p(algMOD_AA) and p(algMOD_AA/AM) with indication of the characteristic peaks and the corresponding bond vibrations.

The similar characteristic peaks of the hydrogels shown in figure 3.3 on the preceding page and 3.4 on page 53 are indicated in grey, either by a line to indicate a sharp peak or simply by text to indicate a broad peak. The presence of the oxygen-hydrogen stretch vibration v(O-H) of the carboxylic acid moieties of both AlgMOD and AA in visualised by the broad peak between $2400 - 3400\,\mathrm{cm}^{-1}$. This peak can also be observed in the spectra of ChiMOD/DMAEMA in figure 3.4 on page 53. At $1700\,\mathrm{cm}^{-1}$, a sharp peak related to the carbon-oxygen double bond stretch vibration v(C=O) of carboxylic acid moieties from both AlgMOD and AA is observed. The peaks at 1170 and $1120\,\mathrm{cm}^{-1}$ correspond to, respectively, the symmetric and asymmetric stretching vibration of the carbon-oxygen-carbon bonds (v(O=C-O)) of the ester groups present in AlgMOD. The addition of AM in AlgAA/AM is visualised by a broad peak introduced in between $3100 - 3500\,\mathrm{cm}^{-1}$ related to the nitrogen-hydrogen stretching vibration v(N-H) of the primary amide of AM, a peak at $1625\,\mathrm{cm}^{-1}$ related to out-of-plane equivalent of the former, and a peak introduced at $1675\,\mathrm{cm}^{-1}$ related to the carbon-oxygen double bond stretch vibration v(C=O) of the amide moiety. The former peak were partly obscured due to the presence of the broad peak introduced by the carboxylic acid from both AlgMOD and AA. The peak at $1700\,\mathrm{cm}^{-1}$ related to AA is relatively larger for AlgAA compared to that of AlgAA/AM, which can be explained by the reduced amount of AA in the hydrogel composition of AlgAA/AM. The peak that was observed at $2930\,\mathrm{cm}^{-1}$ in both hydrogels in figure 3.3 on the previous page is associated with the C-H stretching of CH_2 functionalities, which were induced by the polymerisation reaction.

Table 3.2: Characteristic absorption peaks in the ATR-IR spectra of methacrylated alginate (AlgMOD), methacrylated chitosan (ChiMOD) as well as the monomers acrylic acid, acrylamide and DMAEMA

Wavenumber	*Vibration*	*Width*	*Functionality*
	Methacrylated alginate (AlgMOD)		
1170	v_{as}(C-O)	Sharp	Ester
1220	v_s(C-O)	Sharp	Ester
1700-1720	v(C=O)	Sharp	Carboxylic acid/ester
2400-3400	v(O-H)	Broad	Carboxylic acid
	Acrylic acid (AA)		
1700	v(C=O)	Sharp	Carboxylic acid
2400-3400	v(O-H)	Broad	Carboxylic acid
	Acrylamide (AM)		

Continued on next page

Table 3.2: *Continued from previous page*

Wavenumber	*Vibration*	*Width*	*Functionality*
1625	v_{oop}(N-H)	Sharp	Amide (out-of-plane)
1675	v(C=O)	Sharp	Amide
3100-3500	v(N-H)	Broad	Amide
	Methacrylated chitosan (ChiMOD)		
1150	v_{as}(C-O)	Sharp	Ester
1720	v(C=O)	Sharp	Ester
2400-3400	v(O-H)	Broad	Carboxylic acid
3100-3500	v(N-H)	Broad	Amide
	2-(dimethylamino)ethyl methacrylate (DMAEMA)		
1145	v_{s}(C-O)	Sharp	Ester
1175	v_{as}(C-O)	Sharp	Ester
1720	v(C=O)	Sharp	Ester
2775	v(N-C)	Sharp	Tertiary amine
2825	v(N-C)	Sharp	Tertiary amine
2945	v_{as}(C-H)	Broad	Alkane

In figure 3.4 on the following page, the similar peaks, indicated in grey, are those attributed to the monomer DMAEMA. The carbon-oxygen double bond stretch vibration (v(C=O)) at 1720 cm^{-1} is related to the ester moieties of both ChiMOD and DMAEMA. The peak at 2775 and 2825 cm^{-1} are both related to the nitrogen-carbon bond stretch vibrations (v(N-C)) of tertiary amine functionalities from DMAEMA. The asymmetric carbon-oxygen bond stretch (v_{as}(C-O)) related to the ester functionalities of both ChiMOD and DMAEMA is observed at, respectively, 1150 and 1175 cm^{-1}. At the wavelength interval 3500 to 3100 cm^{-1} of ChiMOD/DMAEMA, a broad peak is situated, corresponding to the nitrogen-hydrogen stretch of the amide on ChiMOD's backbone.

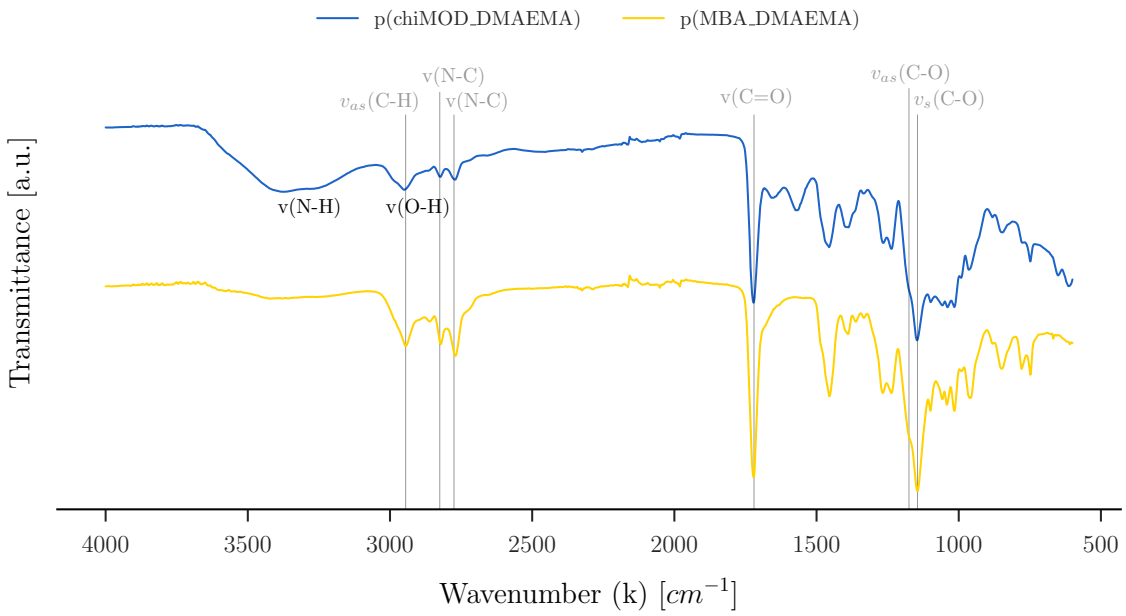

Figure 3.4: ATR-IR spectra of p(chiMOD_DMAEMA) and p(MBA_DMAEMA) with indication of the characteristic peaks and the corresponding bond vibrations

3.1.4 Swelling capacity measurements in aqueous and cement filtrate solutions

The swelling capacity, or absorption capacity, is measured using the filtration method, as explained in subsection 2.2.3.3 on page 34. In previous research by Devisscher (2015) and Mignon et al. (2016), the use of a second method, i.e. the tea bag method, was also considered, but Vermeulen (2016) argued the advantageous use of the filtration method. The swelling capacity is measured for hydrogel powders exposed to aqueous solution of varying pH and a cement filtrate solution for a timespan of 24 h. The results of the filtration test are shown in figure 3.5 on the following page. In addition, potential hydrogel hydrolysis after exposure to the various solutions, a sign of degradation, is examined and discussed. The long-term degradation of the hydrogels exposed to a neutral solution and a cement filtrate solution is discussed in section 3.3 on page 60.

First, the swelling capacity of AlgAA will be discussed. Alginate, covalently cross-linked with acrylic acid (AA), is an anionic polysaccharide composed of β-D-mannuronate and α-L-guluronate blocks with pK_a equal to, respectively, 3.38 and 3.65. When exposed to a solution of pH greater than 3.65, the carboxylic acid functionalities present on alginate will gradually start to deprotonate. Thus, those functionalities, both negatively charged, repel each other and contribute to the increasing swelling capacity. In addition, AA has a pK_a equal to 4.25, implying the deprotonation of carboxylic acid functionalities at a pH above this value. As observed in figure 3.5 on the following page, the swelling capacity of AlgAA

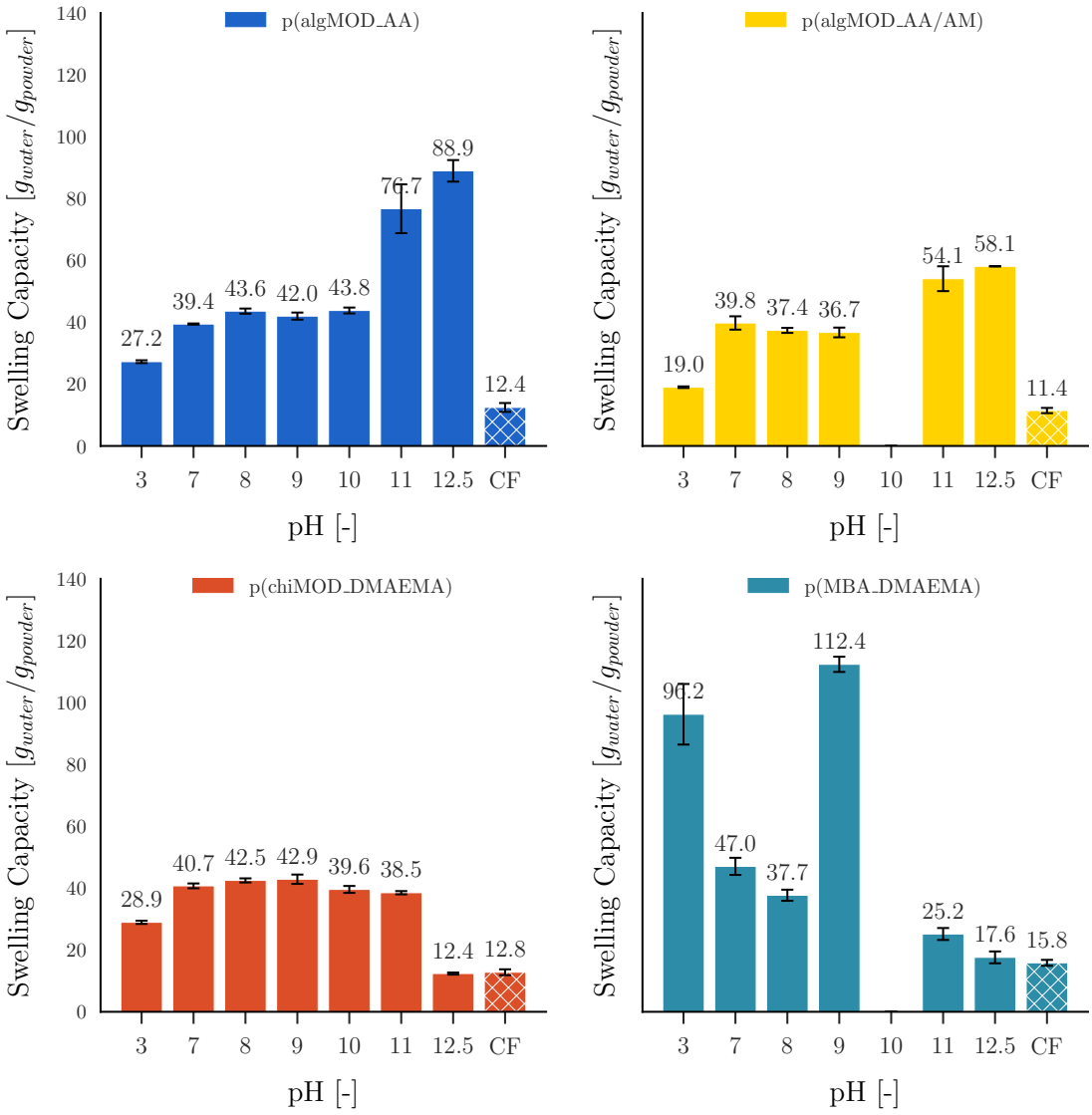

Figure 3.5: The swelling capacity for the synthesised hydrogels, both in aqueous solutions (3-12.5; no hatch) and cement filtrate solutions (CF; hatched)

gradually increases for increasing pH value, reaching a maximum swelling at pH 12.5 equal to $88.9 \pm 3.48\,g_{water}/g_{hydrogel}$. However, a jump in swelling capacity is observed at pH equal to 11, corresponding to a change in ATR-IR spectra of AlgAA at $1540\,cm^{-1}$ shown on figure B.1 on page 112. This peak was originally hidden as a shoulder of the v(C=O) stretch of the carboxylic acid functionality at $1720\,cm^{-1}$ on AlgMOD. The latter will gradually start to hydrolyse, leading to a more open structure with an initial increase in swelling capacity. This result was compared to those of a hydrogel with identical composition examined by Vermeulen (2016). The results lie in a similar range and the same trends occurred [181]. In addition, she

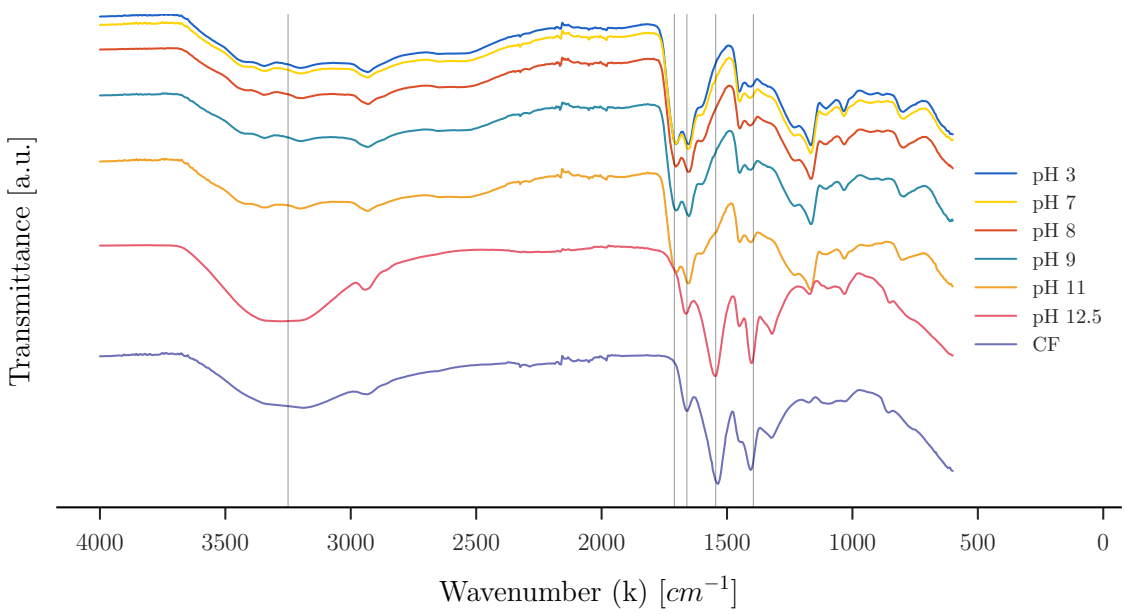

Figure 3.6: ATR-IR spectra of p(algMOD_AA/AM) after exposure to aqueous solutions of varying pH and a cement filtrate solution for a timespan of 1 day. The changes of the spectra of p(algMOD_AA) are similar and can be found in figure B.1 on page 112

noted a reduction in swelling capacity at a pH of 13, related to further decrease in structural integrity of the hydrogel, a trend that is confirmed by the peak shifts observed in the ATR-IR spectra of AlgAA in figure B.1 on page 112. The decreased swelling in a cement filtrate solution may be attributed to a screening effect of ions of the polymeric chain due to the presence of mono- and multivalent cations [60].

On the other hand, acrylamide (AM) cross-linked in AlgAA/AM, which replaces 25 mol% of the acrylic acid compared to the composition of AlgAA, is a hydrophilic monomer, which is not charged within the pH range of interest. Thus, reduction of the overall swelling capacity is expected compared to that of AlgAA. As observed in figure 3.5 on the previous page, this behaviour is confirmed. The same degradation phenomena described in AlgAA are true for AlgAA/AM with the exception of the hydrolyses of acrylamide (AM), visualised by a decrease of the peaks at 794, 1625 and 1675 cm^{-1} in figure 3.6. The former can be attributed to the hydrolysis of the internal amide groups of AM. The maximum swelling capacity is reached at pH 12.5 and is equal to $58.1 \pm 0.08\, \mathrm{g_{water}}/\mathrm{g_{hydrogel}}$, only around 65% of the maximum swelling capacity of AlgAA. Both AlgMOD based hydrogels are prone to partial degradation in an extremely alkaline environment.

Next, the swelling capacity of ChiMOD/DMAEMA and MBA/DMAEMA will be discussed. Both hydrogels are mainly composed out of the basic monomer 2-(dimethylamino)ethyl

methacrylate (DMAEMA). Tertiary amine functionalities of DMAEMA have a pK_a value of 8.4, hence, the monomer will not swell substantially upon exposure to a solution of pH above 8.4. On the other hand, the concentration of positively charged amine functionalities of DMAEMA will increase below pH 8.4, thus, promoting electrostatic interactions between charged functionalities. Chitosan is a cationic polysaccharide that shows an opposite pH-sensitivity in an alkaline environment compared to alginate. However, the pH-sensitivity of chitosan and DMAEMA is similar, though both have a different pK_a. The primary amine functionality of ChiMOD possesses a pK_a of 6.5. The swelling capacity at pH 12.5 only amounted $12.4 \pm 0.34\,g_{water}/g_{hydrogel}$ and increased substantially to $38.5 \pm 0.53\,g_{water}/g_{hydrogel}$ at pH 11. In the mindset of the application of the hydrogels in cementitious materials, this pH responsive behaviour is promising since the hydrogel should ideally swell as least as possible during mixing (pH >12), yet extensively at neutral or slightly alkaline pH. Within the pH range between 7 and 11, the swelling capacity remained stable, varying between 38.5 ± 0.53 and $42.9 \pm 1.50\,g_{water}/g_{hydrogel}$. However, a small decline in swelling at pH 3 can be observed in figure 3.5 on page 54. This decline is greater than that of ChiMOD/DMAEMA synthesised by Vermeulen (2016). The ATR-IR spectra of the ChiMOD/DMAEMA after exposure to various solutions is analysed, in particular in solutions of high alkalinity and high acidity. At pH 3, a broad peak emerges in the range $3100 - 3600\,cm^{-1}$. This peak tends to decrease after exposure to a more acidic solution and can be attributed to the nitrogen-hydrogen stretch v(N-H) associated with the amides of ChiMOD. In addition, a shoulder peak is observed at $1170\,cm^{-1}$ at pH 3, whereas this shoulder disappears at higher pH values.

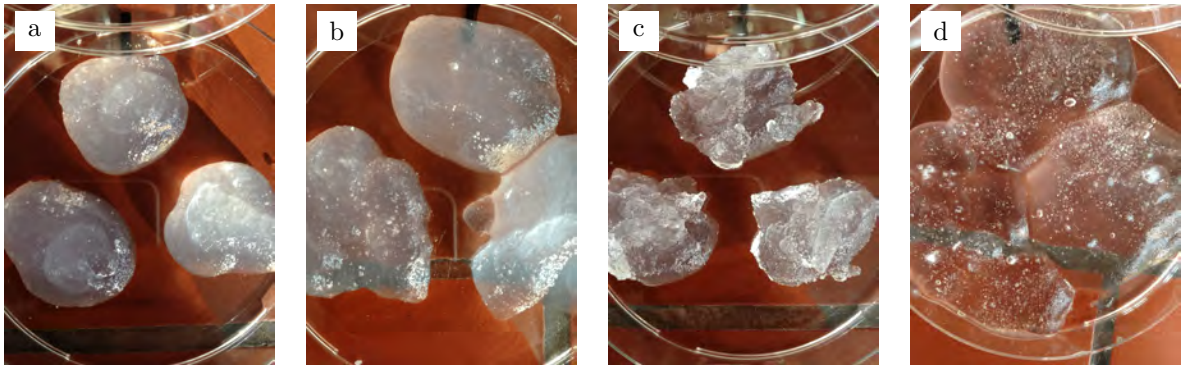

Figure 3.7: Swollen hydrogel after filtration test: (a) poly(algMOD_AA), (b) poly(algMOD_AA/AM), (c) poly(chiMOD_DMAEMA), and (d) poly(MBA_DMAEMA)

MBA/DMAEMA is composed out of the previously discussed DMAEMA and the synthetic cross-linker N,N'-methylene bisacrylamide (MBA). The cross-linker MBA possesses internal neutral amide moieties. The hydrogel exhibited a low swelling at the most alkaline conditions, ranging from $17.6 \pm 1.92\,cm^{-1}$ to $25.2 \pm 1.93\,cm^{-1}$ for, respectively, pH 12.5 and 11.

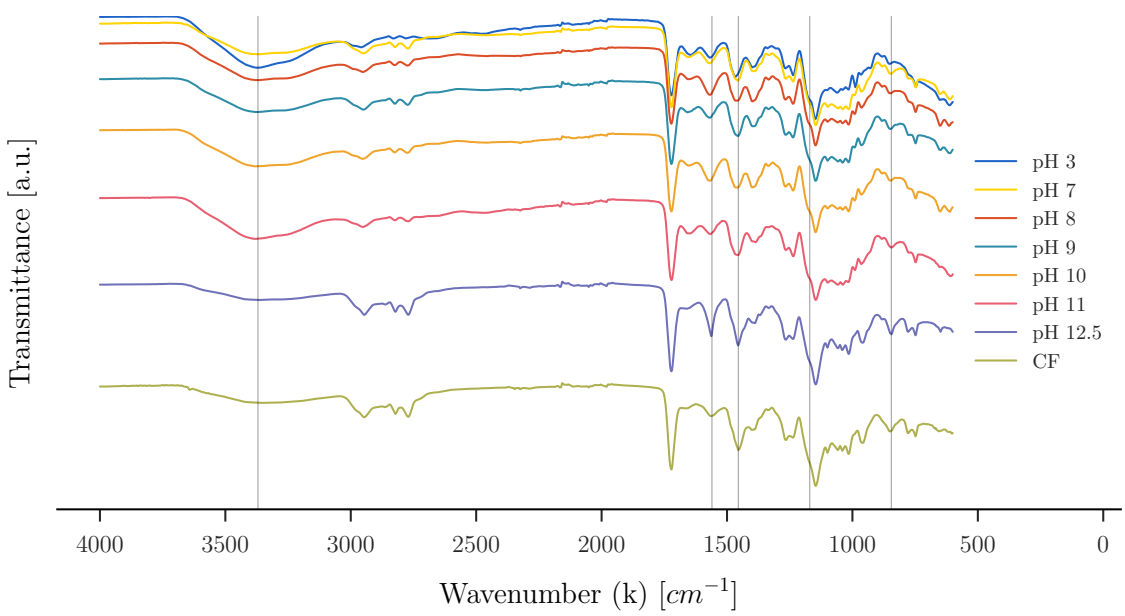

Figure 3.8: ATR-IR spectra of p(chiMOD_DMAEMA) after exposure to aqueous solutions of varying pH and a cement filtrate solution for a timespan of 1 day. The changes of the spectra of p(MBA_DMAEMA) are similar and can be found in figure B.4 on page 113

The swelling gradually increased after exposure to more acidic solutions, reaching a swelling of $96.2 \pm 9.80\,g_{water}/g_{hydrogel}$ at pH 3. This can be explained by the protonation of tertiary amine functionalities of DMAEMA at lower pH. However, a tremendous swelling is observed at pH 9 for MBA/DMAEMA on figure 3.5 on page 54 compared to the adjacent results. Unfortunately, in case of the filtration test at pH 9, hydrogel powders of a different batch MBA/DMAEMA had to be used due to a limited amount of powders available of a first batch of the hydrogel. The first batch amounted to a theoretical mass of 18.40 g, whereas the second batch amounted to 50.0 g of MBA/DMAEMA. The upscaling of the free radical polymerisation reaction might influence the hydrogel's composition. As observed by [60], a lower MBA concentration lead to a higher swelling as anticipated due to its less dense network. The upscaling of MBA/DMAEMA synthesis might not have been successful, hence cross-linking MBA at a lower concentration than anticipated. This results should highlight the importance of characterising each batch, regardless of the fact that the nature and synthesis of the hydrogel is the same. Because of the lack of hydrogel powders of the original batch, the swelling at pH 10 was not evaluated. The presence of mono- and multivalent cations in the cement filtrate solution further reduces the swelling of MBA/DMAEMA up to $15.83 \pm 0.96\,g_{water}/g_{hydrogel}$. However, MBA/DMAEMA possesses the highest swelling capacity of all synthesised hydrogels. The signals at 1550 and 1410 cm^{-1} associated with, respectively, the asymmetric (v_{as}(C-O)) and the symmetric (v_s(C-O)) stretch are only slightly more pronounced. They are related

to hydrolysis, hence it could be concluded that MBA/DMAEMA showed a negligible amount of degradation.

3.2 Implementation of hydrogels in mortar

The primary reason to use pH responsive hydrogels over normal hydrogels as a carrier for bacterial spores for self-healing concrete, is its potential to conserve the mechanical properties of the concrete. For this reason, the flexural and compressive strength of mortar specimens with and without the addition of hydrogel particles was evaluated. In addition, the influence of the amount of hydrogel powders in mass% of the Portland cement was examined. No additional water was added to compensate for the swelling of the hydrogel powders, whereas other researchers argue that additional water is required to obtain a mortar mixture of the same slump [60, 134, 181]. However, Vermeulen (2016) noted that the amount of water that the hydrogel powders will absorb is hard to predict [181]. For this reason, no additional water was added. Hence, mixtures including hydrogels exhibited a reduced workability compared to the control specimen.

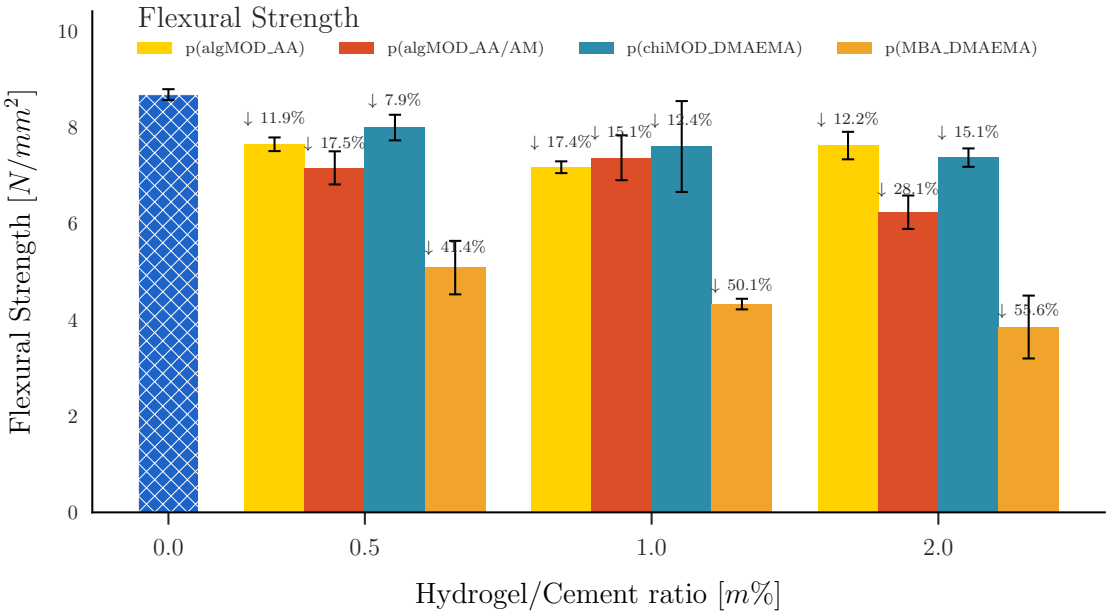

Figure 3.9: Flexural strength of the reference mortar specimen (blue; hatched) and mortar specimens with addition of the synthesised hydrogels

The flexural and compressive strength results are listed in table C.1 on page 119. A graphical interpretation is shown in figure 3.9 and 3.10 on page 60. In addition to the preparation of a control specimen, mortar specimens containing 0.5, 1 or 2% hydrogel relative to the mass of the cement were made. The addition of 0.5m% of MBA/DMAEMA had a great

impact on the flexural and compressive strength, significantly decreasing it by respectively 41.4 and 50.2% compared to the reference sample, whereas the other hydrogels encountered less strength reduction. This severe strength reduction may be related to the absorption rate and the swelling of MBA/DMAEMA during mixing. The swelling behaviour was tested in a cement filtrate solution, however this method is questioned to be a representative approach since the mixing process of mortar only takes a few minutes while the cement filtrate was prepared by exposing cement particles to an aqueous solution for three hours. Moreover, the absorption rate of the hydrogels was not tested in this master's dissertation. Even after addition of 1m% of hydrogel, the flexural and compressive strength decrease remained within the range of, respectively, 12.4-17.4% and 4.7-12.8% for semi-synthetic hydrogels. However, this is still a significant decrease compared to the strength properties of the control specimen. The synthetic hydrogel, MBA/DMAEMA, experienced an even greater strength decrease. Thus, the synthetic hydrogels may only be used in applications where the reduction in mechanical strength is of minor importance compared to the self-sealing ability. Furthermore, the addition of MBA/DMEAMA showed a more severe reduction in strength compared to the results of a hydrogel of the same composition in the research conducted by Mignon et al. (2016). This may be attributed to the use of additional water to compensate for the swelling of the hydrogel, as was done by Mignon et al. (2016). In addition, the MBA/DMAEMA synthesised for the addition in mortar specimens belonged to the batch of hydrogel that showed a significant increased swelling compared to the batch of MBA/DMAEMA that was synthesised for filtration tests. As aforementioned, this swelling behaviour may be explained by a low cross-linking efficiency and consequently loose hydrogel network. At last, a significant decrease in compressive strength was observed for 2m% addition of any of the synthesised hydrogels compared to the samples containing only 1% hydrogel relative to the mass of the cement. Furthermore, the magnitude of the difference was large.

In order to promote the self-sealing and -healing of cracks, the largest possible amount of hydrogels should be added to the cementitious material without compromising the mechanical properties. Hence, the addition of 1% hydrogel relative to the mass of the cement is chosen to be used for the preparation of the specimens containing hydrogel immobilised bacterial spores. Based on the strength properties of mortar specimens after addition of the hydrogels, AlgAA and ChiMOD/DMAEMA are selected as the most promising carriers to be included in the cementitious material. The addition of AlgAA shows no significance difference regarding the compressive strength compared to the control specimen, whereas the addition of ChiMOD/DMAEMA does decrease the compressive strength by 11.8%. On the other hand, the flexural strength is decreased by 17.4 and 12.4% on average compared to the control specimen for respectively AlgAA and ChiMOD/DMAEMA. The runner-up is AlgAA/AM whose results does not differ significantly from those of ChiMOD/DMAEMA, but was not selected because the hydrogel is of the same nature as AlgAA.

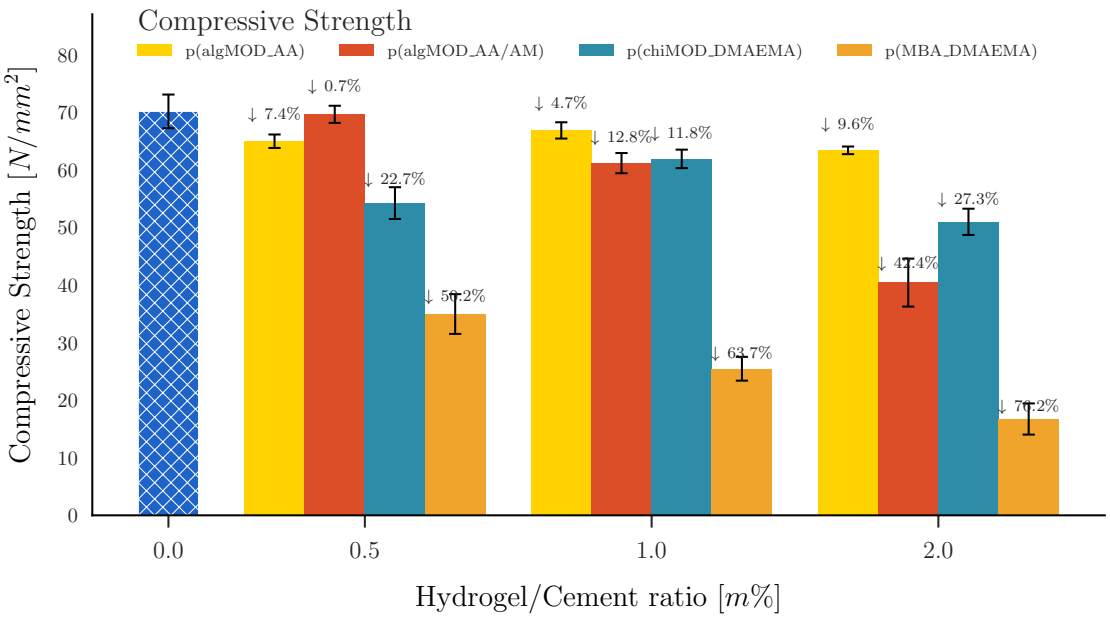

Figure 3.10: Compressive strength of the reference mortar specimen (blue; hatched) and mortar specimens with addition of the synthesised hydrogels

3.3 Degradation study of hydrogel exposed to aqueous and cement filtrate solution

When applied in cementitious materials, the self-healing functionality of hydrogel immobilised bacteria must be maintained over the relatively long service life of the civil infrastructures, ranging from fifty to a hundred years. Both the hydrogel as the bacterial spores should possesses a shelf life as long as the service life of the infrastructure, as was included as one of the six robustness criteria by Li and Herbert (2012) to evaluate the feasibility of a self-healing approach [12]. Thus, the degradation of the hydrogel, i.e. its shelf life, should be evaluated upon quantifying the robustness of this self-healing approach since it possess the ability to seal cracks upon formation and act as a water reservoir to promote spore germination, and hence, facilitate the precipitation of $CaCO_3$. The degradation study involves a filtration test and subsequently an analysis of the ATR-IR spectra of the hydrogels exposed to an aqueous solution of neutral pH and a cement filtrate solution for a timespan of 1, 7, 28, 90 and 180 days.

In figure 3.11 and 3.13 on page 64, a visual overview of the hydrogels after filtration is given in order to clarify to morphology of the hydrogels. The first figure represents the hydrogels after exposure to an aqeous solution of neutral pH, whereas the latter shows the hydrogels after exposure to a cement filtrate solution of pH 12.5. In the fourth column of figure 3.11 on the

following page, an increased MBA/DMAEMA hydrogel volume over time after filtration is visually observed. It should be noted that filtration test MD_{180} represents the volume of only two times 0.20 g swollen hydrogel, whereas the third sample was stored in another petri dish because it could not fit into one. After addition of the hydrogel to a cement filtrate solution, the hydrogel either sticked to the bottom or float around in the suspension. The former behaviour was observed for AlgAA and AlgAA/AM, whereas the other hydrogels floated in the suspension. During the filtration test, the hydrogel at the bottom of the cup in case of AlgAA and AlgAA/AM was not destroyed. Afterwards, it was collected in a petri dish and it released some of its entrapped solution, as can be seen in sample AA_{90} in figure 3.13 on page 64. All samples were filtered by paper filters with a particle retention of 12 to 15 µm. In figure 3.12 on page 63, the swelling capacity in function of time after exposure to an aqueous solution of neutral pH is showed. As for the first hydrogel, i.e. AlgAA, there is a significant difference between the means of the swelling capacity after different exposure time. The swelling of AlgAA increases over time, reaching maximum swelling capacity for 90 and 180 days. As earlier discussed in subsection 3.1.4 on page 53, AlgMOD based hydrogels are prone to degradation, which can cause the significant increase in swelling capacity because of loosening of the hydrogel's network. However, in a cement filtrate solution the trend is less clear. The swelling of AlgAA after exposure for 1 day is significantly lower than that of 7, 90 and 180 days. Furthermore, no significant differences could be observed between the other samples. ATR-IR spectra analysis must indicate whether or not degradation emerges shortly after initial exposure to the cement filtrate solution.

In case of AlgAA/AM exposed to an aqueous solution, no immediate trend is observed. However, there is a significant difference between samples of different exposure time. No visual differences in morphology is observed in the subset AM_x in figure 3.11 on the following page. This hydrogel may be less prone to degradation compared to AlgAA, which showed a significant increase in swelling over time when exposed to an aqueous solution. When AlgAA/AM is added to a cement filtrate solution, by visual interpretation, a trend in swelling of the hydrogel seems to emerge over time. However, the longer the hydrogel is exposed to the solution, the wider the range becomes in which the values of the swelling capacity lie. Thus, it should be concluded that no significant difference is observed between the samples of different exposure time to a cement filtrate solution. The consistency of the swelling property over time of AlgAA/AM is doubtful, and hence, its use would suggest a lack of reliability of the particular self-healing approach.

The swelling properties of ChiMOD/DMAEMA over time when exposed to an aqueous solution of neutral pH do not differ significantly. Nevertheless, a small reduction of swelling is observed for the samples of 7 and 28 days compared to the sample of 1 day. When added to a cement filtrate solution, there is a significant difference within the test results. The mutual difference between the swelling properties of the sample of 7 and that of 90 days is recognised.

However, the result at 180 days with a maximum swelling capacity in cement filtrate solution of 17.2 $g_{water}/g_{hydrogel}$, does not distinguish itself from the other test results because of the wide deviation of the test results.

At last, the swelling capacity over time of the synthetic hydrogel MBA/DMAEMA is discussed. In an aqueous solution of neutral pH, the hydrogel tends to increase over the course

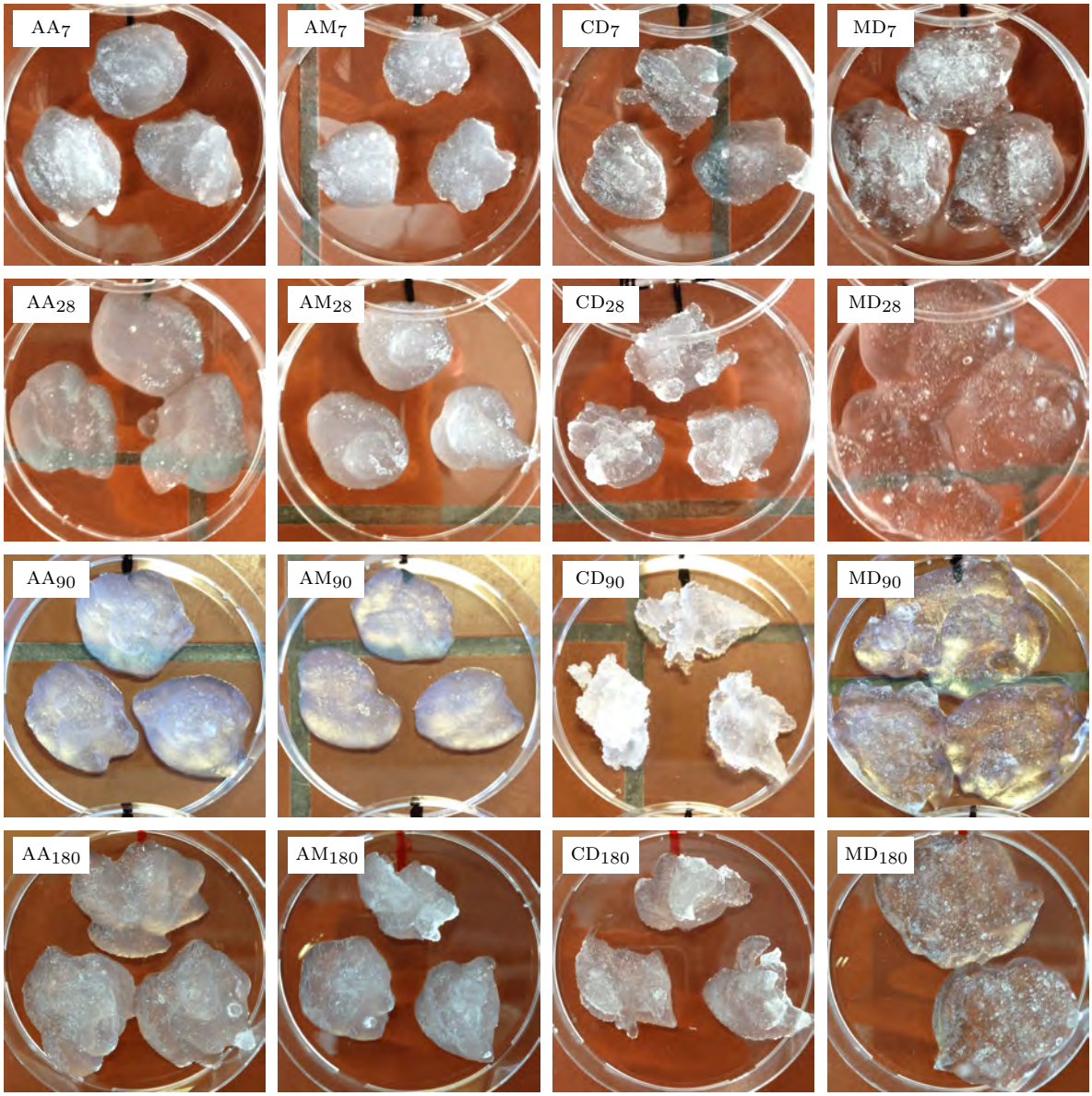

Figure 3.11: Swollen hydrogel after filtration test: (AA_x) poly(algMOD_AA), (AM_x) poly(algMOD_AA/AM), (CD_x) poly(chiMOD_DMAEMA), and (MD_x) poly(MBA_DMAEMA). The subscript $_x$ equals to the amount of days the samples were exposed to an aqueous solution of neutral pH

of time. A Dunnett T3 post hoc test revealed that the swelling after 1 day of exposure time was statistically significantly lower than the swelling at 7 and 28 days. However, there was no significantly difference between 90 nor 180 days and the swelling at 1, 7 and 28 days. This can be attributed to the large amount of variation in the results for 90 and 180 days. ATR-IR spectra analyses should clarify if MBA/DMAEMA is prone to degradation. Lastly, the influence of the exposure time to a cement filtrate solution of samples containing MBA/DMAEMA showed no significant difference on the swelling properties of the hydrogel.

All statistical interpretations were supported by a univariate ANOVA test, followed by a Levene's test to test the homogeinity of the variances. If the assumption of equal variances was not violated, the test was continued by a Tukey post-hoc test, whereas a Brown-Forsythe and Dunnett's T3 post-hoc test were performed if the assumption was violated. Potential significant differences ($p < 0.05$) were identified using the statistical program SPSS.

The ATR-IR spectra of the hydrogels were analysed after the filtration tests and are available in section B.2 on page 114. In general, no significant degradation of the hydrogels exposed to both an aqueous and a cement filtrate solution is observed. However, changes in the ATR-IR spectra will be discussed for all synthesised hydrogels. In the case of AlgAA, no significant difference, nor a trend is spotted in the ATR-IR spectra after exposure to an aqueous solution of neutral pH over the course of time. The only change is observed for the sample of 28 days. Its peak at 1550 cm^{-1} corresponding to the asymmetric carbon-oxygen bond stretch

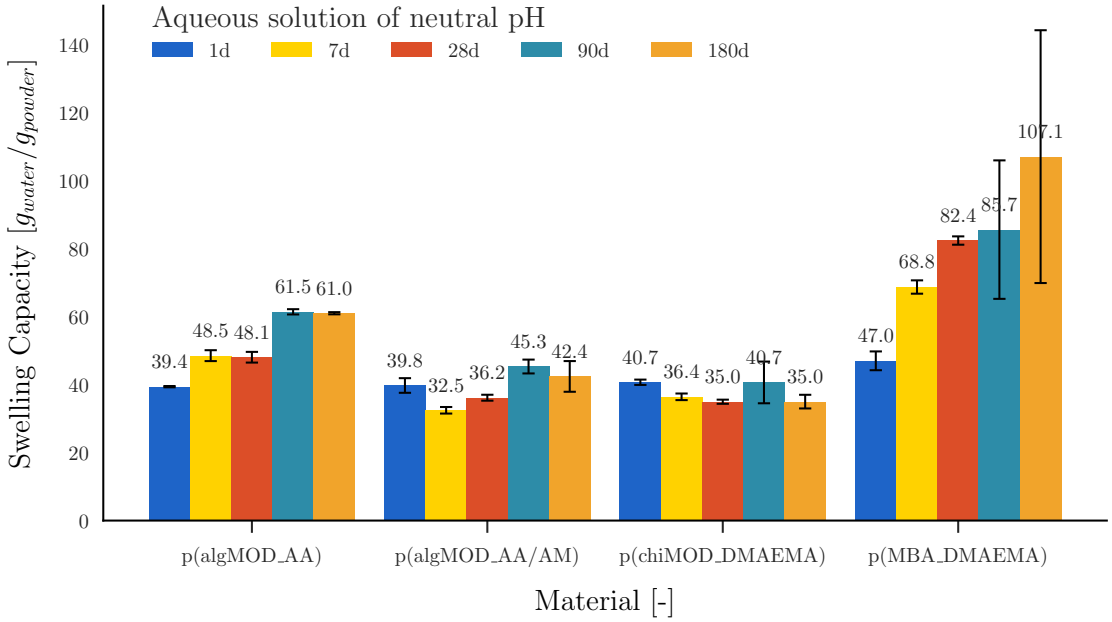

Figure 3.12: Swelling capacity of the synthesised hydrogels in function of time, after exposure to an aqueous solution of neutral pH.

vibration v(C-O) is slightly more distinguishable compared to the other samples. In addition, the peak around 2940 cm^{-1} is slightly more pronounced. This might indicate the hydrolysis of incorporated methacrylate ester functionalities of AlgMOD, but then a decrease of carbon-oxygen double bond stretch v(C=O) at 1700 cm^{-1} is to be expected. However, the latter is not the case so the significant increase in swelling capacity in an aqueous solution due to a less densely cross-linked network after degradation could not be confirmed by ATR-IR spectra analysis. When AlgAA is exposed to a cement filtrate solution, the ATR-IR spectra of the hydrogel shows signs of degradation even after one day of exposure time. The incorporated methacrylate ester moieties at 1700 cm^{-1} almost completely disappeared. Their only sign of existence is a small shoulder visible in the peak related to carboxylate functionalities v_{as}(C-O) at 1550 cm^{-1} which emerged after the hydrolyses of the aforementioned ester moieties from AA and AlgMOD. In addition, the broad oxygen-hydrogen bond stretch v(O-H) associated with the hydroxyl functionalities, in particular in the range of $3000 - 3500\,cm^{-1}$, are more

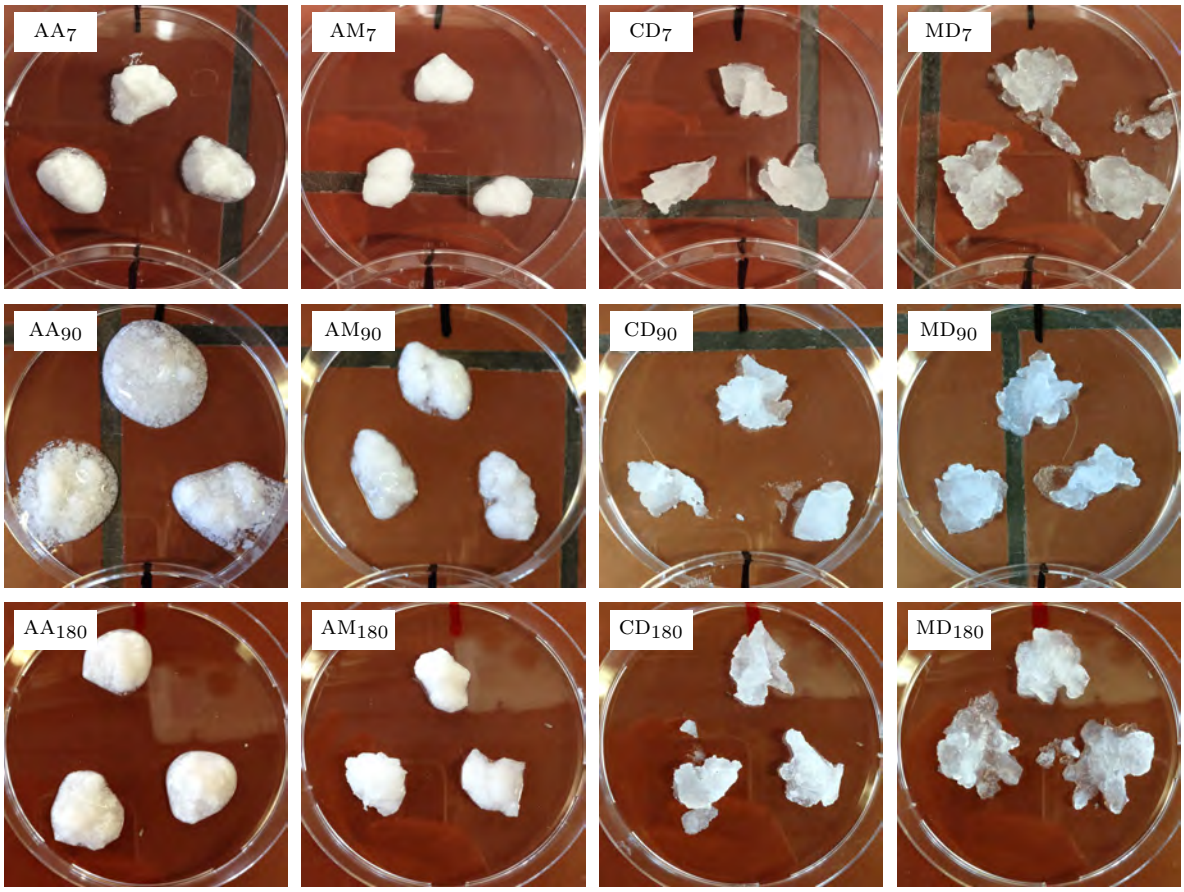

Figure 3.13: Swollen hydrogel after filtration test: (AA_x) poly(algMOD_AA), (AM_x) poly(algMOD_AA/AM), (CD_x) poly(chiMOD_DMAEMA), and (MD_x) poly(MBA_DMAEMA). The subscript $_x$ equals to the amount of days the samples were exposed to an cement filtrate solution

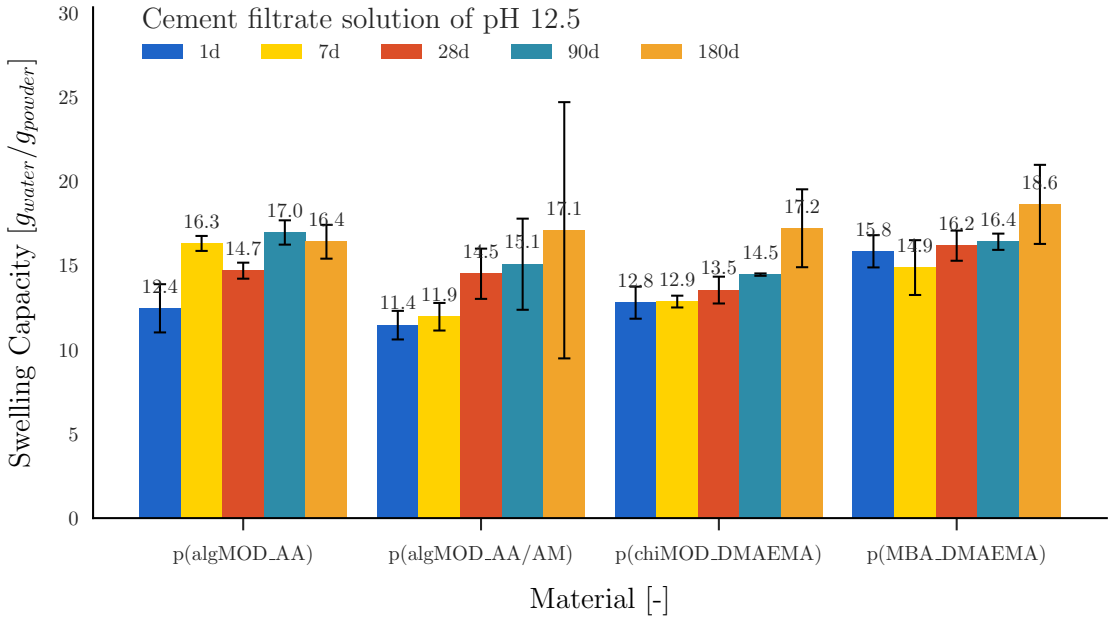

Figure 3.14: Swelling capacity of the synthesised hydrogels in function of time, after exposure to an aqueous solution of neutral pH.

pronounced compared to samples exposed to an aqueous solution of neutral pH, and hence are another indication of degradation. However, no significant mutual differences where observed between the samples, with exception of the sample of 90 days, whose peaks at around 2940, 1410 and in the range of $1030 - 1150\,\mathrm{cm}^{-1}$ increased slightly compared to the other adjacent peaks in the spectra.

When analysing the ATR-IR spectra of AlgAA/AM exposed to an aqueous solution of neutral pH, no signs of degradation over time are observed. The only noticeable difference is spotted at $1550\,\mathrm{cm}^{-1}$ for the sample of 28 days. This peak is related to the asymmetric carbon-oxygen bond v_{as}(C-O) of carboxylate moieties. The ATR-IR spectra at the peak follows a convex curve, whereas a concave form is observed in the spectra of the other samples. Thus, this indicates a slight increase of the peak in the sample of 28 days. In case of the addition of AlgAA/AM to a cement filtrate solution, the same degradation compared to the samples exposed to an aqueous solution are observed. They were described in the above paragraph. No significant differences between the samples were observed. Thus, the increased variation in the swelling properties over time, as observed in figure 3.14, could not be attributed to severe degradation.

Over the course of time, a slight increase of the peak at $1410\,\mathrm{cm}^{-1}$, related to the symmetric carbon-oxygen stretch vibration v_s(C-O), is observed for samples containing ChiMOD/D-MAEMA who were exposed to an aqueous solution of neutral pH. When the hydrogel was

exposed to cement filtrate solution, the sample of 28 days possesses a slightly different ATR-IR spectra. The peak at 1700 cm^{-1} decreased, whereas the peaks at 1550 and 1410 cm^{-1} increased slightly compared to the adjacent peaks. This can be attributed to the hydrolyses of incorporated methacrylate ester functionalities of ChiMOD which results in the formation of carboxylate moieties. However, this phenomena is only visible in the sample of 28 days and no significant difference is observed between the other samples.

Despite a sign of degradation over the course of time was expected in samples of MBA/DMAEMA exposed to an aqueous solution of neutral pH, no significant difference is observed in the ATR-IR spectra of the different samples. However, a small peak at 1550 cm^{-1} emerged for the sample of 28 days. When MBA/DMAEMA is added to a cement filtrate solution, this peak is observed in all samples and it tends to increase over time, but at a very slow pace. The peak is related to the asymmetric carbon-oxygen bond strength v_{as}(C-O) of carboxylate functionalities which could be a result of the hydrolysis of the ester v(C=O) peak in DMAEMA at 1720 cm^{-1}. However, no significant reduction of this peak is observed.

Chapter 4

Evaluation of pH responsive hydrogel encapsulated bacteria for self-healing mortar

4.1 Immobilisation of the bacterial spores into the hydrogel

The spores of *B. sphaericus* were encapsulated as explained in section 2.2.2.4 on page 33. Previously, the immobilisation of bacterial spores during polymerisation was done according to a process called "UV Curing", in which ultraviolet light (UV) is used to initiate a photochemical reaction that generates a polymeric network. After UV radiation for 1 hour, a hydrogel sheet of about 10 g polymer solution (20m% hydrogel) is acquired. This polymerisation technique is found to be an effective immobilisation method for bacterial spores, without compromising their viability [62]. However, in order to synthesize a large amount of hydrogel, the procedure needed to be repeated several times. For this reason, a free radical polymerisation in solution was proposed to synthesise the hydrogels. The immobilisation involved the addition of 0.5 ml bacterial spores stored in a 8.5 g/l NaCl saline solution per 1 g theoretical synthesised hydrogel before the addition of the radical initiator ammonium persulfate (APS). The bacterial spores suspension used for viability tests contained 10^9 cells/ml, whereas the suspension used for the evaluation of self-sealing and crack closure of mortar specimens contained twice as much bacterial spores.

In order to improve the survival of the bacterial spores during synthesis, the author reduced the temperature on which the synthesis should be performed according subsection 2.2.2 on page 31. However, after the addition of bacterial spores which were injected in a saline suspension, the polymerisation reaction failed. The failure could be attributed to one or more of the following parameters: (1) the change in temperature at which the synthesis took place, (2) to duration of the flushing cycle after addition of the bacterial suspension, (3) the saline

solution in which the bacterial spores were stored. To determine the cause of the failure, a hydrogel was synthesised with the addition of a 8.5 g/l NaCl saline solution. It was found that this was one of the failure mechanisms, consequently before addition of the bacterial solution, the bacterial spores where harvested by centrifuge at 7000 rpm and added to an equal amount of Milli-Q water to preserve the bacterial suspension concentration.

4.2 Viability of hydrogel encapsulated spores

In order to prove the concept of hydrogel immobilised bacteria, the bacteria should survive the polymerisation reaction and consecutive processing before obtaining the final product, a fine dry hydrogel powder. Therefore, specific batches of hydrogels were prepared to be subjected for a viability test. After removal of the hydrogel from the three-neck flask, the hydrogel was cut into small pieces. A sample was taken from those pieces before and after dialyses, after freeze drying via lyophilisation and consequently after grinding, all of an equal portion by mass. Prior to freeze drying (Christ Alpha 2-4 LSC, Germany) of the samples, they were put into a freezer at $-20\,^{\circ}\mathrm{C}$, just long enough to let the sample freeze completely. After lyophilisation, the dried hydrogel was grinded into a fine powder with an IKA A 11 basic Analytical mill. Eventually, the four samples were subjected to the viability test, as described in 2.3.4 on page 38. The viability test is comprised of the evaluation of decomposed urea after exposure of the sample to a growth medium. Both hydrogels with and without incorporated spores are tested. Because of favourable condition of the growth medium, the bacterial spores are supposed to germinate into active viable cells and decompose urea through their ureolytic activity. The growth medium contains 20 g/l of urea of which about ± 18 g/l remains available after autoclaving. During autoclaving a small amount of urea was hydrolysed to liberate ammonia. Thus, about 1 to 2 g/l of the decomposed urea shown in figure **??** on page ?? can be attributed to this phenomena.

The viability test related to the results shown in figure 4.1 on the next page were performed on hydrogels who were synthesized according the methods described in subsection 2.2.2 on page 31 and 2.2.2.4 on page 33. Both ChiMOD/DMAEMA and MBA/DMAEMA were successfully synthesized, provided that the temperature of the original synthesis method was retained. In addition, this temperature was maintained for 24 hours to favour the polymerisation as was described by Mignon et al. (2016). On average, 4 g/l urea was decomposed after three days of exposure to the growth medium. This amount may be attributed to both the decomposition of urea after autoclaving of the medium and presence of some contamination. The hydrogels were synthesized in non-sterile conditions and besides that, some bacterial strains from the air can also decompose urea. For practical reasons, only one replicate per stage per hydrogel was subjected to the viability test. Thus, no conclusions could be substantiated by statistical evidence. A slight increase in the amount of decomposed urea was

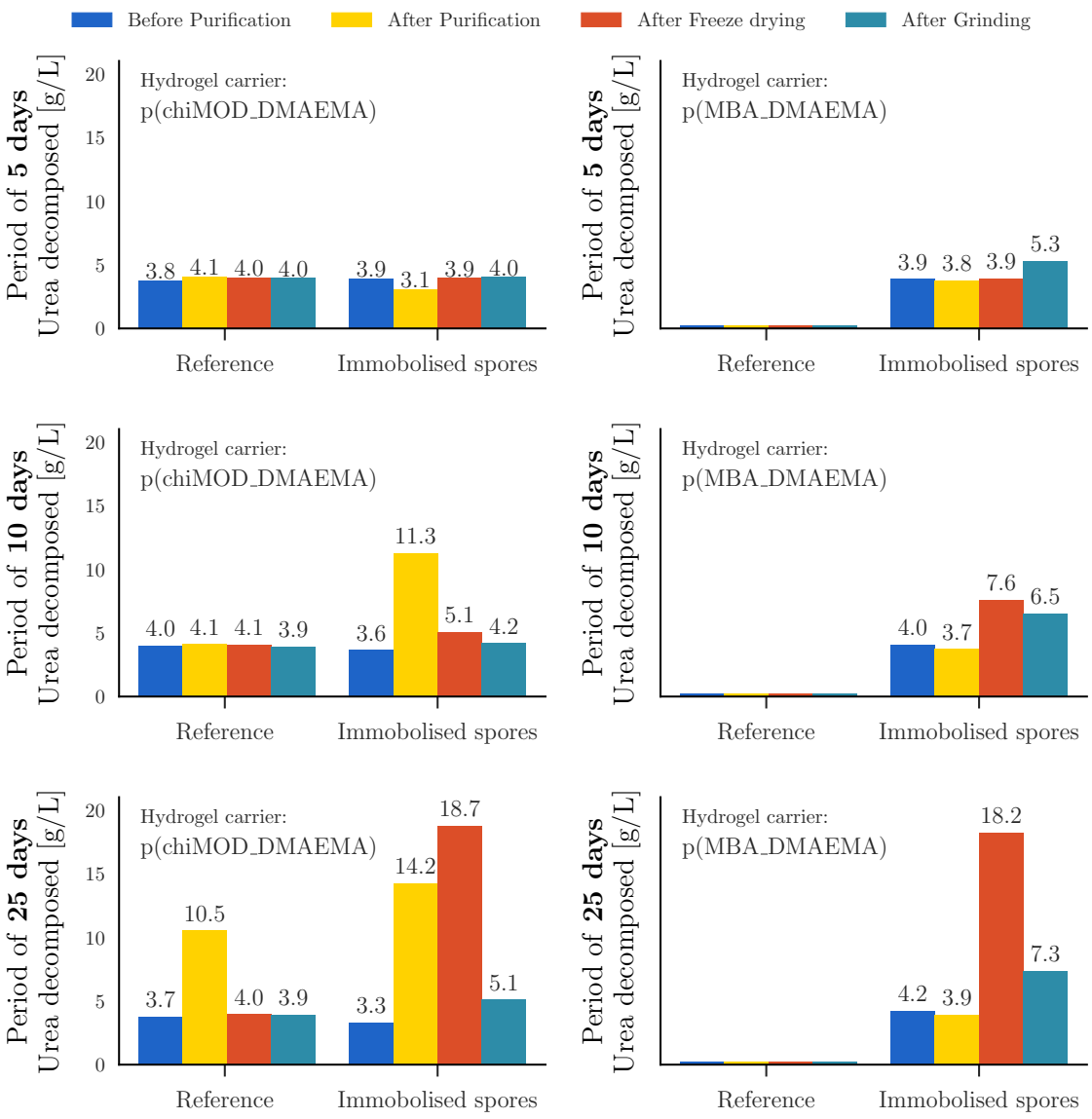

Figure 4.1: Urea decomposed in a growth medium with the addition of hydrogels with and without bacterial spores evaluated over 5, 10 and 25 days.

observed after grinding the sample of MBA/DMAEMA immobilised spores. By grinding the hydrogel in small particles, the available surface area increases, and hence bacterial spores can be more easily exposed to the growth medium. Even after 10 days, no clear trend was observed. Half of the urea was decomposed in the sample containing ChiMOD/DMAEMA immobilised bacteria after purification (AP), whereas the reference sample, as well as the samples of other stages show little or no activity. During synthesis of ChiMOD/DMAEMA, a small amount of acetic acid was added to the mixture to improve the solubility of ChiMOD. During purification, the acetic acid can leach out of the hydrogels in which it was trapped. By

consequence, the pH of the hydrogel sample after purification should be higher than that of the sample before purification (BP). Thus, germination of bacterial spores and the ureolytic activity can be promoted if the sample reaches a favourable pH of ±8.5 . However, the pH of samples after and before purification equals to respectively 7.53 and 7.56. In case of MBA/D-MAEMA, a slight increase was noticed for the samples after freeze drying and grinding. After being exposed for 25 days to the growth medium, still no significant ureolytic activity after grinding was observed for samples containing hydrogel immobilised bacteria. However, urea was almost completely decomposed for bacterial spores after freeze drying. In addition, half of the urea was decomposed of the reference sample before purification. Over time, the risk of contamination increases and thus, this is attributed to the latest observation. Since the temperature during synthesis cannot be changed, it was proposed to try to minimise the time on which the polymerisation reaction was maintained.

In what follows, hydrogels of a shorter synthesis time are used for testing. Once a solid hydrogel was formed during synthesis, the three-neck flask was removed from the oil bath and the sealed N_2 environment was opened. Synthesis of AlgAA, AlgAA/AM and ChiMOD/D-MAEMA used for viability tests as shown in figure 4.2 took respectively 1, 5 and 5 hours.

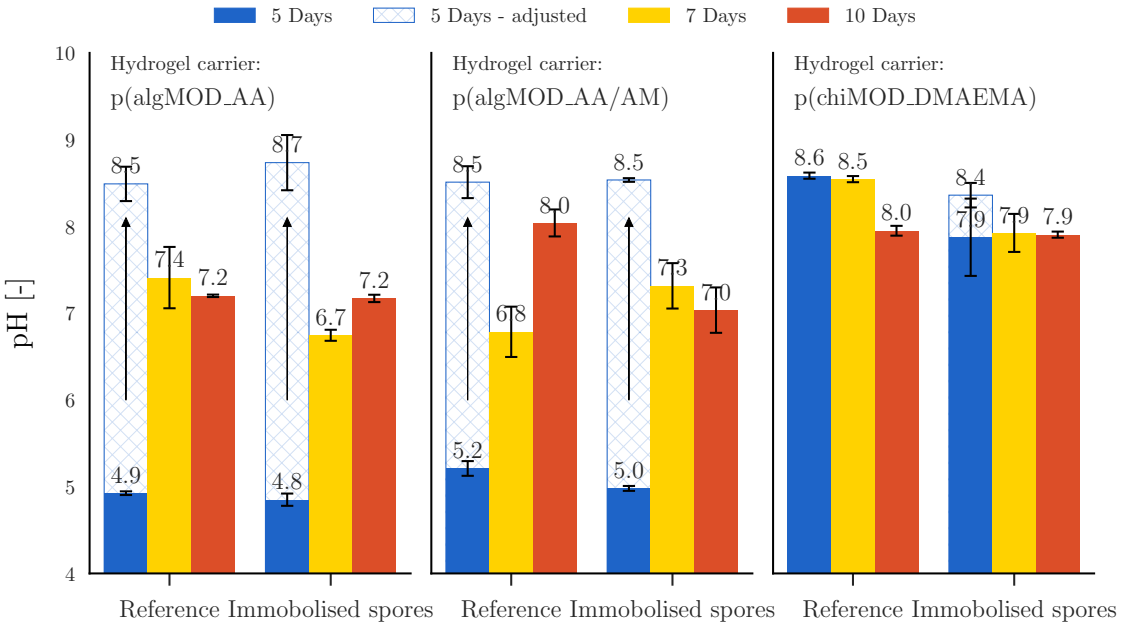

Figure 4.2: pH measurement of the growth medium with the addition of hydrogels of reduced synthesis time with and without bacterial spores evaluated over 5, 7 and 10 days. After 5 days, the pH of the samples were adjusted to ±8.5 by a 5M NaOH solution in order to promote the germination and consequently the ureolytic activity of the bacterial spores.

Due to problems related to the TAN measurements, pH measurement which were earlier used as a supplementary technique to verify the TAN measurements, became the primary indicator to verify bacterial activity. It should be noted that this indicator is not quantitative. The pH measurements were performed on samples containing 0.3 g hydrogel per 25 ml growth medium and are shown in figure 4.2 on the previous page. In this figure, the dependant variable pH is displayed on a scale from 4 to 10 in order to make small changes more clear. An increase in pH over time can be attributed to the decomposition of urea, producing ammonia molecules which get protonated under physiological pH and result in a net increase in pH [97]. The pH was measured after 5 days and a significant drop compared to that of the growth medium ($\pm$9) was noticed for the samples containing hydrogels composed out of acrylic acid (AA) monomers. In addition, a slight decrease is noticed for ChiMOD/DMAEMA. This drop in pH can be attributed to the presence of carboxylic acid moieties on the hydrogels backbone. To compensate this reduction, a 5M NaOH solution is added to adjust the pH to $\pm$8.5. After two more days, all samples encountered a decrease of pH. The final measurement was performed after 10 days and the results could not provide a decisive answer regarding the viability of the bacterial spores. A slight increase was noticed for the sample of AlgAA immobilised spores, whereas that of its reference dropped. The opposite behaviour is observed in the case of AlgAA/AM, presumably due to contamination of its reference sample, though this does not explain the decrease in pH of its sample containing immobilised bacteria. While the pH of the sample containing ChiMOD/DMAEMA immobilised bacteria remained stable, a significant drop is observed after 10 days for its reference sample. Despite that no increase is observed in the former, there might be some bacterial activity that causes the pH to remain stable.

Selecting appropriate hydrogel carrier for the application in cementitious materials

The use of hydrogel immobilised spores for the application in self-healing concrete is only appropriate if the mechanical properties of the cementitious materials are not compromised while bacterial spores should still be viable and able to germinate upon crack formation. AlgAA and ChiMOD/DMAEMA are preferred over the other synthesised hydrogels regarding the mechanical performance of the mortar specimens after addition of the hydrogels, as discussed in subsection 3.2 on page 58. However, based on previous tests, it could not be concluded that the spores were still viable after immobilisation in hydrogels. Furthermore, the hydrogels composed out of acrylic acid (AA) monomers had a major influence on the pH of their surrounding medium, decreasing the ability of spores to germinate. Despite the remaining uncertainty regarding the viability of the hydrogel immobilised spores, AlgAA and ChiMOD/DMAEAM were selected to further develop. A large batch ($\pm$12 g) with and without bacterial spores ($4.6 \cdot 10^9$ spores per 1 g hydrogel) of each material was made and a viability test was performed on the final powder of each hydrogel. After hydrogel immobilisation and the subsequent processing (dialysis, freeze drying via lyophilisation and grinding), spores were still viable. This was confirmed by both pH measurements and evaluation of

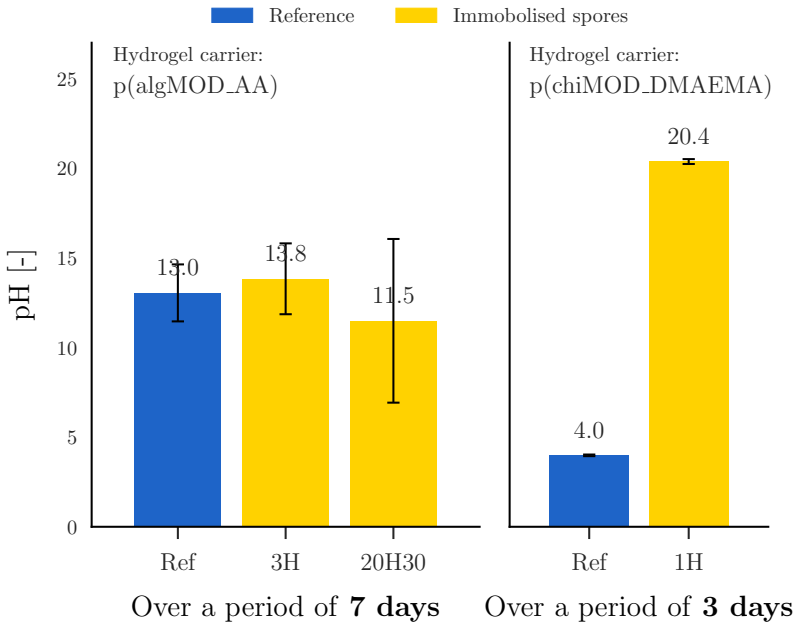

Figure 4.3: Urea decomposed in a growth medium with the addition of p(algMOD_AA) and p(chiMOD_DMAEMA) with and without bacterial spores evaluated over respectively 7 and 3 days. After 3 days, the pH of the samples containing p(algMOD_AA) were adjusted to ±9 by a 5M NaOH solution in order to promote the germination and consequently the ureolytic activity of the bacterial spores.

decomposed urea, as shown in figure 4.3. The viability test was performed on samples containing 100 ml growth medium in addition to 0.8 g of hydrogel powder. After three days, the pH of the samples containing AlgAA were adjusted to ±9 by 5M NaOH solution. The amount of decomposed urea of those samples was measured four days afterwards and showed a similar urea decomposition and pH around 9.5 for both samples with and without bacteria. It should be noted that two different large batches of AlgAA immobilised bacteria were synthesised. During grinding, a small amount of AlgAA without bacteria was mixed with AlgAA with bacteria (3H) that was synthesised over 3 hours. Consequently a new polymerisation reaction was set up but failed to form a firm gel after 3 hours. The gelation took place overnight and was terminated after 20 hours 30 minutes (20H30). On the other hand, samples of ChiMOD-/DMAEMA immobilised spores (1H) showed a complete decomposition of urea within three days, while its reference showed a very limited urea decomposition.

4.3 Leakage of spores from hydrogel

After being immobilised inside the hydrogel, bacterial spores can still escape from their carrier. Thus, the leakage of the spores from the hydrogel is evaluated as described in subsection 2.3.3

on page 37. This method is also used to determine the amount of spores in the original suspension, which appears to be equal to $4.6 \cdot 10^9$ spores/ml. However, spores are harvested using a centrifuge and are resuspended in half of the original amount of solution, resulting in spore concentration of $9.2 \cdot 10^9$ spores/ml. Subsequently, 0.5 ml spore suspension was added to a theoretical 1 g of synthesised hydrogel. Thus, the theoretical amount of bacterial spores can be estimated at $4.6 \cdot 10^9$ spores/$g_{hydrogel}$. The leakage test is closely related to the viability tests since the leakage is expressed as the number of colonies formed on the agar plates. Those colonies could only be related to viable cells. The leakage was evaluated for samples in contact with a steril NaCl solution for 5 minutes, 1 and 2 days. The series in which colonies were expected to be attributed to contamination will not be discussed. In general, the leaked amount of spores was negligible or even nonexistent. A consistent increase in leakage ratio is observed for ChiMOD/DMAEMA immobilised bacteria, increasing from 0.0002% at 5 minutes immersion, 0.002% at 1 day immersion and 0.02% after 3 days of immersion. Thus, it can be concluded that most of the spores were still inside the hydrogels.

4.4 Self-healing efficiency

In what follows, the self-healing efficiency is evaluated based on the ability to restore the water transport properties upon crack formation, as described in subsection 2.4.1.3 on page 41, and the crack closure by means of an optical microscope which is described in subsection 2.4.2 on page 42. The strength regain of the mortar specimens was not evaluated.

4.4.1 Evaluation of water transport properties by means of a water flow test

The development of water transport properties over the course of time under full immersion were analysed for a pre-cracked sample of controlled crack width. Despite the effort to discard the influence of the crack width on the sealing efficiency (SE) by closely targeting the initial crack width by a displacement sensor, some deviation in average initial crack width is observed. The targeted crack width on the apparatus during loading varied between 240 and 280 µm. However, some of the crack width is recovered after unloading. Consequently, the displacement sensor measured values between 150 and 225 µm after unloading. Crack measurement at the particular location, i.e. the side of the specimen where the displacement sensor was glued, showed that the real crack width varies between 79 µm and 256 µm for R1 and AAS20H30, respectively. It should be noted that the series are labeled by their name (R, N, etc.) in addition of an integer (1, 2 or 3) referring to the particular replica. If a series is indicated merely by its name, than average values over the three replicas will be given. The average crack width of the crack at the bottom varied between 124 µm and 296 µm for R1 and CD3, respectively. However, 76.6% of samples have an average crack width that lie between 200 and 275 µm. The water flow test itself is performed as described in section 2.4.1.3 on

page 41. The water flow was measured after 3 days, 4 weeks and 10 weeks while preserving the samples under full immersion.

Influence of initial crack width

Not a single sample stopped the water flow completely. The water transport properties are evaluated by the sealing efficiency (SE), a parameter which rates the decline of the average flow rate compared to its initial rate. The influence of the initial crack width on the final self sealing for each replica within a particular series varies. For samples AAS3H and CD, the smallest sealing efficiency of about 53.8 and 80% is obtained for its largest initial crack width equal to 275 and 296 µm, respectively. On the other hand, the replica of minimal initial crack width of samples AA, AA+S, AAS20H, CDS and N possesses the lowest self sealing within the particular series. Thus, regardless the nature of the sample, it can be concluded that a higher sealing efficiency is obtained in samples of greater initial crack width. If the distribution of the initial crack width over the different series is taken into account, it is observed that only average sealing efficiencies of samples within the range of 200 to 250 µm are representative for the global behaviour. Hence, the previous conclusion is confirmed.

Table 4.1: Influence of the initial crack width on the sealing efficiency (SE)

Crack width range	*Series*	*SE* [%]
(100, 125]	R	69.08
(125, 150]		
(150, 175]	AA+S	38.47
(175, 200]	AA, AA+S	55.63 ± 9.24
(200, 225]	R, N, NS, AAS20H30	66.09 ± 10.95
(225, 250]	R, N, NS, AA, AA+S, AAS3H, AAS20H30, CD, CDS	71.24 ± 11.52
(250, 275]	AAS3H, AAS20H, CD, CD+S	70.98 ± 11.83
(275, 300]	CD, CDS	83.59 ± 5.04

Water transport properties

The results of the water flow tests can be found in section D.1 of appendix D on page 120. An overview of development of the sealing efficiency is shown in figure 4.4 on the next page. In this representation, the influence of the initial crack width is not taken into account. However, the conclusion of previous paragraph is kept in mind. The highest average sealing ratio of 85.9% was found for the sample CDS. Specimen incorporating ChiMOD/DMAEMA with and without the addition of bacterial spores perform better than both the reference samples

and samples including AlgMOD/AA hydrogel. After the first incubation period, swollen hydrogel particles were visible on the surface of the specimen incorporating AlgMOD/AA, whereas the surface of specimens incorporating ChiMOD/DMAEMA showed no presence of hydrogel particles. Thus, due to the swelling of AlgMOD/AA, some surface damage occurred and the surface became more rough. Despite this substantial swelling at the surface, no significant improvement in sealing efficiency is observed compared with samples containing ChiMOD/DMAEMA. Moveover, the series containing ChiMOD/DMAEMA seems to perform better than the series containing AlgMOD/AA, though no statistically significant difference, with the exception of AA+S - CDS and AA - CD, is observed between those samples using a Dunnett T3 post hoc test ($p = 0.05$). The large deviation of the average sealing efficiency for each series is not only related to the initial crack widths of its replicates since the third largest deviation, that of the sample CD+S, is found for replicas whose widths lie within the narrow range of 250 and 275 µm.

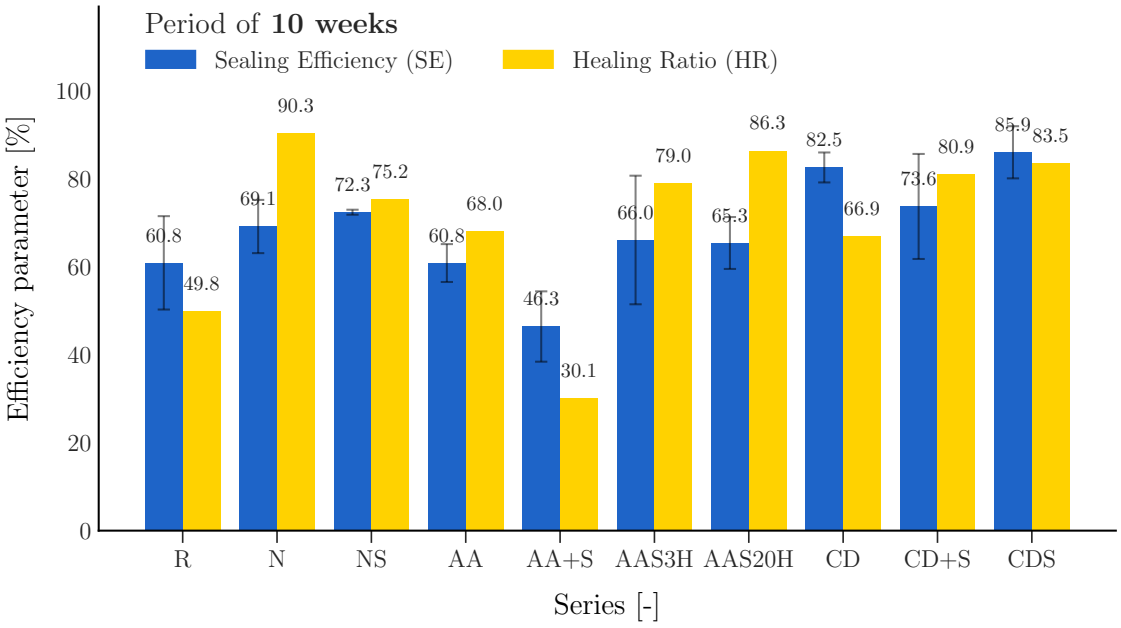

Figure 4.4: Sealing efficiency for the different series under full immersion over a period of 10 weeks.

Crack closure evaluation

Aside the sealing efficiency, the healing ratio is showed in figure 4.4 as well. It was noticed that even if a high healing ratio (HR) is obtained, the sealing efficiency can still be substantially lower. This was the case for the specimens N and AAS20H. In those particular series, the cracks at the bottom were closed completely up to a great extend, whereas the crack at the side remained open. Thus, the majority of the water left the specimen along the side and subsequently dropped into the container. The relative difference between the

two efficiency parameters is smaller for the specimens containing ChiMOD/DMAEMA then for those containing AlgMOD/AA. Thus, the sealing efficiency is relatively larger when compared to its associated healing ratio for the ChiMOD/DMAEMA specimens. This difference with AlgMOD/AA may be explained by the increased availability of hydrogel particles in the specimens containing ChiMOD/DMAEMA compared to that of AlgMOD/AA incorporated specimens. The water flow tests were performed within 10 minutes after removal of the specimens from their incubation medium in order to prevent water uptake by the cementitious matrix and to rely on fully swollen particles. Due to the presence of those swollen particles, the sealing efficiency might get promoted. However, if those hydrogel particles get flushed out of the crack after several water flow tests, they no longer promote but instead reduce the sealing efficiency. This might have happened to the sample AA+S. Initially, hydrogel particles blocked a considerable amount of liquid during the water flow test, but get flushed out during subsequent tests and because of degradation. As can be seen in figure 4.5, healing products are especially formed in the vicinity of the edge. Furthermore, more healing products are formed near the bottom of the sample in comparison to the top.

Figure 4.5: A typical pattern of healing products observed for specimens under full immersion

Conclusions

Specimens containing ChiMOD/DMAEMA performed better than both the reference specimens and those containing AlgMOD/AA. AlgMOD/AA is prone to degradation as was discussed in section 3.3 on page 60 and consequently might get flushed out during incubation because of its looser network compared to the ChiMOD/DMAEMA hydrogel. Initially, the hydrogel particles of AlgMOD/AA slow down a substantially amount of water during testing, scoring a relatively low water flow rate (WF_{avg}). However, after some of the hydrogel particles leave the crack, the water flow rate is mainly influenced by the crack closure due to formation of minerals and less affected by the presence of hydrogel particles. Thus, this phenomena inhibits a rapid increase of the sealing efficiency. Moreover, in figure D.5 and D.7 on page 122 an increase in water flow rate between 4 and 10 weeks is noticed. This can be explained by

the previously discussed phenomena. Due to a substantially reduction of hydrogel particles in the crack, their beneficial effect on the water flow rate disappears. This is not the case for the specimens containing ChiMOD/DMAEMA where a significant improvement in sealing efficiency is noticed between 4 and 10 weeks, whereas the improvement of AlgMOD/AA specimens is less extensive and tends to stagnate. An in depth study into the crack closure behaviour is necessary to further compare specimens with or without hydrogel encapsulated spores. The crack closure test will be performed on specimens in addition of ChiMOD/DMAEMA. This hydrogel is selected based on the viability tests discussed in section 4.2 on page 68 in this chapter and the conclusion drawn in this particular section.

4.4.2 Microscopic evaluation of crack closure

4.4.2.1 Crack closure evaluation over the course of time

The crack closure was evaluated over a period of 1, 2, 3, 4 and 10 weeks using an optical microscope. Six different series were prepared as described in subsection 2.4.2 on page 42. Each series consists of two replicas of which one is brought under full emersion and the other under wet/dry cycles of 2 hours immersion alternated by a drying period of 4 hours. A detailed overview per series of the crack closure evolution over time is given in section D.2 on page 123 of Annex D. In what follows, the samples under full immersion will be discussed first followed by the samples under wet/dry cycles. As will be further discussed, the maximum completely healed crack width does not give a good indication of the expected average healing efficiency. Therefore, the crack closure should be discussed in detail.

Full immersion

Crack healing in the specimens of the R series under full immersion was primarily limited to the bottom face of the specimen (figure D.11 on page 124). The crack widths up to 0.22 mm of the bottom face had an obvious decrease in the first week. The crack closure after the first week happened at a slower pace. This is confirmed by the development of the slope of the trend line, decreasing from 0.60 at 1 week to 0.30 after 10 weeks. The complete crack closure of the cracks at the side face remains below 0.20 mm and becomes obvious after 4 weeks. Cracks at the top surface are more difficult to heal, whereas their maximum completely healed crack width is below 0.15 mm.

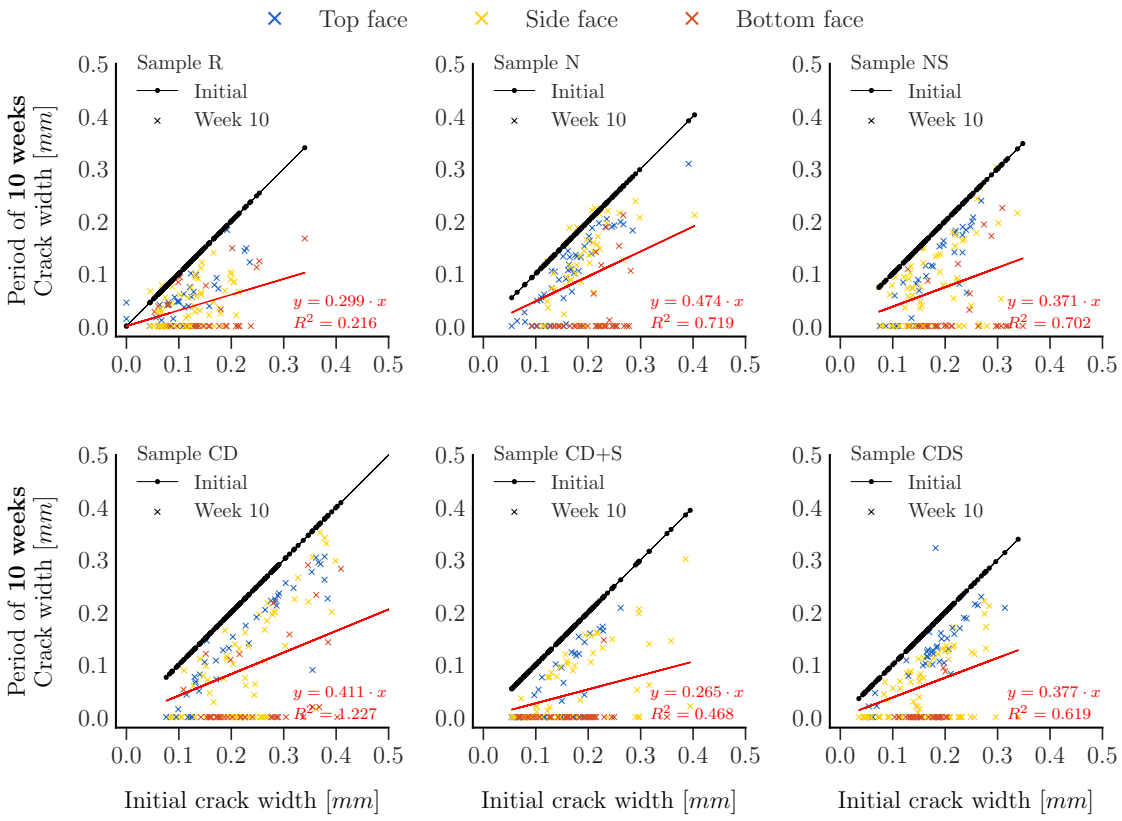

Figure 4.6: Overview of the development of crack widths in specimens under full immersion over a period of 10 weeks

The specimen N had a somewhat similar self-healing efficiency compared to R. Again, the bottom face had the highest maximum crack closure ability. By exception of one crack, all cracks below 0.10 mm were healed after 4 weeks. The slope of the trend line decreased from 0.74 at 1 week to 0.48 after 10 weeks. After 10 weeks, the maximum completely healed crack width for the bottom face lies around ±0.28 mm, whereas that of the other crack faces lies below 0.2 mm.

The specimens embedding both nutrients and non-encapsulated spores (NS) had a similar gradual decrease of crack widths compared to R and N. However, the maximum completely healed crack width was about 0.34 mm and multiple completely healed cracks of the side surface fell within the range of 0.2 to 0.3 mm, as can be observed in figure D.13 on page 126. Thus, the direct addition of bacterial spores might improve to healing of larger cracks. Furthermore, the measurement points in figure D.13 dissociates themselves further from the initial line than both R and N samples do.

Within one week, the sample of the CD series under full immersion healed particularly well in the 0.02 to 0.23 mm. The crack widths above this threshold only started to heal gradually

after 2 weeks. The healing of cracks at the bottom face progresses at a slower pace than in previously discussed series. However, cracks up to 0.4 mm were able to heal completely after 10 weeks, whereas the maximum completely healed crack width after 4 weeks was limited to about 0.3 mm. The crack closure at the top face of the specimen was limited to 0.17 mm.
Similarly to CD, crack healing up to 0.21 mm started after 1 week. The maximum completely healed crack widths was about 0.3 mm and was reached after 3 weeks. However, the healing of cracks beyond that extend is halted after 3 weeks. All cracks, with the exception of one of 0.23 mm, of the bottom face were completely closed within 10 weeks under full immersion. In the end, the slope of the trend line dropped to 0.265. The crack closure at the top face of the specimen was limited to 0.18 mm.
Considerable crack healing already occurred in the first week in the specimen of the CDS series. Cracks up to 0.24 mm were entirely closed. At a slow pace, cracks widths gradually decrease over time. The maximum completely healed crack width is observed after 2 weeks and equals about 0.34 mm. After 10 weeks, almost all cracks of the bottom face were completely closed. No significant improvement regarding the crack closure at the top face is observed. The performance of the series NS, CD, CD+S and CDS are very similar. Compared to the series R and S, they have a higher potential to completely close cracks within the range 0.3 to 0.4 mm. In figure 4.6 on the previous page, the crack width decrease after 10 weeks for all six series under full immersion is showed.

Wet/dry cycles

A limited amount of crack healing occurred in the specimens of the R series under wet/dry cycles, as can be observed in figure D.11 on page 124. The crack width decrease observed after one week remains unchanged up to 4 weeks. Thus, no cracks were closed completely. After 10 weeks, crack closure results are more dispersed and more crack closure is observed, though only a few cracks of maximum 0.1 mm are closed completely.
The specimen of the N series showed a significant increase in crack closure efficiency. After 1 week, some cracks up to 0.14 mm were entirely closed, whereas the maximum completely closed crack width after 10 weeks was equal to about 0.24 mm. Most of the crack width decrease occurred within the first week. Cracks at the top surface closed at a much slower pace than those at the other surfaces and cracks closed completely were limited to 0.18 mm. Whereas crack decrease was barely noticed above 0.25 mm in the specimen of the N series, this is no longer true for the specimen of the NS series. Most of the crack width decrease occurred within the first 2 weeks. The maximum completely closed crack width within those 2 weeks is equal to about 0.26 mm. However, no larger cracks were closed over the course of time. Even cracks larger than 0.25 mm were partially closed.

The sample of series CD showed a poor crack closure behaviour compared to the one of series N, though both include nutrients in the same amount. It is observed in figure D.14 on page 127 that only a limited amount of crack decrease occurred after 1 week under wet/dry

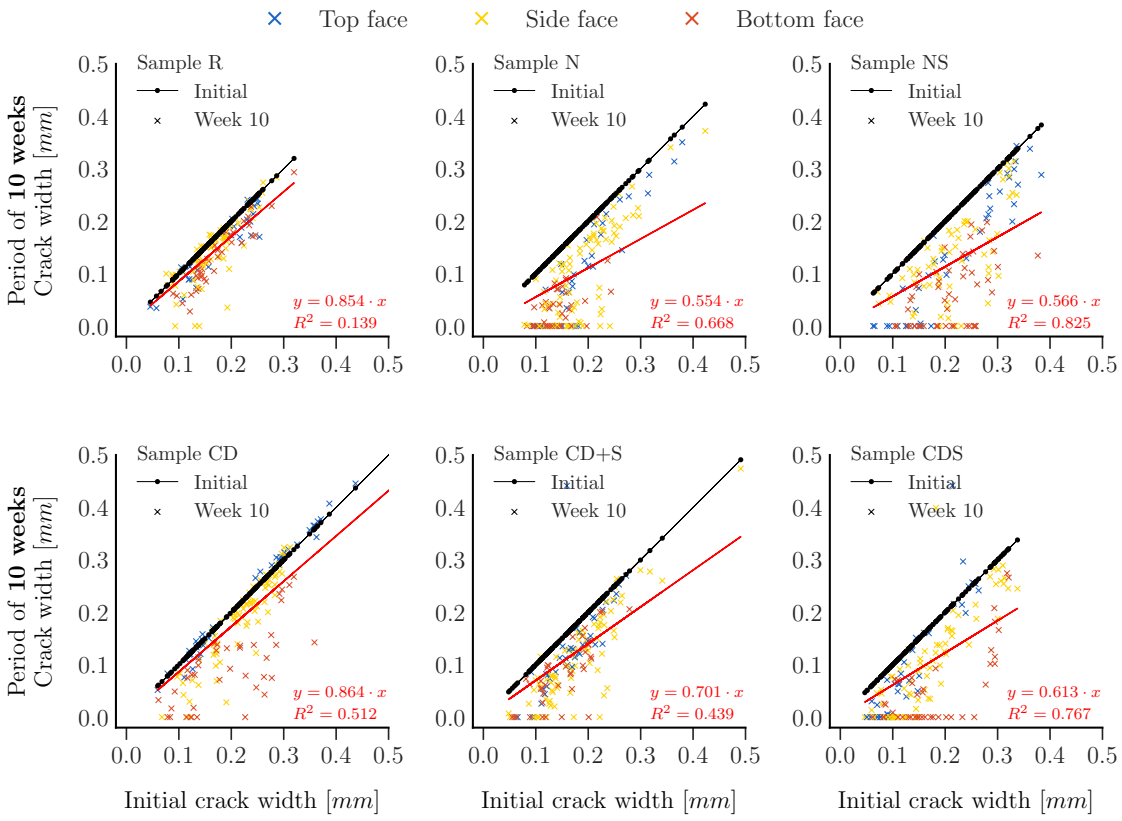

Figure 4.7: Overview of the development of crack widths in specimens under wet/dry cycles (2 hours wet alternated by 4 hours dry) over a period of 10 weeks

cycles. After 2 weeks till 10 weeks, the crack width changes were not obvious anymore. The maximum completely closed crack width was limited to about 0.22 mm. However, in general, about half of the cracks up to 0.14 mm located at the bottom face of the specimen were entirely closed. Above this threshold, partially closure was observed for cracks at the bottom surface, whereas no change of the crack widths at the top surface was observed.

Obvious crack closure over the course of time is limited to crack widths up to 0.23 mm for the specimen of the CD+S series. However, over the course of time, almost all cracks start to deviate from their initial crack width. This was not the case for the specimen of the CD series. Complete crack closure occurred especially below 0.13 mm and the maximum complete crack closure was about 0.21 mm.

A slight improvement of the crack closure over the CD+S series is observed for specimens of the CDS series, incorporating hydrogel immobilised bacteria, as can be seen in figure D.16 on page 129. Up to 0.2 mm an obvious decrease in crack width occurred after 1 week and gradually increases over the course of time. After 2 weeks, a considerable number of cracks below 0.2 mm were entirely closed, most of them positioned at the side and bottom face of the

specimen. Moreover, most of the cracks located at the top which are smaller than 0.1 mm, were entirely closed after 10 weeks. The crack width decrease of cracks beyond 0.2 mm progresses at a slow pace, though an obvious decrease is observed between 4 and 10 weeks.
In figure 4.7 on the previous page, the crack width decrease after 10 weeks for all six series under full immersion is showed. The maximum completely closed crack width was similar for the samples of series N, NS, CD+S and CDS. The crack closure results of the NS series are way more dispersed than those of the N series, and hence more distanced from their initial crack width position. Thus, direct addition of bacterial spores may increase the potential to partially heal cracks below 0.25 mm. In specimens of series CD+S and CDS, the cracks are either completely closed or slightly decreased in size. The number of completely closed cracks is considerably larger for series CDS than for series CD+S, respectively 51 and 19, whereas that of series NS equals to 31 cracks.

The slope of the trend line in figure 4.6 on page 78 and 4.7 on the previous page indicate the development of the crack closure. Cracks of a higher initial width will have a greater influence on the slope than smaller cracks since the trend line is pivoted around zero. Thus it reflect the efficiency of the crack closure with great importance to larger cracks. However, this is not a qualitative approach since the cracks are not distributed evenly and the maximum crack width differs between the several samples, and hence it should not be used to compare different series. However, it can still be used to compare the crack closure of a particular sample over the course of time and is displayed on the figures found in section D.2 on page 123.

4.4.2.2 Healing ratio evaluation after 10 weeks

The crack healing ratio (HR) is calculated as described in subsection 2.4.2.4 on page 44. The healing ratio both depends on the initial crack width and the type of specimens, included as independent variables in figure 4.8 on the following page and 4.8 on the next page. As earlier discussed, the crack closure also depends on the orientation of the samples during immersion, and hence could be used as third independent variable. However, the aim of this section is to get a general view of the healing within distinct cracks ranges of 50 µm. In addition, the healing ratio at each crack location is presented to give an idea about the spread of the results.

Full immersion

Overall, the healing ratio decreased for increasing crack width. It should be noted that the cracks widths were not perfectly homogeneously spread. No cracks of size within the range of 350 to 400 µm of series R, NS and CDS are measured. Within each crack width range, the average healing ratio for the R series is higher than 50%. The highest average healing ratio is for the R series is found between 50 and 200 µm and is equal to about 76%. The series N had a high HR of about 91% for cracks between 50 and 100 µm and reaches a stable HR between

150 and 300 µm but eventually experienced a significant decline beyond that boundary.

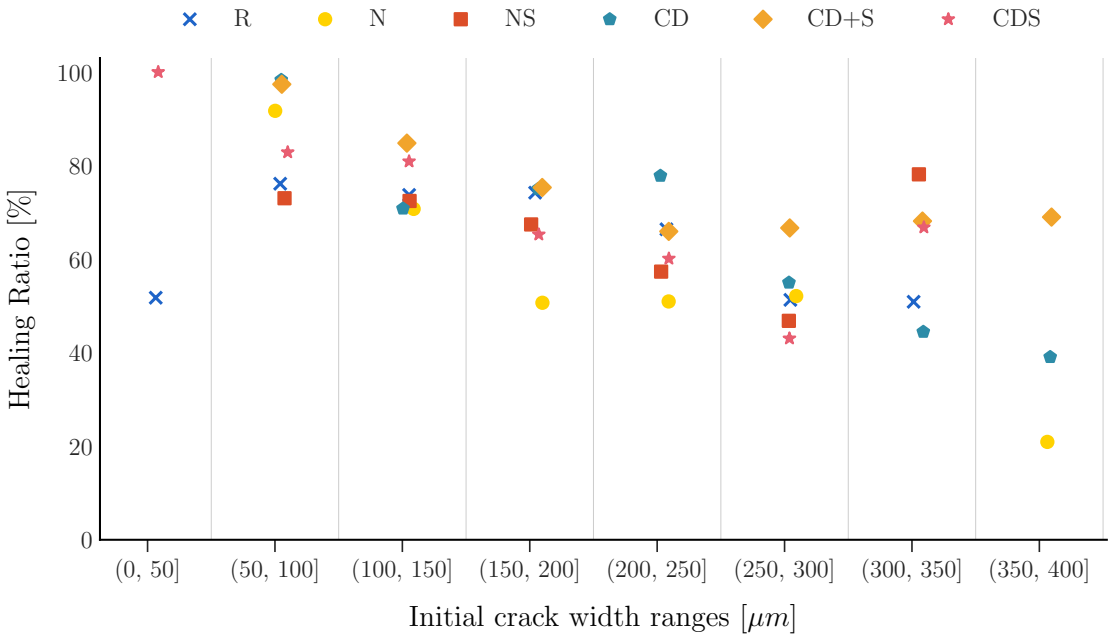

Figure 4.8: Average crack healing ratio in different ranges of crack widths of specimens under full immersion over a period of 10 weeks

In that particular range, a higher HR was obtained after direct addition of bacterial spores (NS series). The NS series performed in particular well in the range of 300 to 350 µm, having an average healing ratio of about 78% for 10 cracks within this range, whereas a moderate HR was experienced for smaller cracks, varying between 46 and 73%. The HR for the CD series for cracks between 50 and 100 µm is equal to about 98% followed by a range in which the HR varies around 74%, while beyond 250 µm, the HR drops gradually and becomes 39% for cracks between 350 and 400 µm. The development of the healing ratio for samples of direct addition of bacterial spores in addition of hydrogel particles (CD+S series) is very stable, though the average healing ratios for crack widths beyond 250 µm were determined on a small number of measurements. The maximum HR that series CD+S obtained was 97% within the range of 50 to 100 µm and dropped to a more or less stable value about 66% for the entire range between 200 and 400 µm. At last, the HR development of the CDS series is discussed. Of the 7 measured crack widths below 50 µm, all of them were completely closed within 10 weeks. Then, a gradual decrease is noticed until an initial crack width of 300 µm. In the range of 250 to 300 µm, the HR is outperformed by all other specimens. However, the average healing ratio of the 2 cracks of an initial crack width varying between 300 and 350 µm is equal to 67% which is higher than that of series R and CD. To conclude, it seems that specimens containing bacterial spores, whether or not immobilised in a hydrogel, had a better crack closure efficiency (HR $>$ 60%) than specimens without bacterial spores within the range of

250 to 400 µm. In figure 4.9 a clear view of the healing ratio for each individual crack is given.

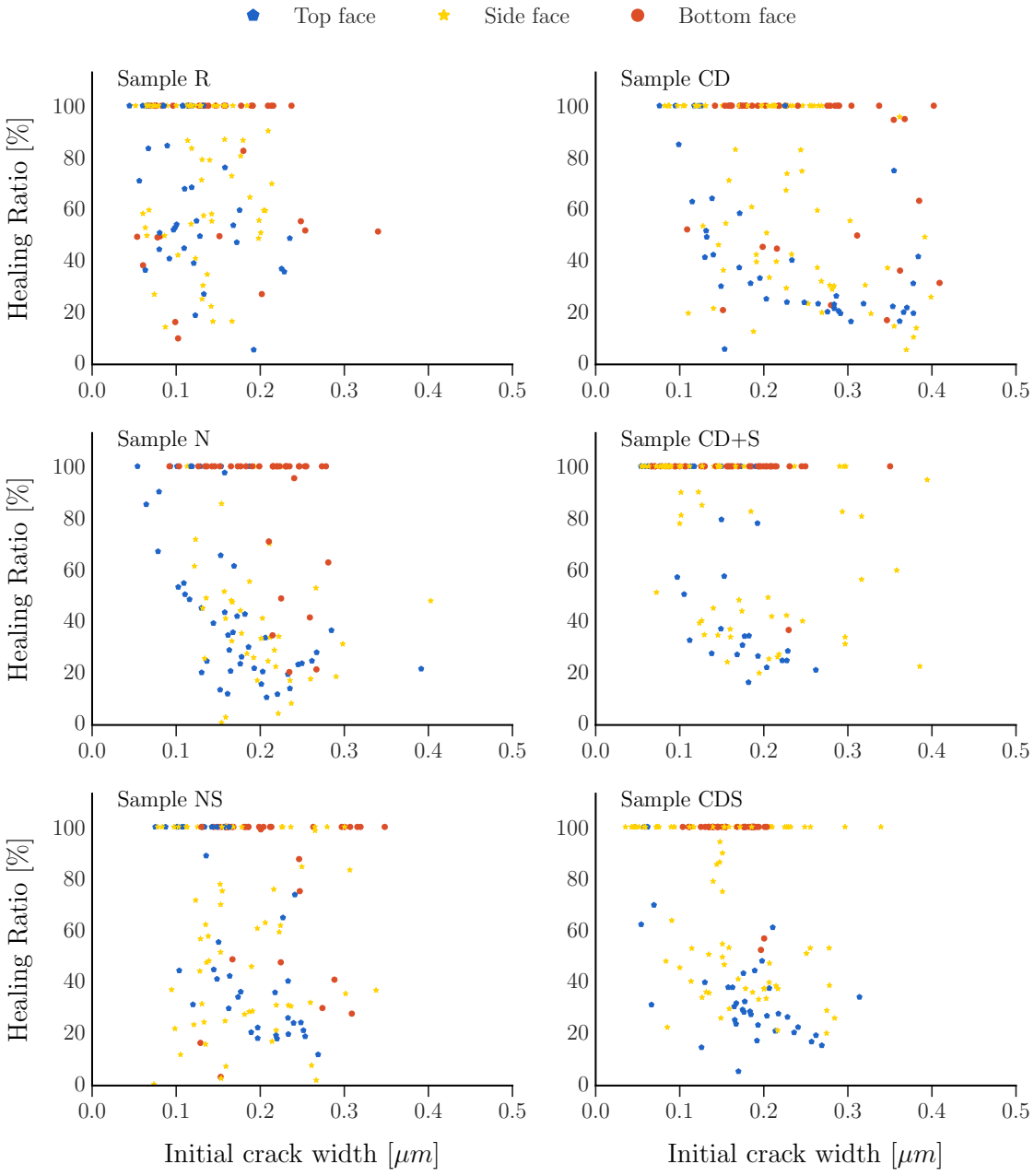

Figure 4.9: The healing ratio at each crack location, categorised by crack surface, in the specimen under full immersion over a period of 10 weeks

The initial crack width and crack surface face are the two independent variables. It is observed that cracks located at the bottom face have the highest ability to completely close after a period of 10 weeks. Furthermore, the maximum completely closed crack is for five of the six series found at the bottom surface of the sample. Limited crack healing occurred at the top

face of the sample. It should be noted that there are two side faces, each representing about 40 points in the figure. In accordance with figure 4.8 on page 82, aside from the completely closed cracks, the data cloud tends to decrease for increasing initial crack width. In samples R, N, NS and CDS, cracks beyond 0.25 mm are either completely closed or partially closed below 50% of their initial crack width, while CD and CD+S possess more cracks that are nearly completely closed. For the sample R and NS, the result are dispersed whereas those of N, CD, CD+S and CDS can be clustered into two distinct groups, i.e. completely closed and partially closed to an extend of 50% of their initial crack width.

Wet/dry cycles

As observed in figure 4.10 on the following page, the healing ratios of samples under wet/dry cycles are much smaller than those of samples under full immersion which can be found in figure 4.8 on page 82. In addition, the healing rate of the former decreases at a much larger pace than the latter. More than 60% of the average healing ratios of samples under wet/dry cycles dropped below a HR level of 40%, whereas only 2 average healing ratios over the entire crack width range dropped below 40% for sample under full immersion. The sample of series R experienced a maximum HR of 28% in the range of 100 to 150 mm. However, all other crack ranges had a lower HR. The sudden increase can be explained by the high amount of cracks within the range of 100 to 150 µm at the bottom of the specimen. Merely adding nutrients to the reference mixture (N series) already has an obvious increase in healing ratio compared to the sample of the R series. Moreover, its HR value outperforms all other samples within a range of 50 to 100 µm. Still, a sudden drop in performance is observed beyond 200 µm.

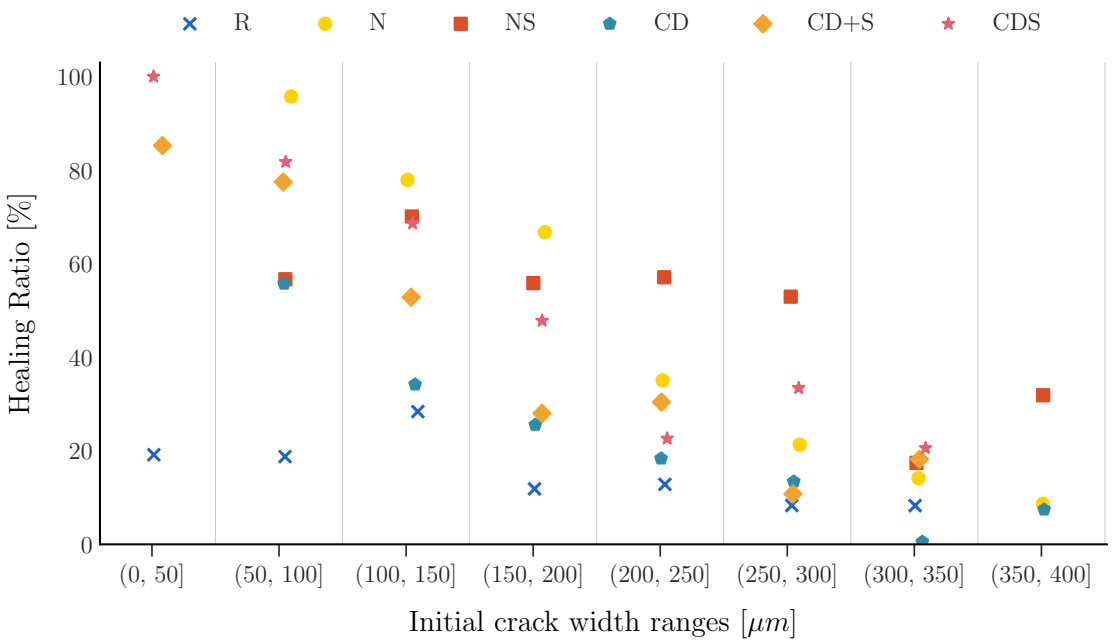

Figure 4.10: Average crack healing ratio in different ranges of crack widths of specimens under full immersion over a period of 10 weeks

In that particular region, the sample of series NS performed extremely well, with the exception of the HR within 300 to 350 µm which is only moderate, compared to all other samples. The overall size of the cracks whitin this sample lay between 100 and 350 µm. Below this range cracks are found that belong merely to either the top or side surface, and hence the obvious decrease in HR compared to its adjacent crack width range is explained. The sample of series CD is hardly any better than that of series R. Even after direct addition of bacterial spores in addition of hydrogel particles (CD+S series), no better performance is observed compared to both the N and NS series. However, a similar healing ratio (±17%) is noticed in the range of 300 to 350 µm for the three particular series. The sample of the CDS series is the second most best performing series after NS within the range of 200 to 350 µm. However, the difference with NS is still great. Thus, the best performing series for large cracks is definitely NS, ranging between an HR of 17 and 57%. It is concluded that the addition of hydrogels did not improve the average self healing of the specimens. Furthermore, no conclusion regarding the influence of bacterial spores, whether or not immobilised in hydrogel particles, could be drawn. A view of the healing ratio in function of the initial crack width for each crack location is given in figure 4.11 on the following page. Compared to figure 4.9 on page 83 related to samples under full immersion, the data cloud is much denser which means less cracks are completely closed within 10 weeks of wet/dry cycles. The data cloud of sample R and CD+S has a triangular shape skewed to the left side of the graph. Small cracks either close completely or experience a low crack closure. For crack widths ranging between about

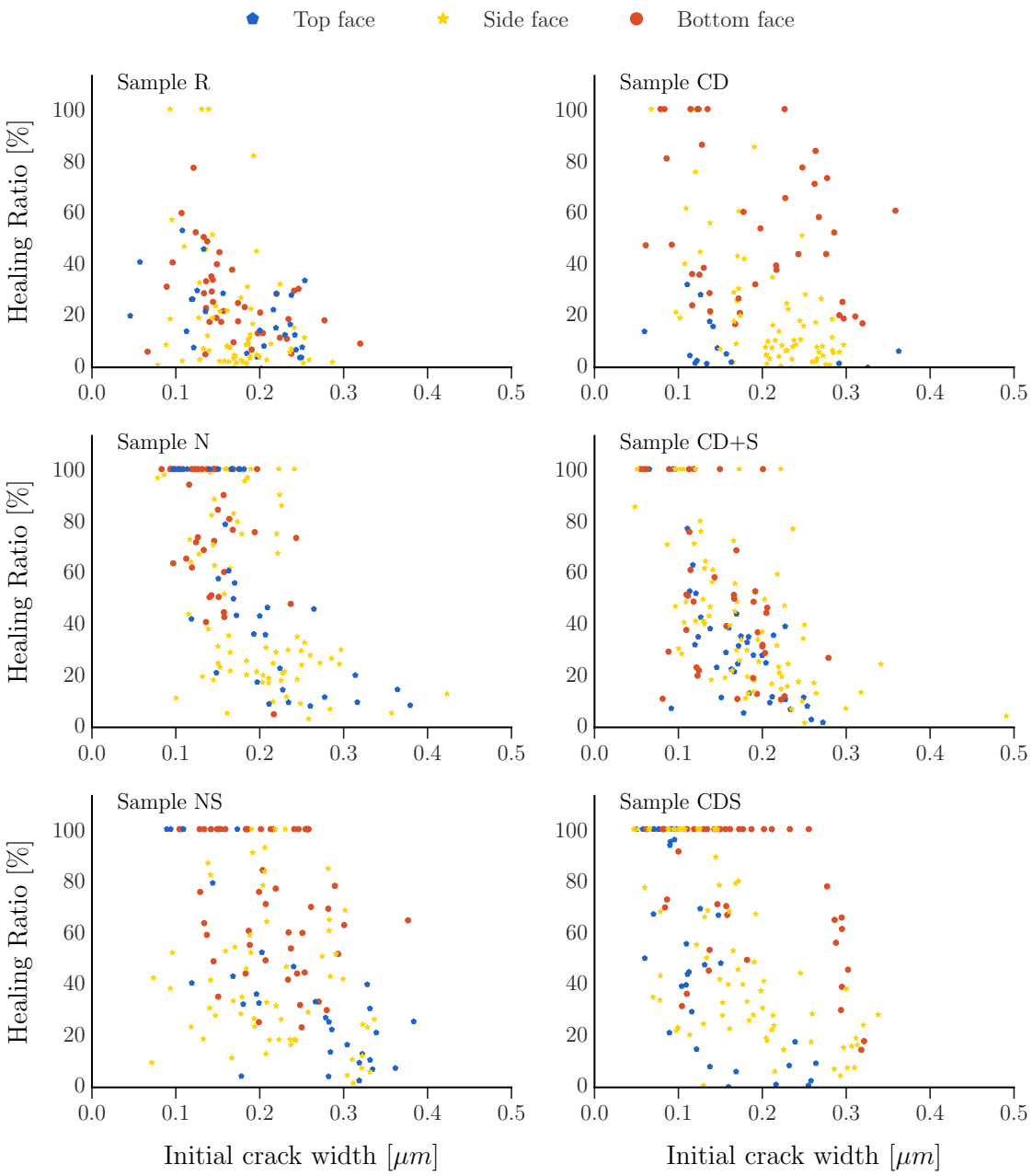

Figure 4.11: The healing ratio at each crack location, categorised by crack surface, in the specimen under full immersion over a period of 10 weeks

$0.10 - 0.35$ mm for R and CD+S, the maximum partially healing ratio reduces from 65 and 80% to 0% respectively. The least dense point cloud, i.e. points for partially closed cracks, is observed for the sample CDS (109) and followed by N (111) with respectively 31.9 and 29.7% of the total amount of cracks completely closed. It seems like the addition of merely hydrogel particles (CD) ceases the crack closure ability of the sample compared to sample N. This can

be attributed to a change in crack surface.

4.4.2.3 Optical microscope images of maximum closed cracks widths

Figure 4.12 on the following page to figure 4.23 on page 91 show the maximum completely or partially closed crack widths for both samples under full immersion and under wet/dry cycles.

Full immersion

Despite the specimens were handled with care, some healing products might get damaged during handling. Thus, a crack can be completely closed in week 2 while after 10 weeks it is observed to be only partially closed. The maximum closed crack widths for specimens R, N, NS, CD, CD+S and CD are about 0.21, 0.25, 0.35, 0.40, 0.30 and 0.34, respectively. Cracks took 1 week (R) up to 10 weeks (NS, CD and CDS) to completely close.

Wet/dry cycles

In the case of samples under wet/dry cycles, crack closure developed at a slower pace compared to those under full immersion. On average cracks took 5 weeks to close completely. The maximum completely closed crack widths for specimens N, NS, CD, CD+S and CD are about 0.26, 0.24, 0.23, 0.20 and 0.25, respectively. b

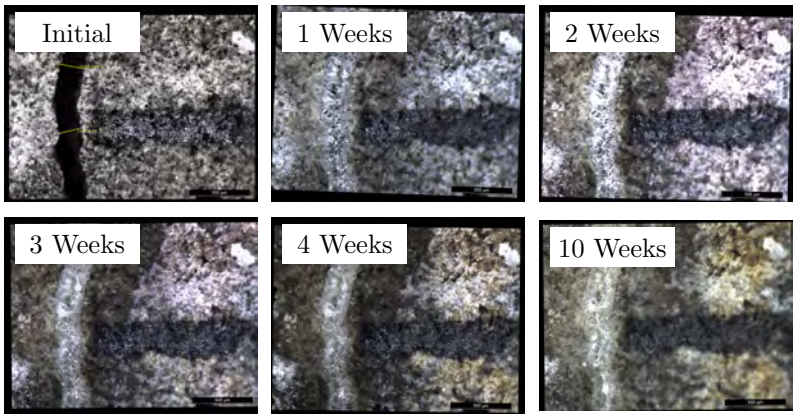

Figure 4.12: The maximum completely healed crack width (209.14 µm) in the specimen R under full immersion

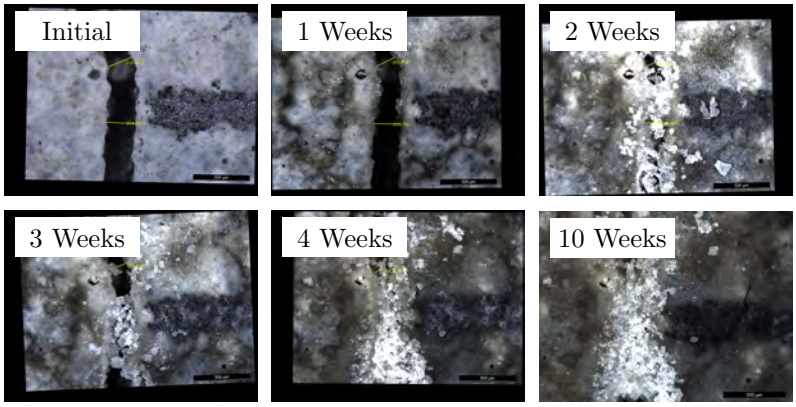

Figure 4.13: The maximum completely healed crack width (254.81 µm) in the specimen N under full immersion

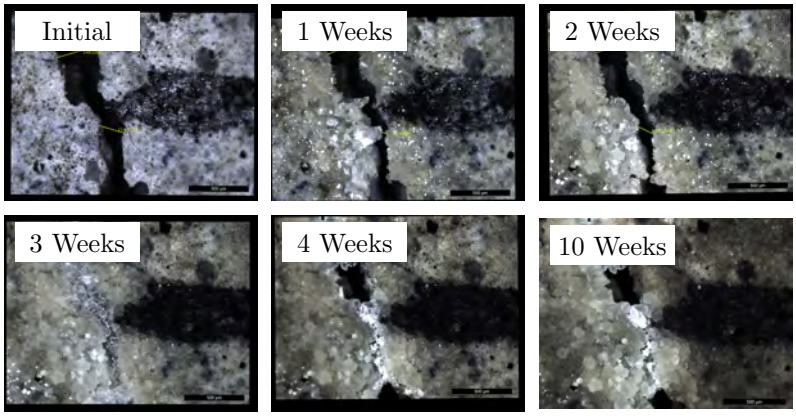

Figure 4.14: The maximum completely healed crack width (348.08 µm) in the specimen NS under full immersion

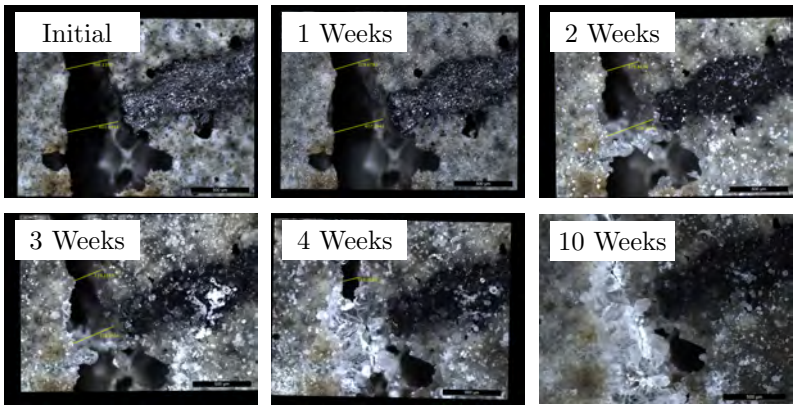

Figure 4.15: The maximum completely healed crack width (401.19 µm) in the specimen CD under full immersion

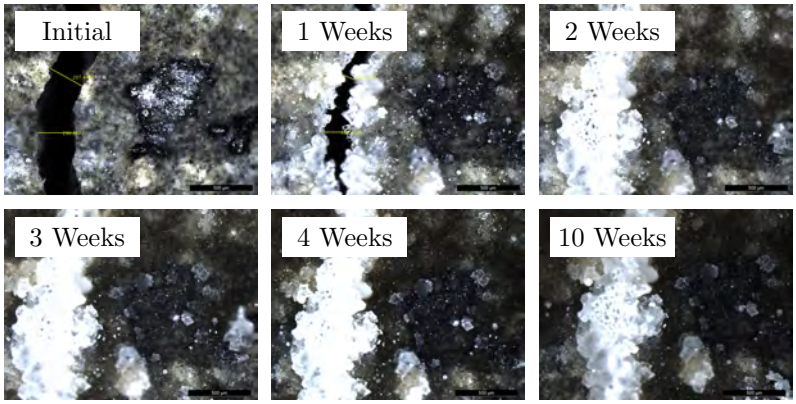

Figure 4.16: The maximum completely healed crack width (297.44 µm) in the specimen CD+S under full immersion

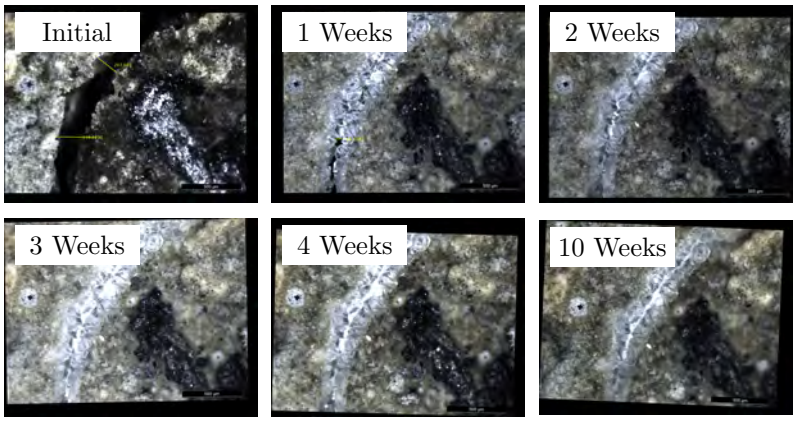

Figure 4.17: The maximum completely healed crack width (339.23 µm) in the specimen CDS under full immersion

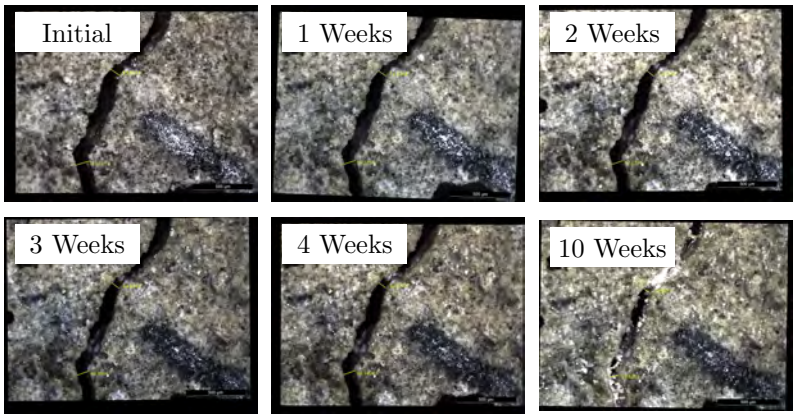

Figure 4.18: The maximum partially healed crack width (123.72 to 59.62 µm; HR = 51.86%) in the specimen R under wet/dry cycles

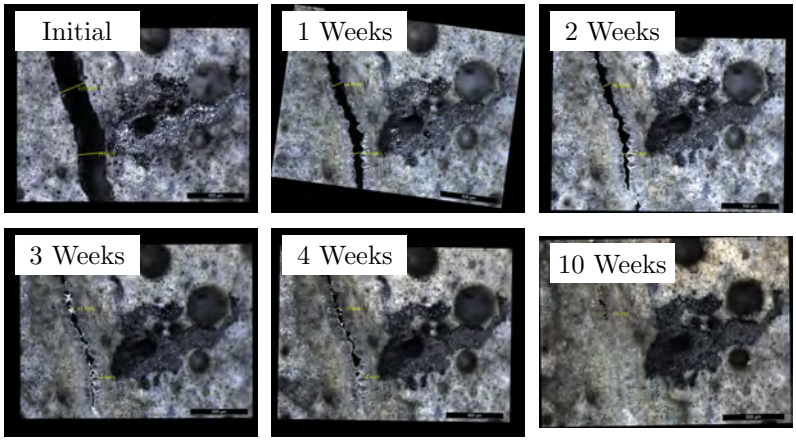

Figure 4.19: The maximum completely healed crack width (258.18 µm) in the specimen N under wet/dry cycles

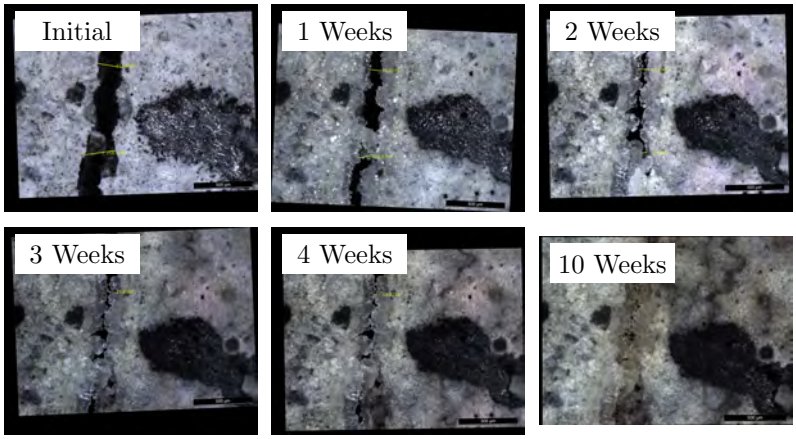

Figure 4.20: The maximum completely healed crack width (241.27 µm) in the specimen NS under wet/dry cycles

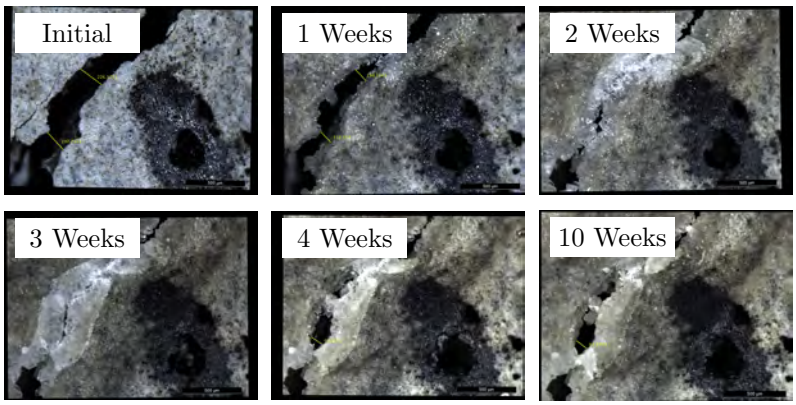

Figure 4.21: The maximum completely healed crack width (226.53 µm) in the specimen CD under wet/dry cycles

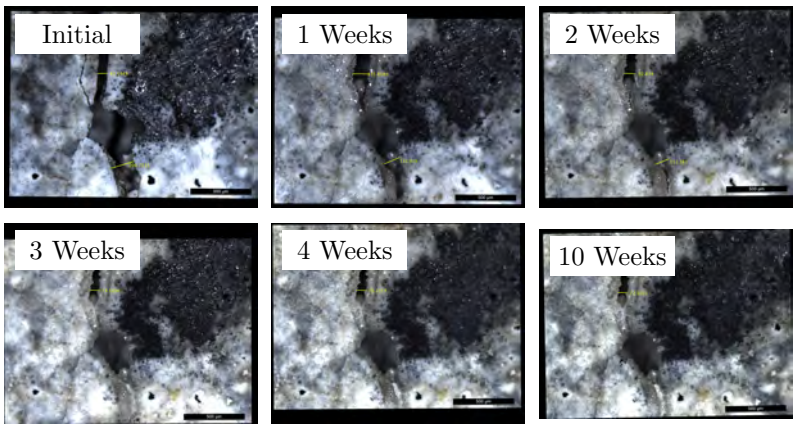

Figure 4.22: The maximum completely healed crack width (200.73 µm) in the specimen CD+S under wet/dry cycles

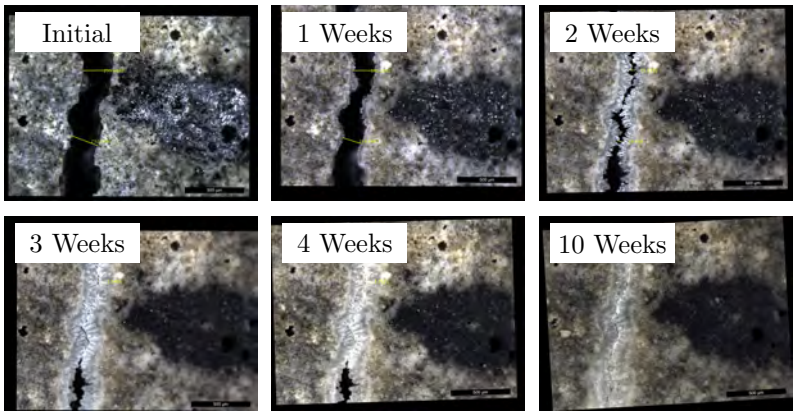

Figure 4.23: The maximum completely healed crack width (255.45 µm) in the specimen CDS under wet/dry cycles

Chapter 5

Conclusion

In this research, the application of pH responsive hydrogel immobilised bacterial spores in mortar specimens is evaluated. This evaluation is based on the performance of several synthesised hydrogels on the reduction of mechanical properties of mortar, viability of bacterial spores *B. sphaericus*, self-sealing and -healing efficiency of cracked mortar samples. Based on previous research by Mignon et al. (2016) into the development of pH responsive SAPs for the use in cementitious materials, four hydrogels were selected as a potential carrier for hydrogel immobilised spores. Methacrylated alginate (AlgMOD) and chitosan (ChiMOD) were synthesised and cross-linked to acrylic monomers, i.e., acrylic acid (AA) and acrylamide (AM), and 2-(dimethylamino)ethyl methacrylate (DMAEMA), respectively. In addition, a synthetic hydrogel consisting of N,N'-methylene bisacrylamide (MBA) cross-linked to DMAEMA is prepared. Thus four hydrogels were synthesised and subsequently characterised by means of swelling tests and attenuated total reflectance-infrared (ATR-IR) spectroscopy. AlgMOD of a high degree of substitution is made according the method described by Vermeulen (2016), though a higher DS is obtained in comparison with that in the related research, respectively 29.6% and 18.9%. The direct consequence was a slightly lower swelling capacity due to a denser hydrogel network compared to that of Vermeulen (2016). Gel fraction quantification revealed that hydrogels were synthesised with a high production capacity, similar to that of Mignon et al. (2016). The chemical structure of the synthesised hydrogels was characterised using ATR-IR spectroscopy and revealed that the materials were correctly built-in. Swelling tests in aqueous solution of varying pH and cement filtrate solution were conducted to evaluate the pH responsiveness of the hydrogels. Carboxylic acid functionalities of AlgMOD covalently cross-linked with AA (AlgMOD/AA) and with both AA and AM (AlgMOD/AA+AM) get deprotonated above pH 3.38, resulting in a gradually increase of swelling capacity in a more alkaline medium and reaching a maximum value at pH 12.5 equal to 88.9 and 58.1 $g_{water}/g_{hydrogel}$, respectively. However, the substantial swelling is limited when exposed to a cement filtrate solution due to the presence of mono- and multivalent cations which shield off functionalities of the hydrogels backbone. In addition, ATR-IR spec-

troscopy revealed that the structural integrity of the hydrogel decreases substantially above pH 11. Hydrogels based on ChiMOD and MBA, both covalently cross-linked with DMAEMA (ChiMOD/DMAEMA; MBA/DMAEMA), are less prone to degradation. The swelling capacity of ChiMOD/DMAEMA increases at a slow pace when exposed to a more acidic solution, whereas that of MBA/DMAEMA increases faster, reaching a maximum of 96.2 $g_{water}/g_{hydrogel}$ at pH 3. The swelling capacity of ChiMOD/DMAEMA reaches a stable value equal to about 40.8 $g_{water}/g_{hydrogel}$ within the range of pH 7 to 11. In case of MBA/DMAEMA, a tremendous increase in swelling capacity was noticed at pH 9 and could be attributed to batch variation. A slight change in cross-linking concentration of MBA has a high influence on the swelling behaviour, as was evaluated by Mignon et al. (2016). Thus, the higher swelling than anticipated might be related to a lower MBA concentration. Overall, the swelling capacity in a cement filtrate solution lie around 12.2 $g_{water}/g_{hydrogel}$ with the exception of MBA/DMAEMA which is equal to 15.8 $g_{water}/g_{hydrogel}$. When applied in cementitious materials, hydrogels of a low swelling capacity in a cement filtrate solution are expected to result in smaller macro-pores during hardening, and hence minimise the mechanical strength reduction compared to those samples incorporating normal hydrogels. The mechanical properties, i.e. flexural and compressive strength, of hydrogel incorporated mortar specimens under varying quantities were compared with those of a control sample. For series MBA/DMAEMA, a significant reduction of the mechanical properties was observed, even after addition of only 0.5m% hydrogel relative to the mass of the cement. The addition of 1m% hydrogel of series AlgMOD/AA, AlgMOD/AA+AM and ChiMOD/DMAEMA was found to comply with the demands to not compromise the mechanical properties significantly while still be available in a considerable amount in order promote the self-sealing and -healing of cracks. For those series, the flexural strength is decreased between 12.4 and 17.4% and the compression strength between 4.7 and 11.8%. The degradation of the hydrogels over time is evaluated by measurement of the swelling capacity and consequently ATR-IR spectroscopy and revealed that no significant degradation emerged over time. Hence, the degradation of the hydrogel after 1 day of exposure to an aqueous or cement filtrate solution is a good indicator of the degradation over a long period. Taking the aforementioned properties into account, ChiMOD/DMAEMA and AlgMOD/AA were the most promising materials regarding the mechanical properties of the mortar specimens and the preferable swelling behaviour.

Secondly, the use of hydrogel immobilised bacterial spores to improve self-sealing and -healing efficiency of mortar specimens is evaluated by optical microscopy, water transport properties and viability of the bacterial spores. To increase the viability of the spores, the synthesis time of the polymerisation reaction had to be decreased. MBA/DMAEMA was no longer recognised as a potential carrier because of its negatively influence on the mechanical properties or mortar specimens and its poor viability test results. The final batches of series ChiMOD/DMAEMA and AlgMOD/AA, to be applied in mortar specimens, showed bacterial

activity within 3 and 7 days, respectively. However, the bacterial activity of AlgMOD/AA was similar to that in its reference specimen, and hence no conclusion regarding the viability of the immobilised spores could be drawn. The water transport properties of mortar specimens containing ChiMOD/DMAEMA and AlgMOD/AA were evaluated by means of a water flow test. The water flow through a pre-cracked specimen was measured and the test revealed that the sealing efficiency is closely related to the crack closure. The sealing efficiency of specimens incorporating AlgMOD/AA is lower than that of ChiMOD/DMAEMA, though the crack closure is more obvious in the former specimens. AlgMOD/AA is prone to degradation and consequently might escape from the crack surface over the course of time due to a looser network and the reduction of its strength. Initially, the hydrogel particles slow down the flow, but over the course of time they leave the crack and the flow is no longer limited by its presence. The crack closure will then become the primary mechanism to reduce the flow rate. Furthermore, ChiMOD/DMAEMA exhibits a more consistent sealing efficiency over time than AlgMOD/AA specimens, though no significant difference was observed between specimens with and without bacterial spores. Next, an in depth crack closure study for specimens containing ChiMOD/DMAEMA immobilised spores was conducted. Specimens were either subjected to incubation under full immersion or under wet/dry cycles of 2 hours immersion alternated by a dry period of 4 hours. Overall, the range of initial crack widths in which completely closure was observed, was higher for specimens under full immersion, ranging up to 401 µm for a specimen containing merely ChiMOD/DMAEMA. However, on average, specimens under full immersion can close cracks completely within 10 weeks up to about 300 µm. The bottom face of the specimens experience the best crack closure efficiency and could often not be tested up to their full potential because of the lack of wider cracks. Thus, the overall crack closure efficiency is closely related to the initial crack widths distribution at the different faces of the specimen. The amount of completely closed cracks for specimens containing ChiMOD/DMAEMA immobilised spores and directly added spores equals to 51.3% and 66.9% respectively, whereas that of the other specimens varies between 34.3% and 46.6%. Furthermore, the average healing ratio above 250 µm was higher for specimens containing bacterial spores, whether or not immobilised in ChiMOD/DMAEMA, than for the specimens without bacteria, though no significant improvement of hydrogel immobilised spores is observed compared to directly added spores. However, optical microscopy of specimens under wet/dry cycles reveal an improved crack closure efficiency of specimens containing hydrogel immobilised spores. The specimen containing ChiMOD/DMAEMA immobilised spores experienced complete crack closure for 31.9% of the measured cracks, whereas the other specimens incorporating ChiMOD/DMAEMA reaches a complete crack closure equal to 12.3 and 5.6%, respectively with and without directly added spores. However, microscopic evaluation of specimens containing solely nutrients or both nutrients and directly added spores reveal a relatively high amount of completely closed crack as well, equal to 29.7 and 21.2% respectively, though the maximum completely closed crack and healing ratio for large cracks (>

250 µm) is higher in specimens containing bacterial spores.

Bibliography

[1] *The Cement Sustainability Initiative - Recycling Concrete*, Geneva. World Business Council for Sustainable Developments, wbcsdcement.org.

[2] CEMBUREAU. Activity Report 2015. Technical report, The European Cement Association.

[3] CEMBUREAU. Activity Report 2016. pages 1–36, June 2017.

[4] C. Meyer. The greening of the concrete industry. *Cement and Concrete Composites*, 31(8): 601–605, September 2009. doi: 10.1016/j.cemconcomp.2008.12.010.

[5] COST Association. Memorandum of Understanding for the implementation of the COST Action "Self-healing As preventive Repair of Concrete Structures" (SARCOS) CA15202. *COST Association*, pages 1–19, March 2016.

[6] BASF. Repairing Concrete: Solutions to Re-Establish Structural Integrity. pages 1–19, December 2013.

[7] V M Malhotra. *Role of supplementary cementing materials in reducing greenhouse gas emissions.* 1999. ISBN 1-84127-051-2.

[8] PBL Netherlands Environmental Assesment Agency & Joint Research Centre. Trends in global CO2-emissions. 2016 Report. pages 1–86, November 2016.

[9] IEA World Business Council for Sustainable Developments. *Cement Technology Roadmap 2009: carbon emissions reductions up to 2050.* World Business Council for Sustainable Development, 2009.

[10] CEMBUREAU. Development of State of the Art-Techniques in Cement Manufacturing: Trying to Look Ahead, 2009.

[11] D W Fowler. Polymers in concrete: a vision for the 21st century. *Cement and Concrete Composites*, 21(5-6):449–452, December 1999. doi: 10.1016/S0958-9465(99)00032-3.

[12] Victor C Li and Emily Herbert. Robust Self-Healing Concrete for Sustainable Infrastructure. *Journal of Advanced Concrete Technology*, 10(6):207–218, 2012. doi: 10.3151/jact.10.207.

[13] Kim Van Tittelboom, Nele De Belie, Willem De Muynck, and Willy Verstraete. Use of bacteria to repair cracks in concrete. *Cement and Concrete Research*, 40(1):157–166, December 2009. doi: 10.1016/j.cemconres.2009.08.025.

[14] PCA. Types and Causes of Concrete Deterioration , 2002.

[15] Salah A Altoubat and David A Lange. Creep, Shrinkage, and Cracking of Restrained Concrete at Early Age. *Materials Journal*, 98(4):323–331, July 2001. doi: 10.14359/10401.

[16] Benoıt Bissonnette, Pascale Pierre, and Michel Pigeon. Influence of key parameters on drying shrinkage of cementitious materials. *Cement and Concrete Research*, 29(10):1655–1662, October 1999. doi: 10.1016/S0008-8846(99)00156-8.

[17] E Tazawa. Autogenous shrinkage of concrete, 1999. doi: 10.1016/S0958-9465(03)00045-3.

[18] D P Bentz and O M Jensen. Mitigation strategies for autogenous shrinkage cracking. *Cement and Concrete Composites*, 26(6):677–685, August 2004.

[19] J G Cabrera. Deterioration of concrete due to reinforcement steel corrosion. *Cement and Concrete Composites*, 18(1):47–59, January 1996. doi: 10.1016/0958-9465(95)00043-7.

[20] J A Gonzalez, J S Algaba, and C Andrade. Corrosion of Reinforcing Bars in Carbonated Concrete. *British Corrosion Journal*, 15(3):135–139, July 2013. doi: 10.1179/bcj.1980.15.3.135.

[21] G K Glass and N R Buenfeld. The presentation of the chloride threshold level for corrosion of steel in concrete. *Corrosion Science*, 39(5):1001–1013, May 1997. doi: 10.1016/S0010-938X(97)00009-7.

[22] Bruno Zuber Michel Pigeon and Jacques Marchand. Freeze/thaw resistance. In *Advanced Concrete Technology*, pages 1–17. Elsevier, 2003. ISBN 9780750656863.

[23] *Alkali-silica reaction in concrete*. Thomas Telford Publishing, July 2015. ISBN 0-7277-4567-0.

[24] D W Hobbs. Structural effects and implications and repair. In *Alkali-silica reaction in concrete*, pages 73–87. Thomas Telford Publishing, July 2015. ISBN 0-7277-4567-0. doi: 10.1680/aric.13179.0004.

[25] Medhat H Shehata and Michael D A Thomas. The effect of fly ash composition on the expansion of concrete due to alkali–silica reaction. *Cement and Concrete Research*, 30(7):1063–1072, July 2000.

[26] William Jason Weiss. Prediction of early-age shrinkage cracking in concrete elements. *ProQuest Dissertations And Theses; Thesis (Ph.D.)–Northwestern University*, November 1999.

[27] Hai-Long Wang, Jian-Guo Dai, Xiao-Yan Sun, and Xiao-Long Zhang. Characteristics of concrete cracks and their influence on chloride penetration. *CONSTRUCTION & BUILDING MATERIALS*, 107:216–225, March 2016. doi: 10.1016/j.conbuildmat.2016.01.002.

[28] A Djerbi, S Bonnet, A Khelidj, and V Baroghel-bouny. Influence of traversing crack on chloride diffusion into concrete. *Cement and Concrete Research*, 38(6):877–883, June 2008. doi: 10.1016/j.cemconres.2007.10.007.

[29] Aalto-yliopisto, Aalto University, Karin Habermehl-Cwirzen, Insinööritieteiden korkeakoulu, and Andrzej Cwirzen. *Internal curing of concrete*. PhD thesis, Karri Kyllästinen, May 2015.

[30] M Palacios and F Puertas. Effect of shrinkage-reducing admixtures on the properties of alkali-activated slag mortars and pastes. *Cement and Concrete Research*, 37(5):691–702, May 2007. doi: 10.1016/j.cemconres.2006.11.021.

[31] T Bakharev, J G Sanjayan, and Y B Cheng. Effect of admixtures on properties of alkali-activated slag concrete. *Cement and Concrete Research*, 30(9):1367–1374, September 2000. doi: 10.1016/S0008-8846(00)00349-5.

[32] K M Lee, H K Lee, S H Lee, and G Y Kim. Autogenous shrinkage of concrete containing granulated blast-furnace slag. *Cement and Concrete Research*, 36(7):1279–1285, July 2006. doi: 10.1016/j.cemconres.2006.01.005.

[33] Dale P Bentz, Ole Mejlhede Jensen, Kurt Kielsgaard Hansen, John F Olesen, Henrik Stang, and Claus-Jochen Haecker. Influence of Cement Particle-Size Distribution on Early Age Autogenous Strains and Stresses in Cement-Based Materials. *Journal of the American Ceramic Society*, 84 (1):129–135, January 2001. doi: 10.1111/j.1151-2916.2001.tb00619.x.

[34] G F Kheder, R S Al-Rawi, and J K Al-Dhahi. A study of the behaviour of volume change cracking in base restrained concrete walls. *Materials and Structures*, 27(7):383–392, August 1994. doi: 10.1007/BF02473441.

[35] A M Paillere, M Buil, and J J Serrano. Effect of fiber addition on the autogeneous shrinkage of silica fume concrete. *ACI Materials Journal*, 86(2):139–144, March 1989.

[36] Dale P Bentz, Pietro Lura, and John W Roberts. Mixture proportioning for internal curing. *ciks.cbt.nist.gov*, February 2005. doi: 10.12952/journal.elementa.000075.t001.

[37] Chiwon Song, Young Cheol Choi, and Seongcheol Choi. Effect of internal curing by superabsorbent polymers – Internal relative humidity and autogenous shrinkage of alkali-activated slag mortars. *CONSTRUCTION & BUILDING MATERIALS*, 123:198–206, October 2016. doi: 10.1016/j.conbuildmat.2016.07.007.

[38] J Justs, M Wyrzykowski, D Bajare, and P Lura. Internal curing by superabsorbent polymers in ultra-high performance concrete. *Cement and Concrete Research*, 76:82–90, October 2015. doi: 10.1016/j.cemconres.2015.05.005.

[39] Graham Tilly. The Durability of Repaired Concrete Structures. *IABSE Symposium Report*, 93 (22):1–8, January 2007. doi: 10.2749/222137807796120030.

[40] S C EDWARDS R T L ALLEN and J D N SHAW edt. The Repair of Concrete Structures. pages 1–238, September 2005.

[41] GEOFF MAYS edt. Durability of Concrete Structures: Investigation, Repair, Protection. pages 1–287, July 2011.

[42] K Van Tittelboom. Self-Healing Concrete through Incorporation of Encapsulated Bacteria-or Polymer-Based Healing Agents ('Zelfhelend beton door incorporatie van . . . , 2012.

[43] Martin D Hager, Sybrand van der Zwaag, Ulrich S Schubert, Peter Greil, and Christoph Leyens. *Self-healing Materials*, volume 273 of *Advances in Polymer Science*. Springer, Cham, July 2016. ISBN 331932778X. doi: 10.1007/978-3-319-32778-5.

[44] K Van Breugel. Is there a market for self-healing cement-based materials. *... of the First International Conference on Self- ...*, 2007.

[45] Nynke ter Heide. *Crack healing in hydrating concrete*. PhD thesis, citg.tudelft.nl, May 2005.

[46] H Huang. Thermodynamics of Autogenous Self-healing in Cementitious Materials. 2014. doi: 10.4233/uuid:249ef3e8-46e7-4608-bc97-8e7d669f6c5b.

[47] Adam Neville. Autogenous Healing—A Concrete Miracle? *Concrete International*, 24(11): 76–82, November 2002.

[48] Carola Edvardsen. Water Permeability and Autogenous Healing of Cracks in Concrete. *Materials Journal*, 96(4):448–454, July 1999. doi: 10.14359/645.

[49] Kenneth R Lauer and Floyd 0 Slate. Autogenous Healing of Cement Paste. *Journal Proceedings*, 52(6):1083–1098, June 1956. doi: 10.14359/11661.

[50] Yingzi Yang, Michael D Lepech, En-Hua Yang, and Victor C Li. Autogenous healing of engineered cementitious composites under wet–dry cycles. *Cement and Concrete Research*, 39(5): 382–390, May 2009. doi: 10.1016/j.cemconres.2009.01.013.

[51] Kim Van Tittelboom and Nele De Belie. Self-Healing in Cementitious Materials—A Review. *Materials*, 6(6):2182–2217, May 2013. doi: 10.3390/ma6062182.

[52] Daisuke Homma, Hirozo Mihashi, and Tomoya Nishiwaki. Self-Healing Capability of Fibre Reinforced Cementitious Composites. *Journal of Advanced Concrete Technology*, 7(2):217–228, June 2009. doi: 10.3151/jact.7.217.

[53] Tomoya Nishiwaki, Marina Koda, Makoto Yamada, Hirozo Mihashi, and Takatsune Kikuta. Experimental Study on Self-Healing Capability of FRCC Using Different Types of Synthetic Fibers. *Journal of Advanced Concrete Technology*, 10(6):195–206, 2012. doi: 10.3151/jact.10.195.

[54] Ya-chuan Kuang and Jin-ping Ou. Passive smart self-repairing concrete beams by using shape memory alloy wires and fibers containing adhesives. *Journal of Central South University of Technology*, 15(3):411–417, June 2008. doi: 10.1007/s11771-008-0077-9.

[55] Yachuan Kuang and Jinping Ou. Self-repairing performance of concrete beams strengthened using superelastic SMA wires in combination with adhesives released from hollow fibers. *Smart Materials and Structures*, 17(2):025020, April 2008. doi: 10.1088/0964-1726/17/2/025020.

[56] Tae-Ho Ahn and Toshiharu Kishi. Crack Self-healing Behavior of Cementitious Composites Incorporating Various Mineral Admixtures. *Journal of Advanced Concrete Technology*, 8(2): 171–186, June 2010. doi: 10.3151/jact.8.171.

[57] T Kishi, T H Ahn, A Hosoda, and S Suzuki. *Self-healing behaviour by cementitious recrystallization of cracked concrete incorporating expansive agent*. Proceedings of the ..., 2007.

[58] K Sisomphon and O Copuroglu. Self healing mortars by using different cementitious materials. *International Conference on ...*, 2011.

[59] D Snoeck and N De Belie. Repeated autogenous healing in strain-hardening cementitious composites by using superabsorbent polymers. *Journal of Materials in Civil Engineering*, 28(1): 04015086, January 2016. doi: 10.1061/(ASCE)MT.1943-5533.0001360.

[60] Arn Mignon, Nele De Belie, and Sandra Van Vlierberghe. Effect of pH-responsive superabsorbent polymers on the self-sealing and self-healing of cracks in concrete . Technical report, September 2016.

[61] D Janssen. *Water encapsulation to initiate self-healing in cementitious materials.* Master's Thesis, 2011.

[62] Jianyun Wang. *Self-Healing Concreteby Means of Immobilized Carbonate Precipitating Bacteria* . PhD thesis, February 2013.

[63] T S Qureshi, A Kanellopoulos, and A Al-Tabbaa. Encapsulation of expansive powder minerals within a concentric glass capsule system for self-healing concrete. *CONSTRUCTION & BUILDING MATERIALS*, 121:629–643, September 2016. doi: 10.1016/j.conbuildmat.2016.06.030.

[64] R Alghamri, A Kanellopoulos, and A Al-Tabbaa. Impregnation and encapsulation of lightweight aggregates for self-healing concrete. *CONSTRUCTION & BUILDING MATERIALS*, 124:910–921, October 2016. doi: 10.1016/j.conbuildmat.2016.07.143.

[65] Benoit Hilloulin, Kim Van Tittelboom, Elke Gruyaert, Nele De Belie, and Ahmed Loukili. Design of polymeric capsules for self-healing concrete. *Cement and Concrete Composites*, 55:298–307, January 2015. doi: 10.1016/j.cemconcomp.2014.09.022.

[66] Yusuf Cagatay Ersan, Filipe Bravo Da Silva, Nico Boon, Willy Verstraete, and Nele De Belie. Screening of bacteria and concrete compatible protection materials. *CONSTRUCTION & BUILDING MATERIALS*, 88:196–203, 2015. doi: 10.1016/j.conbuildmat.2015.04.027.

[67] Henk M Jonkers, Arjan Thijssen, Gerard Muyzer, Oguzhan Copuroglu, and Erik Schlangen. Application of bacteria as self-healing agent for the development of sustainable concrete. *Ecological Engineering*, 36(2):230–235, February 2010. doi: 10.1016/j.ecoleng.2008.12.036.

[68] M Luo and C X Qian. Performance of Two Bacteria-Based Additives Used for Self-Healing Concrete. *Journal of Materials in Civil Engineering*, 2016. doi: 10.1061/(ASCE)MT.1943-5533.0001673.

[69] H G Schlegel. *General Microbiology.* University Press, 7 edition, 1993. ISBN 0 521 43372 X.

[70] Willem De Muynck, Nele De Belie, and Willy Verstraete. Microbial carbonate precipitation in construction materials: A review. *Ecological Engineering*, 36(2):118–136, February 2010. doi: 10.1016/j.ecoleng.2009.02.006.

[71] Maria Angustias Rivadeneyra, Rafael Delgado, Ana del Moral, Maria Rita Ferrer, and Alberto Ramos-Cormenzana. Precipatation of calcium carbonate by Vibrio spp. from an inland

saltern. *FEMS Microbiology Ecology*, 13(3):197–204, January 1994. doi: 10.1111/j.1574-6941.1994.tb00066.x.

[72] Biqin Dong, Yanshuai Wang, Guohao Fang, Ningxu Han, Feng Xing, and Youyuan Lu. Smart releasing behavior of a chemical self-healing microcapsule in the stimulated concrete pore solution. *Cement and Concrete Composites*, 56:46–50, February 2015. doi: 10.1016/j.cemconcomp.2014.10.006.

[73] M M Pelletier, R Brown, and A Shukla. Self-healing concrete with a microencapsulated healing agent. *Cem Concr ...*, 2011.

[74] G Perez, J J Gaitero, E Erkizia, I Jimenez, and A Guerrero. Characterisation of cement pastes with innovative self-healing system based in epoxy-amine adhesive. *Cement and Concrete Composites*, 60:55–64, July 2015. doi: 10.1016/j.cemconcomp.2015.03.010.

[75] Mohammed Al-Ansari, Ala G Abu-Taqa, Marwa M Hassan, Ahmed Senouci, and Jose Milla. Performance of modified self-healing concrete with calcium nitrate microencapsulation. *CONSTRUCTION & BUILDING MATERIALS*, 149:525–534, September 2017. doi: 10.1016/j.conbuildmat.2017.05.152.

[76] J L García Calvo, G Perez, P Carballosa, E Erkizia, J J Gaitero, and A Guerrero. Development of ultra-high performance concretes with self-healing micro/nano-additions. *CONSTRUCTION & BUILDING MATERIALS*, 138:306–315, May 2017. doi: 10.1016/j.conbuildmat.2017.02.015.

[77] T S Qureshi, A Kanellopoulos, and A Al-Tabbaa. Encapsulation of expansive powder minerals within a concentric glass capsule system for self-healing concrete. *CONSTRUCTION & BUILDING MATERIALS*, 121:629–643, September 2016. doi: 10.1016/j.conbuildmat.2016.06.030.

[78] Jiaguang Zhang, Yuanzhen Liu, Tao Feng, Mengjun Zhou, Lin Zhao, Aijuan Zhou, and Zhu Li. Immobilizing bacteria in expanded perlite for the crack self-healing in concrete. *CONSTRUCTION & BUILDING MATERIALS*, 148:610–617, September 2017. doi: 10.1016/j.conbuildmat.2017.05.021.

[79] Jianyun Wang, Arn Mignon, Didier Snoeck, Virginie Wiktor, Sandra Van Vliergerghe, Nico Boon, and Nele De Belie. Application of modified-alginate encapsulated carbonate producing bacteria in concrete: a promising strategy for crack self-healing. *Frontiers in Microbiology*, 6 (125016):1, 2015. doi: 10.3389/fmicb.2015.01088.

[80] Jianyun Wang, Kim Van Tittelboom, Nele De Belie, and Willy Verstraete. Use of silica gel or polyurethane immobilized bacteria for self-healing concrete. *CONSTRUCTION & BUILDING MATERIALS*, 26(1):532–540, January 2012. doi: 10.1016/j.conbuildmat.2011.06.054.

[81] Sookie S Bang, Johnna K Galinat, and V Ramakrishnan. Calcite precipitation induced by polyurethane-immobilized Bacillus pasteurii. *Enzyme and Microbial Technology*, 28(4-5):404–409, March 2001. doi: 10.1016/S0141-0229(00)00348-3.

[82] J Y Wang, N De Belie, and W Verstraete. Diatomaceous earth as a protective vehicle for bacteria applied for self-healing concrete. *Journal of Industrial Microbiology & Biotechnology*, 39(4):567–577, September 2011. doi: 10.1007/s10295-011-1037-1.

[83] Virginie Wiktor and Henk M Jonkers. Quantification of crack-healing in novel bacteria-based self-healing concrete. *Cement and Concrete Composites*, 33(7):763–770, August 2011. doi: 10.1016/j.cemconcomp.2011.03.012.

[84] S K Ramachandran. Remediation of concrete using micro-organisms. *... -American Concrete ...*, 2001.

[85] Pieter Minnebo, Glenn Thierens, Glenn De Valck, Kim Van Tittelboom, Nele De Belie, Danny Van Hemelrijck, and Eleni Tsangouri. A Novel Design of Autonomously Healed Concrete: Towards a Vascular Healing Network. *Materials*, 10(1):49, January 2017. doi: 10.3390/ma10010049.

[86] Alessandra Formia, Salvatore Terranova, Paola Antonaci, Nicola Pugno, and Jean Tulliani. Setup of Extruded Cementitious Hollow Tubes as Containing/Releasing Devices in Self-Healing Systems. *Materials*, 8(4):1897–1923, April 2015. doi: 10.3390/ma8041897.

[87] Haoliang Huang, Guang Ye, and Zhonghe Shui. Feasibility of self-healing in cementitious materials – By using capsules or a vascular system? *CONSTRUCTION & BUILDING MATERIALS*, 63:108–118, July 2014. doi: 10.1016/j.conbuildmat.2014.04.028.

[88] Shannon Stocks-Fischer, Johnna K Galinat, and Sookie S Bang. Microbiological precipitation of CaCO3. *Soil Biology and Biochemistry*, 31(11):1563–1571, October 1999. doi: 10.1016/S0038-0717(99)00082-6.

[89] A Kantzas, L Stehmeier, D F Marentette, F G Ferris, K N Jha, and F M Maurits. *A Novel Method of Sand Consolidation Through Bacteriogenic Mineral Plugging*. Petroleum Society of Canada, January 1992. ISBN 978-1-55563-468-1. doi: 10.2118/92-46.

[90] Deepak Sarda, Huzaifa S Choonia, D D Sarode, and S S Lele. Biocalcification by Bacillus pasteurii urease: a novel application. *Journal of Industrial Microbiology & Biotechnology*, 36(8):1111–1115, May 2009. doi: 10.1007/s10295-009-0581-4.

[91] Frederik Hammes and Willy Verstraete. Key roles of pH and calcium metabolism in microbial carbonate precipitation. *Reviews in Environmental Science and Biotechnology*, 1(1):3–7, March 2002. doi: 10.1023/A:1015135629155.

[92] Sabine Castanier, Gaële Le Métayer-Levrel, and Jean-Pierre Perthuisot. Ca-carbonates precipitation and limestone genesis — the microbiogeologist point of view. *Sedimentary Geology*, 126(1-4):9–23, July 1999. doi: 10.1016/S0037-0738(99)00028-7.

[93] Wasim Khaliq and Muhammad Basit Ehsan. Crack healing in concrete using various bio influenced self-healing techniques. *CONSTRUCTION & BUILDING MATERIALS*, 102:349–357, January 2016. doi: 10.1016/j.conbuildmat.2015.11.006.

[94] Shivani Gupta Gupta, Chhavi Rathi, and Suman Kapur. Biologically Induced Self Healing Concrete: A Futuristic Solution for Crack Repair. *International Journal of Applied Sciences and Biotechnology*, 1(3):85–89, September 2013. doi: 10.3126/ijasbt.v1i3.8582.

[95] MVS Rao, V S Reddy, M Hafsa, P Veena, and P Anusha. *Bioengineered concrete: A sustainable self-healing construction material*. Res J Eng Sci, 2013.

[96] R K Andrews, R L Blakeley, and B Zerner. Urea and urease. *Advances in inorganic biochemistry*, 6:245–283, 1984.

[97] H L Mobley and R P Hausinger. Microbial ureases: significance, regulation, and molecular characterization. *Microbiological reviews*, 53(1):85–108, March 1989.

[98] G MORSDORF and H KALTWASSER. Ammonium Assimilation in Proteus-Vulgaris, Bacillus-Pasteurii, and Sporosarcina-Ureae. *Archives of Microbiology*, 152(2):125–131, July 1989. doi: 10.1007/BF00456089.

[99] Stefan Christians, Joachim Jose, Udo Schäfer, and Heinrich Kaltwasser. Purification and subunit determination of the nickel-dependent Staphylococcus xylosus urease. *FEMS Microbiology Letters*, 80(2):271–275, May 1991.

[100] Doyle J Evans, Dolores G Evans, Stacy S Kirkpatrick, and David Y Graham. Characterization of the Helicobacter pylori urease and purification of its subunits. *Microbial Pathogenesis*, 10(1): 15–26, January 1991. doi: 10.1016/0882-4010(91)90062-F.

[101] Sung-Jin Park, Jong-Myong Park, Wha-Jung Kim, and Sa-Youl Ghim. Application of Bacillus subtilis 168 as a multifunctional agent for improvement of the durability of cement mortar. *Journal of microbiology and biotechnology*, 22(11):1568–1574, November 2012.

[102] V S Reddy, K A Satya, and MVS Rao. A biological approach to enhance strength and durability in concrete structures. *International Journal of . . .*, 2012.

[103] A T Manikandan and A Padmavathi. An Experimental Investigation on Improvement of Concrete Serviceability by using Bacterial Mineral Precipitation. 02(03):46–49., March 2015.

[104] Farzaneh Nosouhian, Davood Mostofinejad, and Hasti Hasheminejad. Concrete Durability Improvement in a Sulfate Environment Using Bacteria. *Journal of Materials in Civil Engineering*, 28(1), January 2016. doi: 10.1061/(ASCE)MT.1943-5533.0001337.

[105] Jan Dick, Wim De Windt, Bernard De Graef, Hans Saveyn, Paul Van der Meeren, Nele De Belie, and Willy Verstraete. Bio-deposition of a calcium carbonate layer on degraded limestone by Bacillus species. *Biodegradation*, 17(4):357–367, February 2006. doi: 10.1007/s10532-005-9006-x.

[106] Malcolm B Burbank, Thomas J Weaver, Barbara C Williams, and Ronald L Crawford. Urease Activity of Ureolytic Bacteria Isolated from Six Soils in which Calcite was Precipitated by Indigenous Bacteria. *Geomicrobiology Journal*, 29(4):389–395, May 2012. doi: 10.1080/01490451.2011.575913.

[107] J Y Wang, H Soens, W Verstraete, and N De Belie. Self-healing concrete by use of microencapsulated bacterial spores. *Cement and Concrete Research*, 56:139–152, February 2014. doi: 10.1016/j.cemconres.2013.11.009.

[108] Mostafa Seifan, Ali Khajeh Samani, and Aydin Berenjian. Bioconcrete: next generation of self-healing concrete. *Applied Microbiology and Biotechnology*, 100(6):2591–2602, March 2016. doi: 10.1007/s00253-016-7316-z.

[109] E Tziviloglou, V Wiktor, H M Jonkers, and E Schlangen. Bacteria-based self-healing concrete to increase liquid tightness of cracks. *CONSTRUCTION & BUILDING MATERIALS*, 122: 118–125, September 2016. doi: 10.1016/j.conbuildmat.2016.06.080.

[110] V Wiktor and H M Jonkers. Bacteria-based concrete: from concept to market. *Smart Materials and Structures*, 25(8):1–8, July 2016. doi: 10.1088/0964-1726/25/8/084006.

[111] J Y Wang, D Snoeck, S Van Vlierberghe, W Verstraete, and N De Belie. Application of hydrogel encapsulated carbonate precipitating bacteria for approaching a realistic self-healing in concrete. *CONSTRUCTION & BUILDING MATERIALS*, 68:110–119, October 2014. doi: 10.1016/j.conbuildmat.2014.06.018.

[112] K Kabiri, H Omidian, S A Hashemi, and M J Zohuriaan-Mehr. Synthesis of fast-swelling superabsorbent hydrogels: effect of crosslinker type and concentration on porosity and absorption rate. *European Polymer Journal*, 39(7):1341–1348, July 2003. doi: 10.1016/S0014-3057(02)00391-9.

[113] Fredric L Buchholz and Andrew T Graham. *Modern Superabsorbent Polymer Technology, Edited by F L Buchholz and A T Graham, Wiley-VCH, New York, 1998, PP xvii + 279.* Wiley-VCH, New York, 1998.

[114] A Mignon, D Snoeck, P Dubruel, and S Van Vlierberghe. Crack Mitigation in Concrete: Superabsorbent Polymers as Key to Success? *Materials*, 10(3):237, 2017. doi: 10.3390/ma10030237.

[115] K S Kazanskii and S A Dubrovskii. Chemistry and physics of "agricultural" hydrogels. In *Polyelectrolytes Hydrogels Chromatographic Materials*, pages 97–133. Springer Berlin Heidelberg, Berlin, Heidelberg, May 2005. ISBN 978-3-540-55109-6. doi: 10.1007/3-540-55109-3_3.

[116] Kirstin Kosemund, Harald Schlatter, Jennifer L Ochsenhirt, Edburga L Krause, Daniel S Marsman, and Geetha N Erasala. Safety evaluation of superabsorbent baby diapers. *Regulatory Toxicology and Pharmacology*, 53(2):81–89, March 2009. doi: 10.1016/j.yrtph.2008.10.005.

[117] Mohammad J Zohuriaan-Mehr and Kourosh Kabiri. Superabsorbent Polymer Materials: A Review. *Polymers for Advanced Technologies*, 19(6):785–792, June 2008. ISSN 1026-1265. doi: 10.1002/pat.1034.

[118] Marcos R Guilherme, Fauze A Aouada, André R Fajardo, Alessandro F Martins, Alexandre T Paulino, Magali F T Davi, Adley F Rubira, and Edvani C Muniz. Superabsorbent hydrogels based on polysaccharides for application in agriculture as soil conditioner and nutrient carrier: A review. *European Polymer Journal*, 72:365–385, November 2015. doi: 10.1016/j.eurpolymj.2015.04.017.

[119] C Demitri, F Scalera, M Madaghiele, A Sannino, and A Maffezzoli. Potential of Cellulose-Based Superabsorbent Hydrogels as Water Reservoir in Agriculture. *International Journal of Polymer Science*, 2013(12):1–6, December 2013. doi: 10.1155/2013/435073.

[120] M J Zohuriaan-Mehr. *Super-absorbents*. Iran Polymer Society, 2006.

[121] Paul J Flory. *Principles of Polymer Chemistry*. Cornell University Press, first edition edition.

[122] P K Chatterjee and B S Gupta. *Absorbent Technology*. Elsevier, March 2002. ISBN 9780080525853.

[123] Marcos R Guilherme, Fauze A Aouada, André R Fajardo, Alessandro F Martins, Alexandre T Paulino, Magali F T Davi, Adley F Rubira, and Edvani C Muniz. Superabsorbent hydrogels based on polysaccharides for application in agriculture as soil conditioner and nutrient carrier: A review. *European Polymer Journal*, 72:365–385, November 2015. doi: 10.1016/j.eurpolymj.2015.04.017.

[124] W E Hennink and C F van Nostrum. Novel crosslinking methods to design hydrogels. *Advanced Drug Delivery Reviews*, 54(1):13–36, January 2002. doi: 10.1016/S0169-409X(01)00240-X.

[125] Syed K H Gulrez, Glyn O Phillips, and Saphwan Al-Assaf. *Hydrogels: Methods of Preparation, Characterisation and Applications*. 2011. ISBN 9789533072685.

[126] Arn Mignon, Geert-Jan Graulus, Didier Snoeck, José Martins, Nele De Belie, Peter Dubruel, and Sandra Van Vlierberghe. pH-sensitive superabsorbent polymers: a potential candidate material for self-healing concrete. *Journal of Materials Science*, 50(2):970–979, October 2014. doi: 10.1007/s10853-014-8657-6.

[127] Yong Qiu and Kinam Park. Environment-sensitive hydrogels for drug delivery. *Advanced Drug Delivery Reviews*, 53(3):321–339, December 2001. doi: 10.1016/S0169-409X(01)00203-4.

[128] Atul R Khare and Nikolaos A Peppas. Release behavior of bioactive agents from pH-sensitive hydrogels. *Journal of Biomaterials Science, Polymer Edition*, 4(3):275–289, January 1993. doi: 10.1163/156856293X00564.

[129] Atsushi Suzuki and Toyoichi Tanaka. Phase transition in polymer gels induced by visible light. *Nature*, 346(6282):345–347, July 1990. doi: 10.1038/346345a0.

[130] K K Lee, E L Cussler, M Marchetti, and M A McHugh. Pressure-dependent phase transitions in hydrogels. *Chemical Engineering Science*, 45(3):766–767, December 1990. doi: 10.1016/0009-2509(90)87019-O.

[131] Roberto F S Freitas and E L Cussler. Temperature sensitive gels as extraction solvents. *Chemical Engineering Science*, 42(1):97–103, January 1987. doi: 10.1016/0009-2509(87)80213-0.

[132] M Dash, F Chiellini, R M Ottenbrite, and E Chiellini. Chitosan—A versatile semi-synthetic polymer in biomedical applications. *Progress in Polymer Science*, 36(8):981–1014, August 2011. doi: 10.1016/j.progpolymsci.2011.02.001.

[133] W M Kulicke and H Nottelmann. Structure and swelling of some synthetic, semisynthetic, and biopolymer hydrogels. 1989. doi: 10.1021/ba-1989-0223.ch002;wgroup:string:ACHS.

[134] Dries Devisscher. Bio-based pH-Sensitive Superabsorbent Polymers for Self-Sealing and -Healing Mortar. pages 1–108, June 2015.

[135] George Odian. *Principles of Polymerization*. John Wiley & Sons, Hoboken, NJ, USA, 2004. ISBN 0471274003. doi: 10.1002/047147875X.

[136] P Trijasson, T Pith, and M Lambla. Hydrophilic polyelectrolyte gels by inverse suspension. *Makromolekulare Chemie. Macromolecular Symposia*, 35-36(1):141–169, March 2011. doi: 10.1002/masy.19900350111.

[137] Ole Mejlhede Jensen and Per Freiesleben Hansen. Water-entrained cement-based materials. *Cement and Concrete Research*, 31(4):647–654, April 2001. doi: 10.1016/S0008-8846(01)00463-X.

[138] B Persson. Self-desiccation and Its Importance in Concrete Technology. 1998.

[139] Viktor Mechtcherine, Egor Secrieru, and Christof Schröfl. Effect of superabsorbent polymers (SAPs) on rheological properties of fresh cement-based mortars — Development of yield stress and plastic viscosity over time. *Cement and Concrete Research*, 67:52–65–65, January 2015. doi: 10.1016/j.cemconres.2014.07.003.

[140] Mateusz Wyrzykowski and Pietro Lura. Controlling the coefficient of thermal expansion of cementitious materials – A new application for superabsorbent polymers. *Cement and Concrete Composites*, 35(1):49–58, January 2013. doi: 10.1016/j.cemconcomp.2012.08.010.

[141] Pietro Lura and Giovanni Pietro Terrasi. Reduction of fire spalling in high-performance concrete by means of superabsorbent polymers and polypropylene fibers. *Cement and Concrete Composites*, 49:36–42, May 2014. doi: 10.1016/j.cemconcomp.2014.02.001.

[142] Maria Araújo, Sandra Van Vlierberghe, João Feiteira, Geert-Jan Graulus, Kim Van Tittelboom, José C Martins, Peter Dubruel, and Nele De Belie. Cross-linkable polyethers as healing/sealing agents for self-healing of cementitious materials. *Materials & Design*, 98:215–222, May 2016. doi: 10.1016/j.matdes.2016.03.005.

[143] H X D Lee, H S Wong, and N R Buenfeld. Self-sealing of cracks in concrete using superabsorbent polymers. *Cement and Concrete Research*, 79:194–208, January 2016. doi: 10.1016/j.cemconres.2015.09.008.

[144] Kenny D'Halluin, Nele De Belie, Didier Snoeck, and Arn Mignon. *Effect of Type of Superabsorbent Polymer on the Self-healing Properties in Cementitious Materials, in Combination with Calcium Carbonate Precipitating Bacteria* . PhD thesis, June 2014.

[145] Didier Snoeck, Kim Van Tittelboom, Stijn Steuperaert, Peter Dubruel, and Nele De Belie. Self-healing cementitious materials by the combination of microfibres and superabsorbent polymers. *Journal of Intelligent Material Systems and Structures*, 25(1):13–24, March 2012. doi: 10.1177/1045389X12438623.

[146] Didier Snoeck. *Self-Healing and Microstructure of Cementitious Materials with Microfibres and Superabsorbent Polymers*. Ghent, 2015.

[147] Marguerite Rinaudo. Main properties and current applications of some polysaccharides as biomaterials. *Polymer International*, 57(3):397–430, 2008. doi: 10.1002/pi.2378.

[148] Marcos R Guilherme, Gilsinei M Campese, Eduardo Radovanovic, Adley F Rubira, Judith P A Feitosa, and Edvani C Muniz. Morphology and water affinity of superabsorbent hydrogels composed of methacrylated cashew gum and acrylamide with good mechanical properties. *Polymer*, 46(19):7867–7873, September 2005. doi: 10.1016/j.polymer.2005.06.068.

[149] P S Keshava Murthy, Y Murali Mohan, J Sreeramulu, and K Mohana Raju. Semi-IPNs of starch and poly(acrylamide-co-sodium methacrylate): Preparation, swelling and diffusion characteristics evaluation. *Reactive and Functional Polymers*, 66(12):1482–1493, December 2006. doi: 10.1016/j.reactfunctpolym.2006.04.010.

[150] A Pourjavadi, Sh Barzegar, and G R Mahdavinia. MBA-crosslinked Na-Alg/CMC as a smart full-polysaccharide superabsorbent hydrogels. *Carbohydrate Polymers*, 66(3):386–395, November 2006. doi: 10.1016/j.carbpol.2006.03.013.

[151] J Zhang, Q Wang, and A Wang. Synthesis and characterization of chitosan-g-poly (acrylic acid)/attapulgite superabsorbent composites. *Carbohydrate Polymers*, 70(2):166–173, 2007. doi: 10.1016/j.carbpol.2007.03.015.

[152] Shuibo Hua and Aiqin Wang. Synthesis, characterization and swelling behaviors of sodium alginate-g-poly(acrylic acid)/sodium humate superabsorbent. *Carbohydrate Polymers*, 75(1): 79–84, January 2009. doi: 10.1016/j.carbpol.2008.06.013.

[153] E Percival. The polysaccharides of green, red and brown seaweeds: their basic structure, biosynthesis and function. *British Phycological Journal*, 14(2):103–117, 1979. doi: 10.1080/00071617900650121.

[154] Arno Verlee, Stein Mincke, and Christian V Stevens. Recent developments in antibacterial and antifungal chitosan and its derivatives. *Carbohydrate Polymers*, 164:268–283, May 2017. doi: 10.1016/j.carbpol.2017.02.001.

[155] Narayan Bhattarai, Jonathan Gunn, and Miqin Zhang. Chitosan-based hydrogels for controlled, localized drug delivery. *Advanced Drug Delivery Reviews*, 62(1):83–99, January 2010. doi: 10.1016/j.addr.2009.07.019.

[156] Florence Croisier and Christine Jérôme. Chitosan-based biomaterials for tissue engineering. *European Polymer Journal*, 49(4):780–792, April 2013. doi: 10.1016/j.eurpolymj.2012.12.009.

[157] Jacek K Dutkiewicz. Superabsorbent materials from shellfish waste—A review. *Journal of Biomedical Materials Research Part A*, 63(3):373–381, January 2002. doi: 10.1002/jbm.10231.

[158] Ali Pourjavadi, Bahareh Farhadpour, and Farzad Seidi. Synthesis and investigation of swelling behavior of new agar based superabsorbent hydrogel as a candidate for agrochemical delivery. *Journal of Polymer Research*, 16(6):655–665, February 2009. doi: 10.1007/s10965-009-9270-2.

[159] Sanju Francis, Manmohan Kumar, and Lalit Varshney. Radiation synthesis of superabsorbent poly(acrylic acid)–carrageenan hydrogels. *Radiation Physics and Chemistry*, 69(6):481–486, April 2004. doi: 10.1016/j.radphyschem.2003.09.004.

[160] Xin Ding, Li Li, Ping Sheng Liu, Jun Zhang, Ning Lin Zhou, Shan Lu, Shao Hua Wei, and Jian Shen. The preparation and properties of dextrin-graft-acrylic acid/montmorillonite superabsorbent nanocomposite. *Polymer Composites*, 30(7):976–981, July 2009. doi: 10.1002/pc.20643.

[161] Yan Bao, Jianzhong Ma, and Na Li. Synthesis and swelling behaviors of sodium carboxymethyl cellulose-g-poly(AA-co-AM-co-AMPS)/MMT superabsorbent hydrogel. *Carbohydrate Polymers*, 84(1):76–82, February 2011. doi: 10.1016/j.carbpol.2010.10.061.

[162] Jihuai Wu, Jianming Lin, Meng Zhou, and Congrong Wei. Synthesis and properties of starch-graft-polyacrylamide/clay superabsorbent composite. *Macromolecular Rapid Communications*, 21(15):1032–1034, October 2000. doi: 10.1002/1521-3927(20001001)21:15⟨1032::AID-MARC1032⟩3.0.CO;2-N.

[163] Hans Grasdalen and Olav Smidsrød. Gelation of gellan gum. *Carbohydrate Polymers*, 7(5): 371–393, January 1987. doi: 10.1016/0144-8617(87)90004-X.

[164] S Damodaran and D C Hwang. Carboxyl-modified superabsorbent protein hydrogel. US Patent Office, 1998.

[165] Der-Chyan Hwang and Srinivasan Damodaran. Equilibrium swelling properties of a novel ethylenediaminetetraacetic dianhydride (EDTAD)-modified soy protein hydrogel. *Journal of Applied Polymer Science*, 62(8):1285–1293, November 1996. doi: 10.1002/(SICI)1097-4628(19961121)62:8⟨1285::AID-APP19⟩3.0.CO;2-6.

[166] Kuen Yong Lee and David J Mooney. Alginate: Properties and biomedical applications. *Progress in Polymer Science*, 37(1):106–126, January 2012. doi: 10.1016/j.progpolymsci.2011.06.003.

[167] J E Scott. Periodate oxidation, pKa and conformation of hexuronic acids in polyuronides and mucopolysaccharides. *Biochimica et Biophysica Acta (BBA) - General Subjects*, 170(2):471–473, December 1968. doi: 10.1016/0304-4165(68)90040-8.

[168] Donald E Clark and Harland C Green. Alginic acid and process of making same. *Google Patents*.

[169] Dennis J McHugh. *A Guide to the Seaweed Industry*. Food & Agriculture Org, 2003.

[170] Uwe Remminghorst and Bernd H A Rehm. Bacterial alginates: from biosynthesis to applications. *Biotechnology Letters*, 28(21):1701–1712, August 2006. doi: 10.1007/s10529-006-9156-x.

[171] P Setlow. Mechanisms which contribute to the long-term survival of spores of Bacillus species. *Journal of Applied Bacteriology*, 76(S23):49S–60S, June 1994. doi: 10.1111/j.1365-2672.1994.tb04357.x.

[172] Peter Setlow. Resistance of Bacterial Spores. In *Bacterial Stress Responses, Second Edition*, pages 319–332. American Society of Microbiology, January 2011. ISBN 9781555816216. doi: 10.1128/9781555816841.ch18.

[173] Willem De Muynck, Dieter Debrouwer, Nele De Belie, and Willy Verstraete. Bacterial carbonate precipitation improves the durability of cementitious materials. *Cement and Concrete Research*, 38(7):1005–1014, July 2008. doi: 10.1016/j.cemconres.2008.03.005.

[174] CEN-Standard Sand EN 196-1, .

[175] Susan Chang. **What is an anomeric carbon?** .

[176] A Kalfon, J F Charles, C Bourgouin, and H De Barjac. Sporulation of Bacillus sphaericus 2297: an Electron Microscope Study of Crystal-like Inclusion Biogenesis and Toxicity to Mosquito Larvae. *Microbiology*, 130(4):893–900, April 1984. doi: 10.1099/00221287-130-4-893.

[177] BS EN 196-1:2016 - Methods of testing cement. Determination of strength. BSI, .

[178] *Vortex-Genie 2*. Scientific Industries, Inc.

[179] V M Ivanov, V N Figurovskaya, Yu A Barbalat, and N I Ershova. Chromaticity Characteristics of NH2Hg2I3 and I2: Molecular Iodine As a Test Form Alternative to Nessler's Reagent. *Journal of Analytical Chemistry*, 60(7):629–632, 2005. doi: 10.1007/s10809-005-0150-6.

[180] Biochrom WPA Lightwave II UV/Visible Spectrophotometer, .

[181] Jolien Vermeulen. *Self-Healing Concrete with Algae and Seaweed. Science or Fiction?* . PhD thesis, Ghent, June 2016.

[182] Bo Wang, Xiao-Ding Xu, Zong-Chun Wang, Si-Xue Cheng, Xian-Zheng Zhang, and Ren-Xi Zhuo. Synthesis and properties of pH and temperature sensitive P(NIPAAm-co-DMAEMA) hydrogels. *Colloids and Surfaces B: Biointerfaces*, 64(1):34–41, June 2008. doi: 10.1016/j.colsurfb.2008.01.001.

Appendix A

Crack measurements using Fiji

Fiji (Fiji Is Just ImageJ) was used to facilitate the crack measurements. It is not intended to give a thorough explanation about how to install the supplied script and how to use them. However, do not hesitate to contact the author to ask for some advice to get started with the Fiji scripts. Please contact trenson.gilles@gmail.com. The scripts can be downloaded from https://gist.github.com/rebot/850e98aa8145c703003b8cb0d0fd8ca0.

The process start with collecting the optical microscopy images and store them in a directory called *Week X*. Its parent directory is named after the short name of the sample (e.g. *CD+S*). Once all images are collected (e.g. *Week 0* up to *Week 4*), the filesystem hierarchy is reorganised in such a way that all images of a particular crack location are stored in the same folder. Next, a script called *Crack_alignment.ijm* was executed and aligned those particular images and saves them in a separate folder. During this operation, the images are not scaled and hence the relation between pixels and the real measurement is not violated. Prior to the batch measurement of the images, the two methods available in *StartupMacros.fiji.ijm* should be installed as startup macros. Then, *Batch_measure.ijm* is executed. The aligned images will open, one at a time, and will automatically float to the right of your monitor. Two lines will appear, indicating the possible measurement locations. The *line* tool is automatically selected and the crack can be indicated by clicking and dragging the mouse pointer. Next, the key n is pressed to record the measurement and indicate the length on the image. Pressing g will move to the next image, while the previous image will still be displayed, but at the right side of the screen. In this way, cracks are indicated at almost exactly the same position and the chance of making mistakes is minimised. However, this setup is far from general and requires a specific filesystem hierarchy.

Appendix B

Attenuated total reflectance-infrared spectroscopy

B.1 ATR-IR spectra for hydrogels exposed to aqueous solution of varying pH and cement filtrate solution over a timespan of 1 day

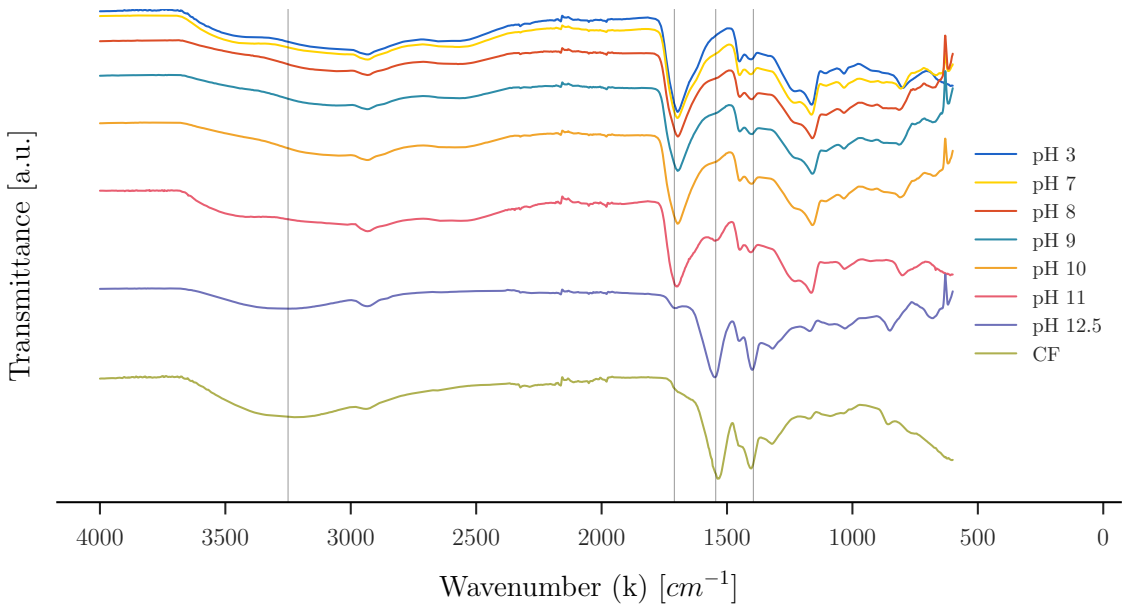

Figure B.1: ATR-IR spectra of p(algMOD_AA) after exposure to aqueous solutions of varying pH and a cement filtrate solution for a timespan of 1 day.

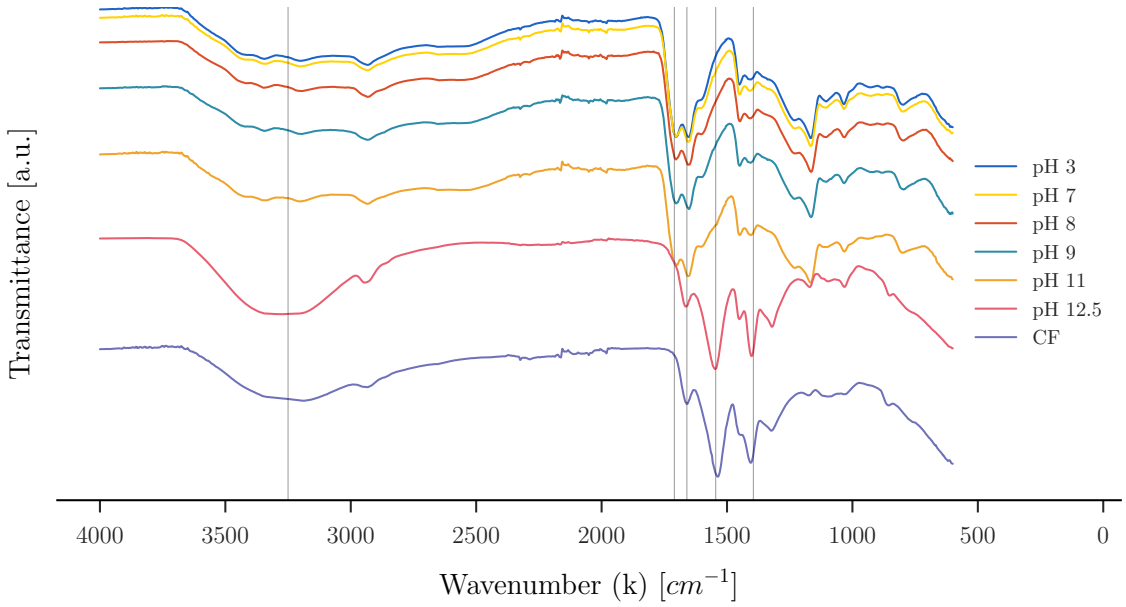

Figure B.2: ATR-IR spectra of p(algMOD_AA/AM) after exposure to aqueous solutions of varying pH and a cement filtrate solution for a timespan of 1 day.

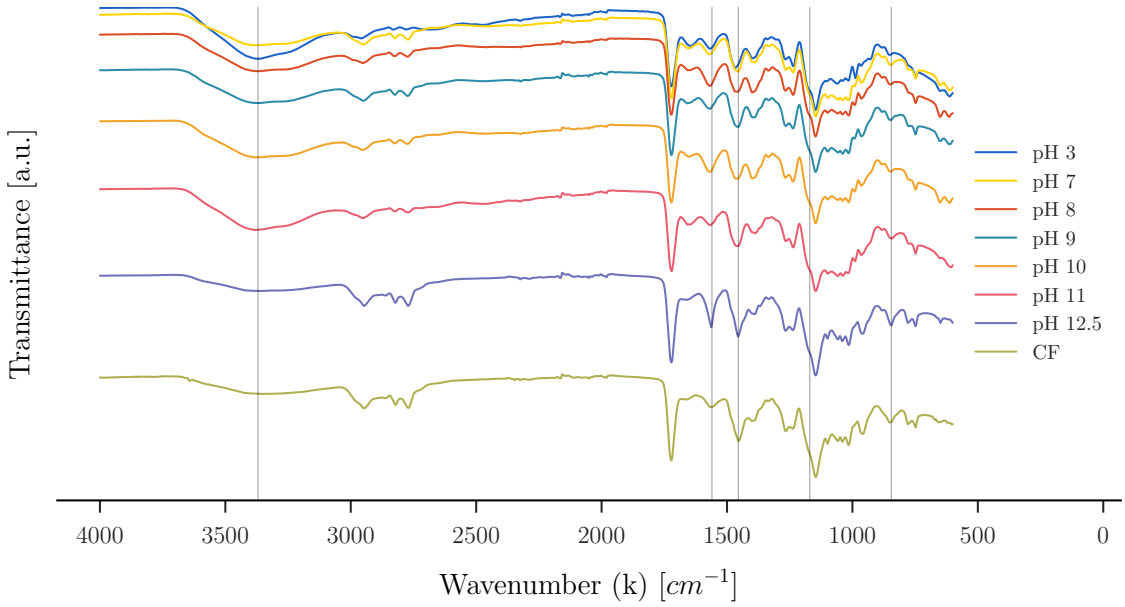

Figure B.3: ATR-IR spectra of p(chiMOD_DMAEMA) after exposure to aqueous solutions of varying pH and a cement filtrate solution for a timespan of 1 day.

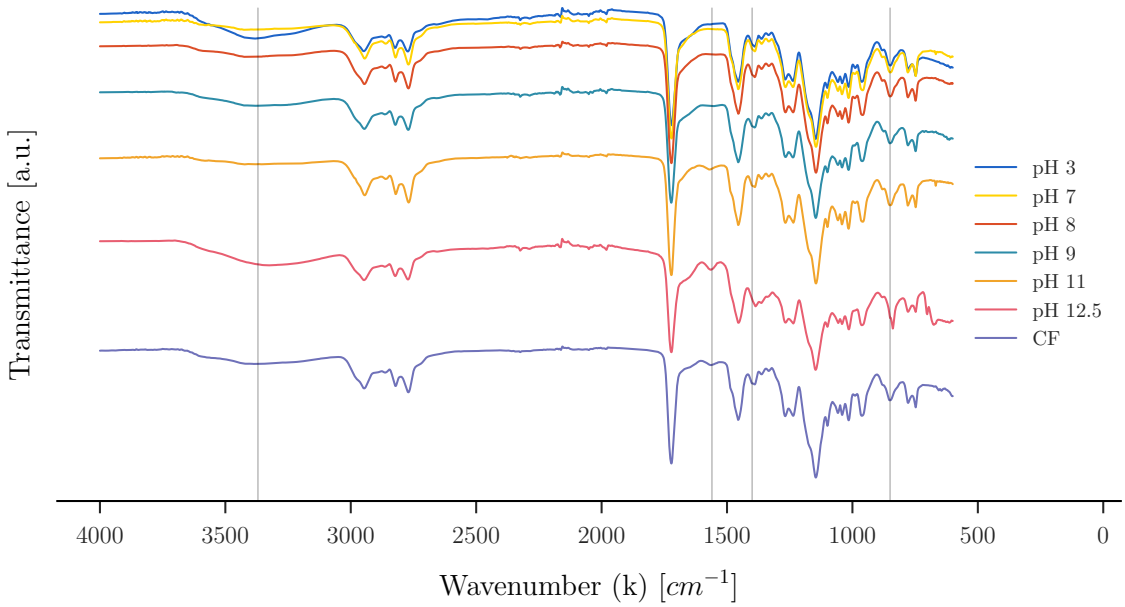

Figure B.4: ATR-IR spectra of p(MBA_DMAEMA) after exposure to aqueous solutions of varying pH and a cement filtrate solution for a timespan of 1 day.

B.2 ATR-IR spectra for hydrogels exposed to aqueous solution of normal pH and cement filtrate solution over the course of time

B.2.1 Exposure to an aqueous solution of neutral pH

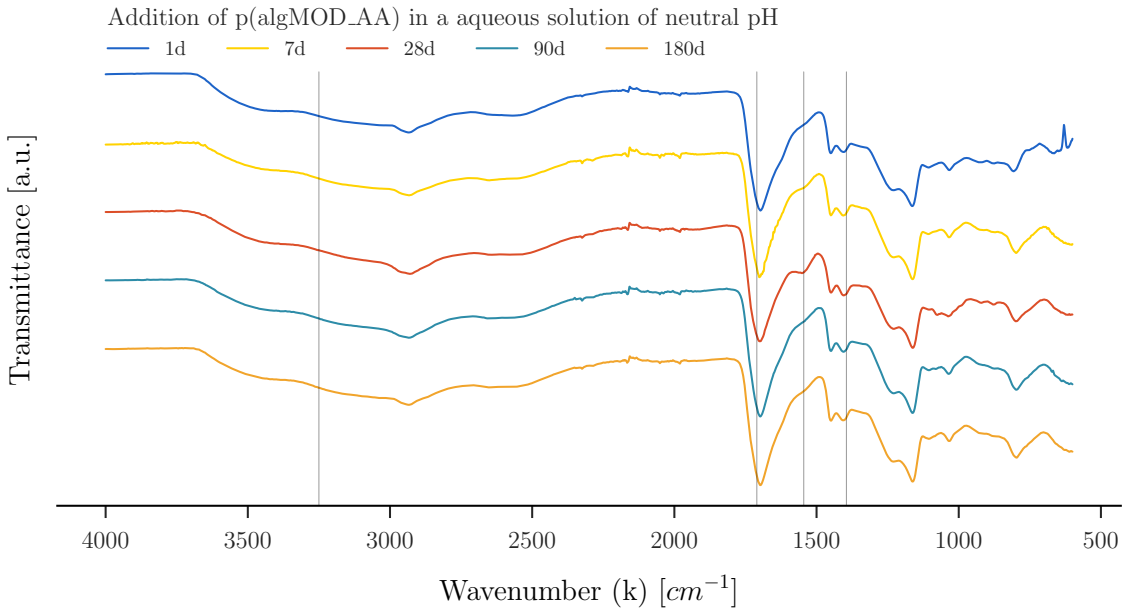

Figure B.5: ATR-IR spectra of p(algMOD_AA) after exposure to an aqueous solutions of neutral pH over the course of time

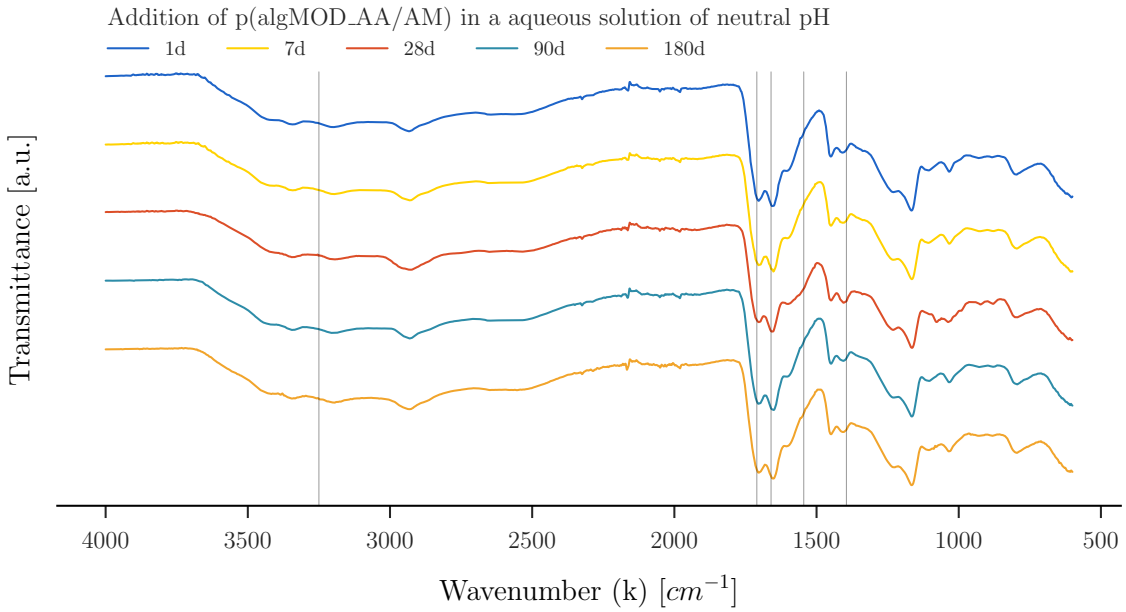

Figure B.6: ATR-IR spectra of p(algMOD_AA/AM) after exposure to an aqueous solutions of neutral pH over the course of time

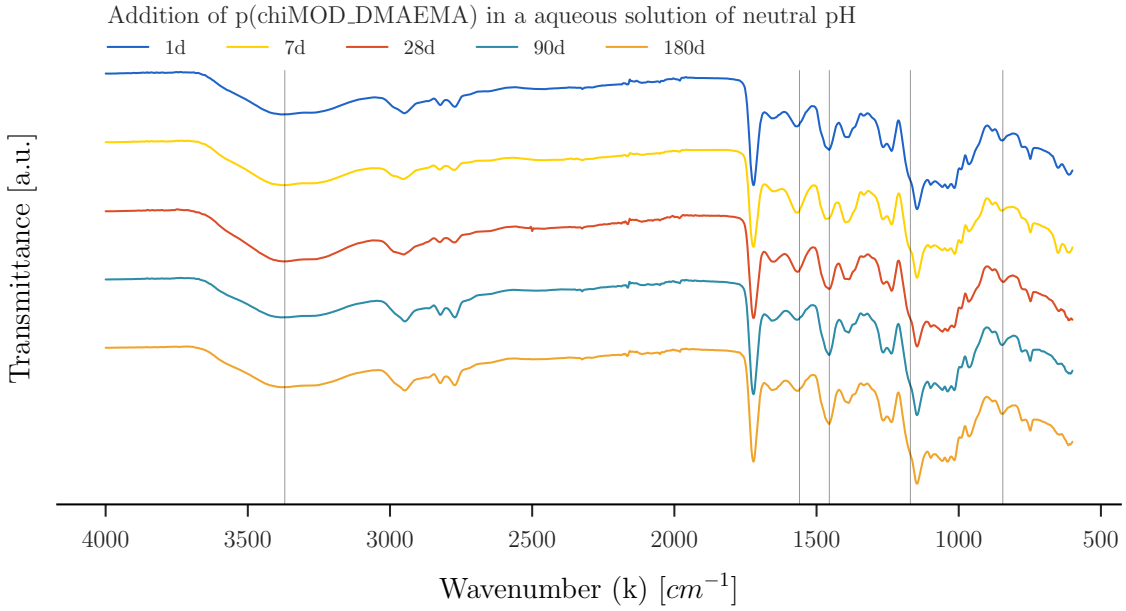

Figure B.7: ATR-IR spectra of p(chiMOD_DMAEMA) after exposure to an aqueous solutions of neutral pH over the course of time

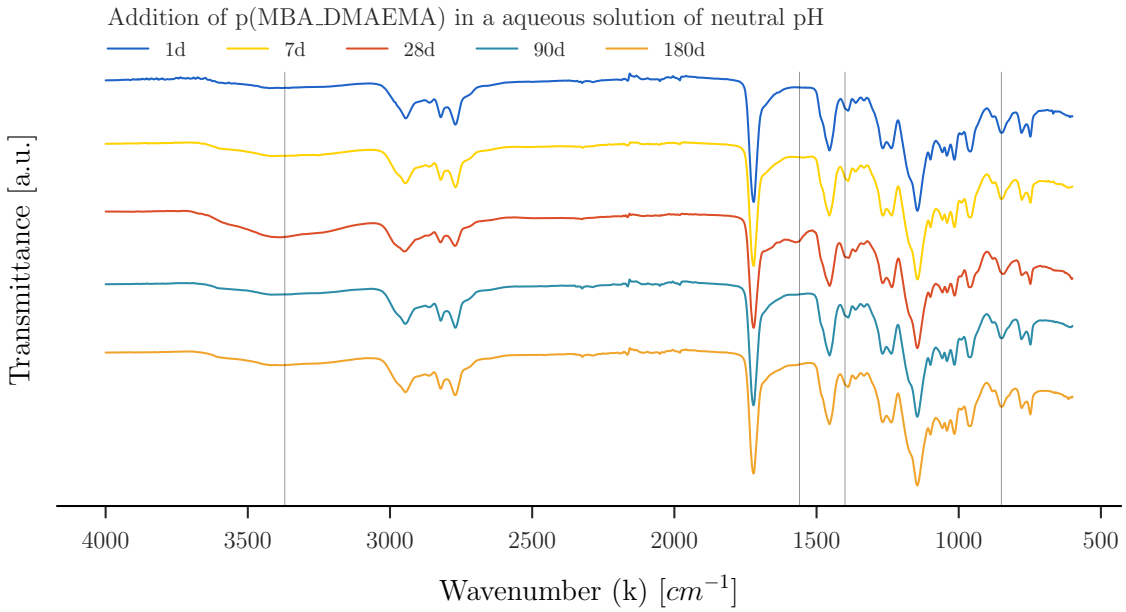

Figure B.8: ATR-IR spectra of p(MBA_DMAEMA) after exposure to an aqueous solutions of neutral pH over the course of time

B.2.2 Exposure to a cement filtrate solution

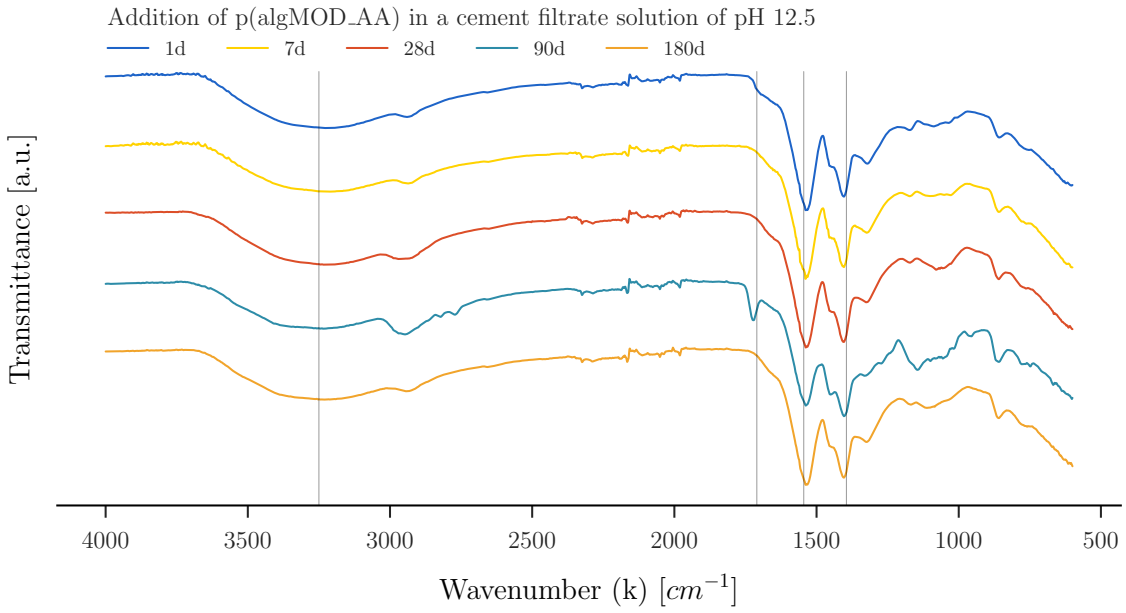

Figure B.9: ATR-IR spectra of p(algMOD_AA) after exposure to a cement filtrate solution of pH 12.5 over the course of time

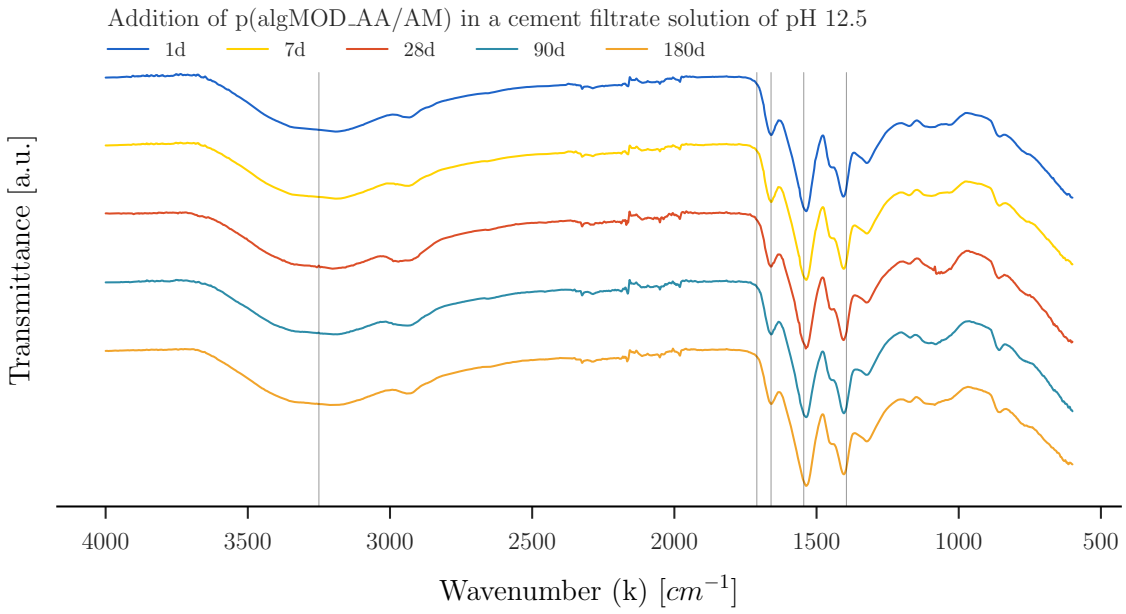

Figure B.10: ATR-IR spectra of p(algMOD_AA/AM) after exposure to a cement filtrate solution of pH 12.5 over the course of time

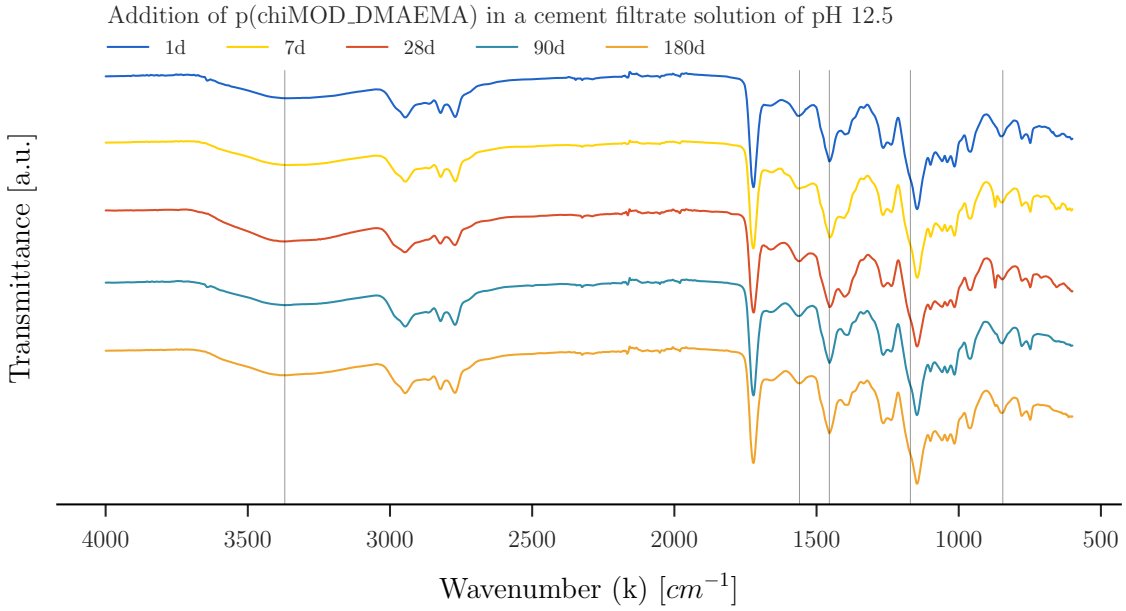

Figure B.11: ATR-IR spectra of p(chiMOD_DMAEMA) after exposure to a cement filtrate solution of pH 12.5 over the course of time

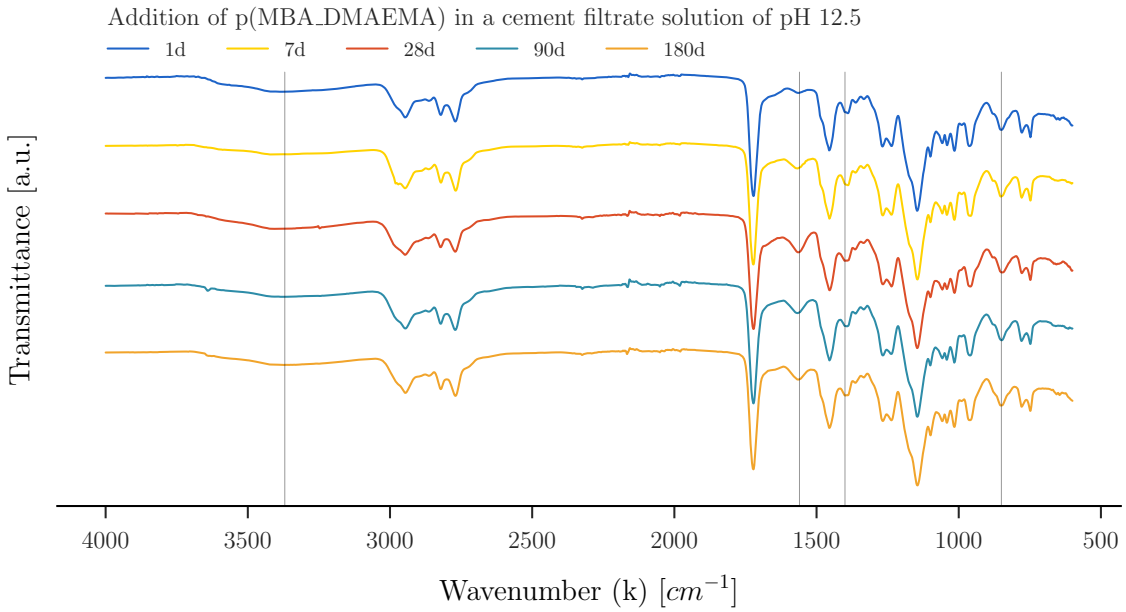

Figure B.12: ATR-IR spectra of p(MBA_DMAEMA) after exposure to a cement filtrate solution of pH 12.5 over the course of time

Appendix C

Flexural and compressive strength

C.1 Flexural and compressive strength of mortar specimens with and without the addition of hydrogels

Table C.1: Flexural and compressive strenth of mortar specimens with and without the addition of synthesised hydrogels

Hydrogel [m%]	*Flexural strength (FS)* [MPa]	*FS Reduction* [%]	*Compressive strength (CS)* [MPa]	*CS Reduction* [%]
		Reference		
0.00	8.7 ± 0.1	—	70.1 ± 2.9	—
		p(algMOD_AA)		
2.25	7.6 ± 0.1	11.9	65.0 ± 1.2	7.4
4.50	7.2 ± 0.1	17.4	66.8 ± 1.4	4.7
9.00	7.6 ± 0.3	12.2	63.4 ± 0.7	9.6
		p(algMOD_AA/AM)		
2.25	7.2 ± 0.3	17.5	69.6 ± 1.5	0.7
4.50	7.4 ± 0.5	15.1	61.2 ± 1.8	12.8
9.00	6.2 ± 0.3	28.1	40.4 ± 4.2	42.4
		p(chiMOD_DMAEMA)		
2.25	8.0 ± 0.3	7.9	54.2 ± 2.8	22.7
4.50	7.6 ± 0.9	12.4	61.9 ± 1.6	11.8
9.00	7.4 ± 0.2	15.1	51.0 ± 2.3	27.3
		p(MBA_DMAEMA)		
2.25	5.1 ± 0.6	41.4	35.0 ± 3.5	50.2
4.50	4.3 ± 0.1	50.1	25.4 ± 2.1	63.7
9.00	3.8 ± 0.7	55.6	16.7 ± 2.7	76.2

Appendix D

Self-healing efficiency

D.1 Water transport properties evaluation by means of water flow test

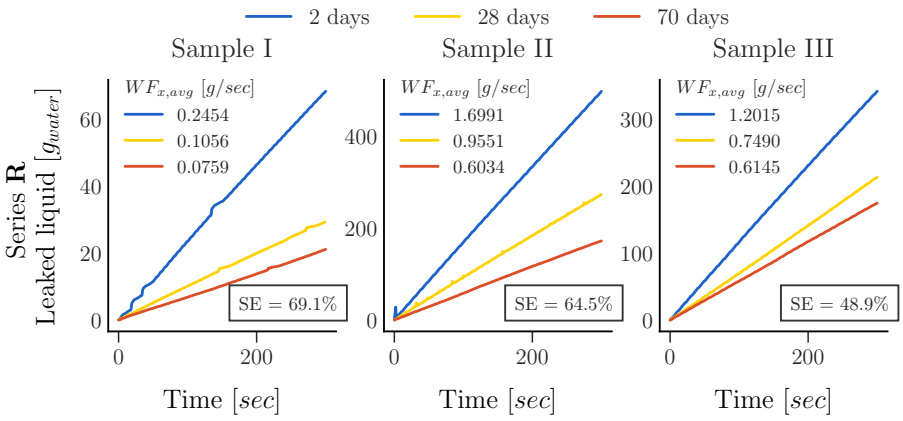

Figure D.1: Development of water flow in the reference specimen (R) under full immersion for three replicates over a period of 1, 4 and 10 weeks

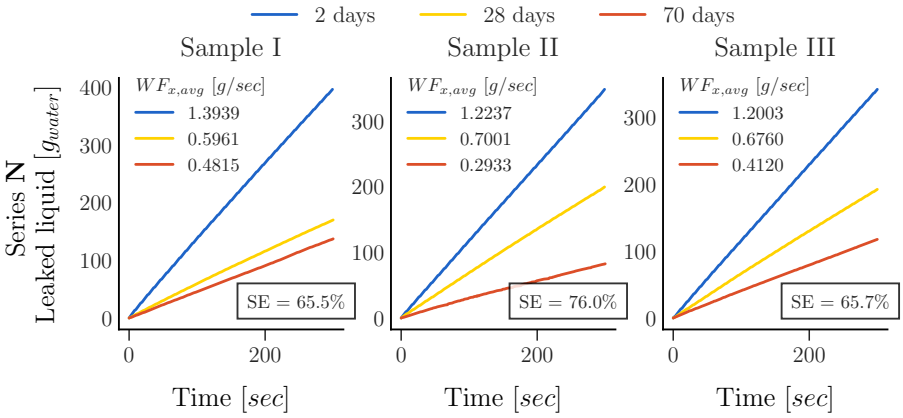

Figure D.2: Development of water flow in the specimen containing nutrients (N) under full immersion for three replicates over a period of 1, 4 and 10 weeks

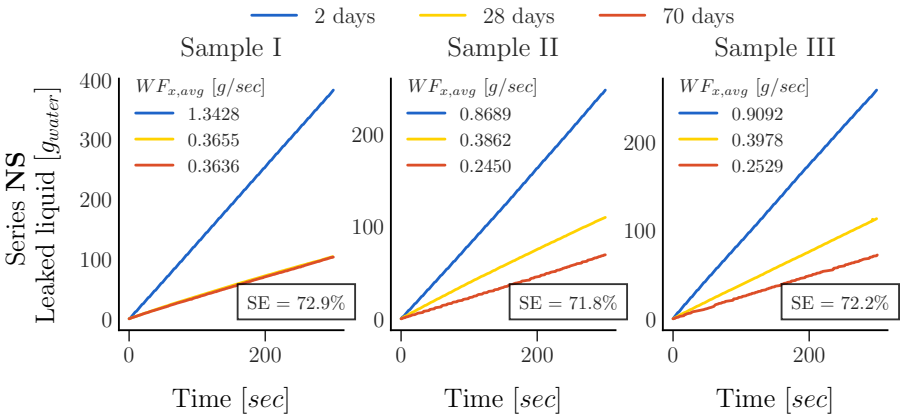

Figure D.3: Development of water flow in the specimen containing both nutrients and non-immobilised spores (R) under full immersion for three replicates over a period of 1, 4 and 10 weeks

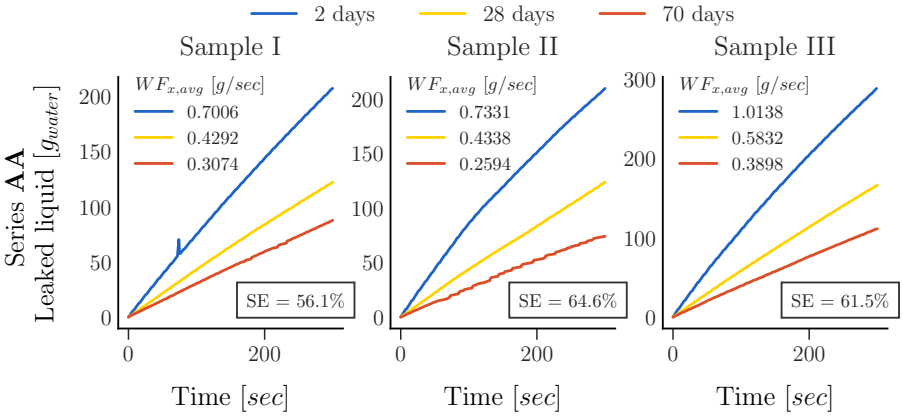

Figure D.4: Development of water flow in the specimen containing AlgMOD/AA (AA) under full immersion for three replicates over a period of 1, 4 and 10 weeks

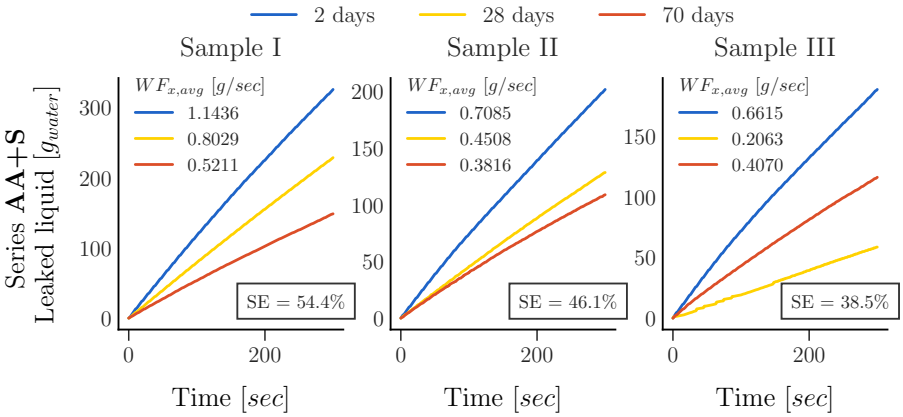

Figure D.5: Development of water flow in the specimen containing AlgMOD/AA and non-immobilised spores (AA+S) under full immersion for three replicates over a period of 1, 4 and 10 weeks

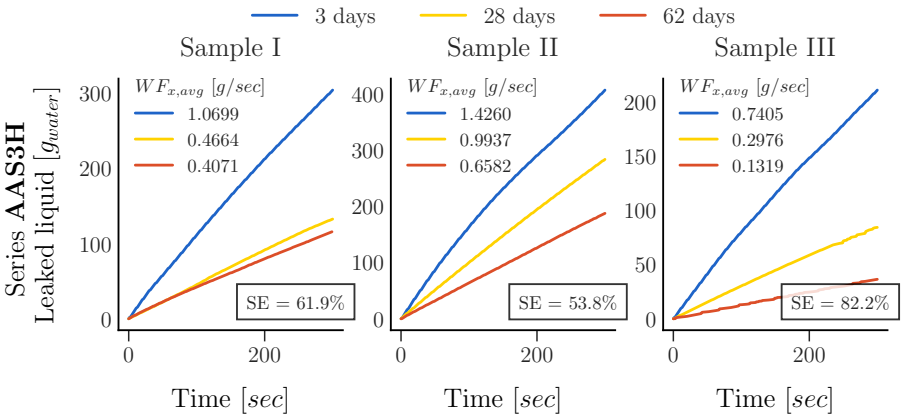

Figure D.6: Development of water flow in the specimen containing AlgMOD/AA immobolised spores (AAS3H) under full immersion for three replicates over a period of 1, 4 and 10 weeks. The hydrogel was synthesised over a period of 3 hours.

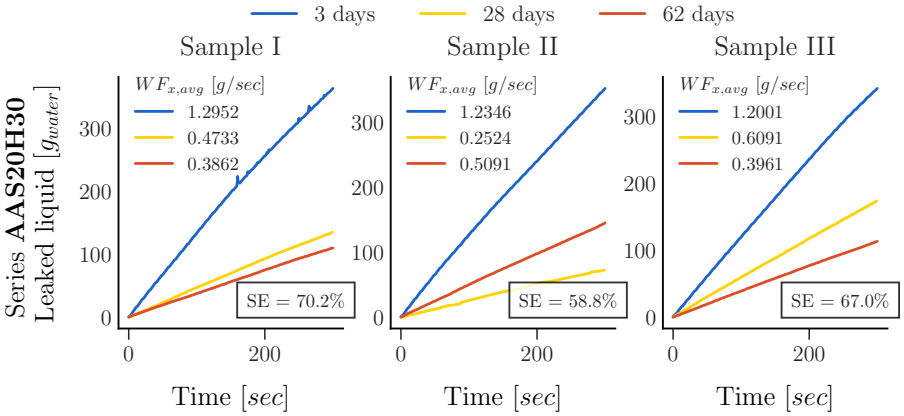

Figure D.7: Development of water flow in the specimen containing AlgMOD/AA immobolised spores (AAS20H30) under full immersion for three replicates over a period of 1, 4 and 10 weeks. The hydrogel was synthesised over a period of 20 hours and 30 minutes.

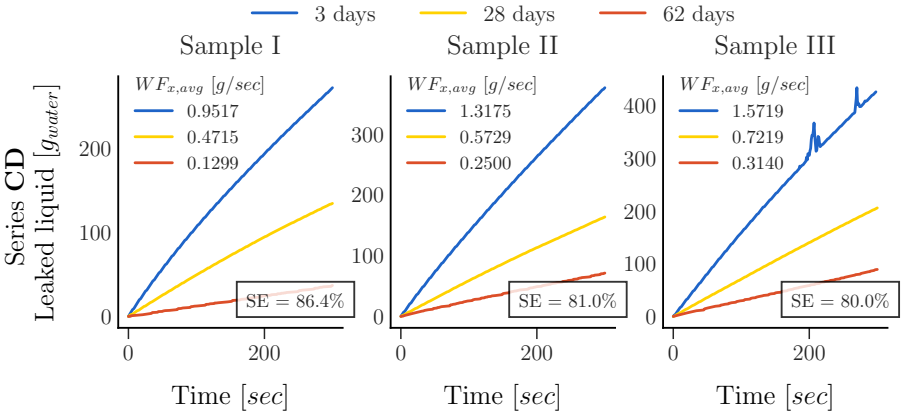

Figure D.8: Development of water flow in the specimen containing ChiMOD/DMAEMA (CD) under full immersion for three replicates over a period of 1, 4 and 10 weeks

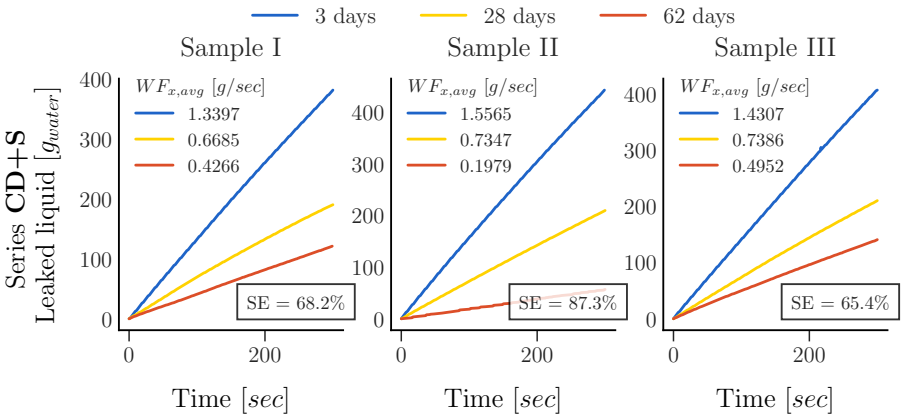

Figure D.9: Development of water flow in the specimen containing ChiMOD/DMAEMA and non-immobilised spores (CD+S) under full immersion for three replicates over a period of 1, 4 and 10 weeks

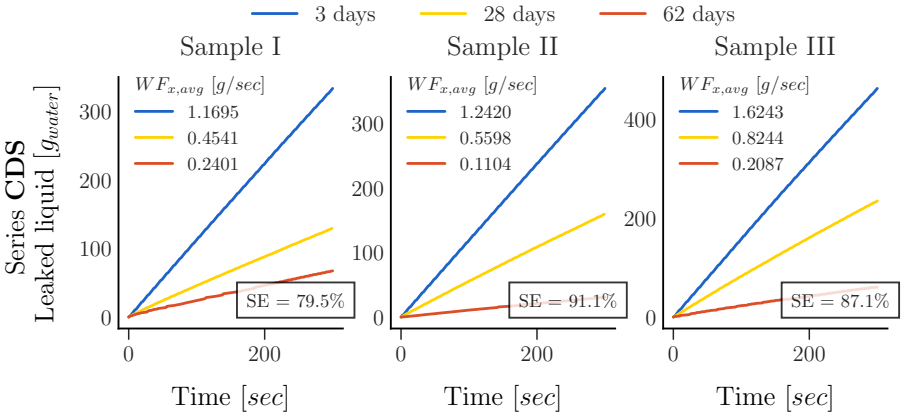

Figure D.10: Development of water flow in the specimen containing ChiMOD/DMAEMA immobilised spores (CDS) under full immersion for three replicates over a period of 1, 4 and 10 weeks

D.2 Microscopic evaluation of crack closure

The crack closure of the specimens over time is evaluated using optical microscopy as described in subsection 2.4.2 on page 42. The different series where subjected to two different incubation methods, either under full immersion or under wet/dry cycles consisting of 2 hours immersion alternated by a dry period for 4 hours.

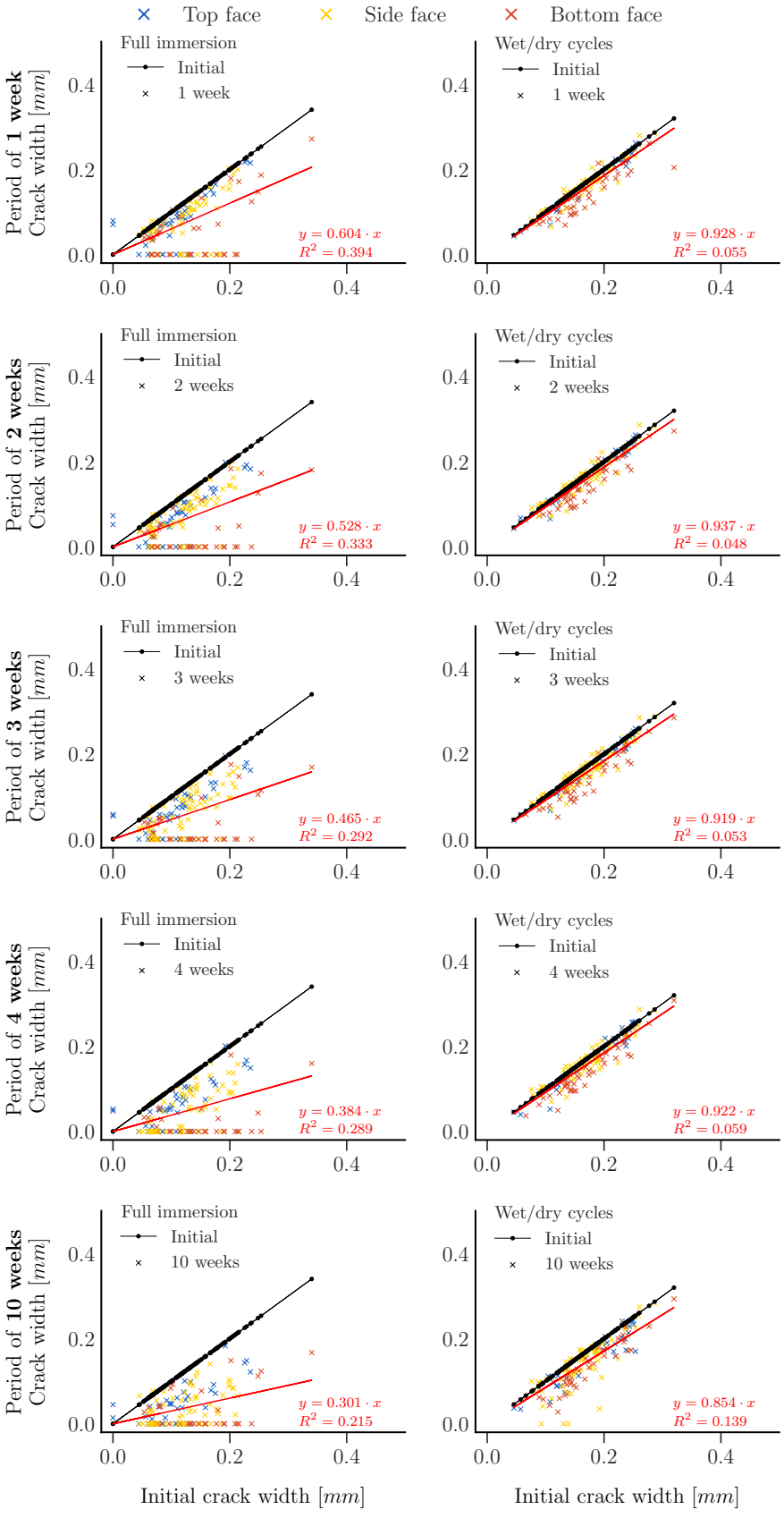

Figure D.11: Development of crack widths in the reference specimens (R) under full immersion (left) and wet/dry cycles (right; 2 hours wet alternated by 4 hours dry) over a period of 1, 2, 3, 4 and 10 weeks

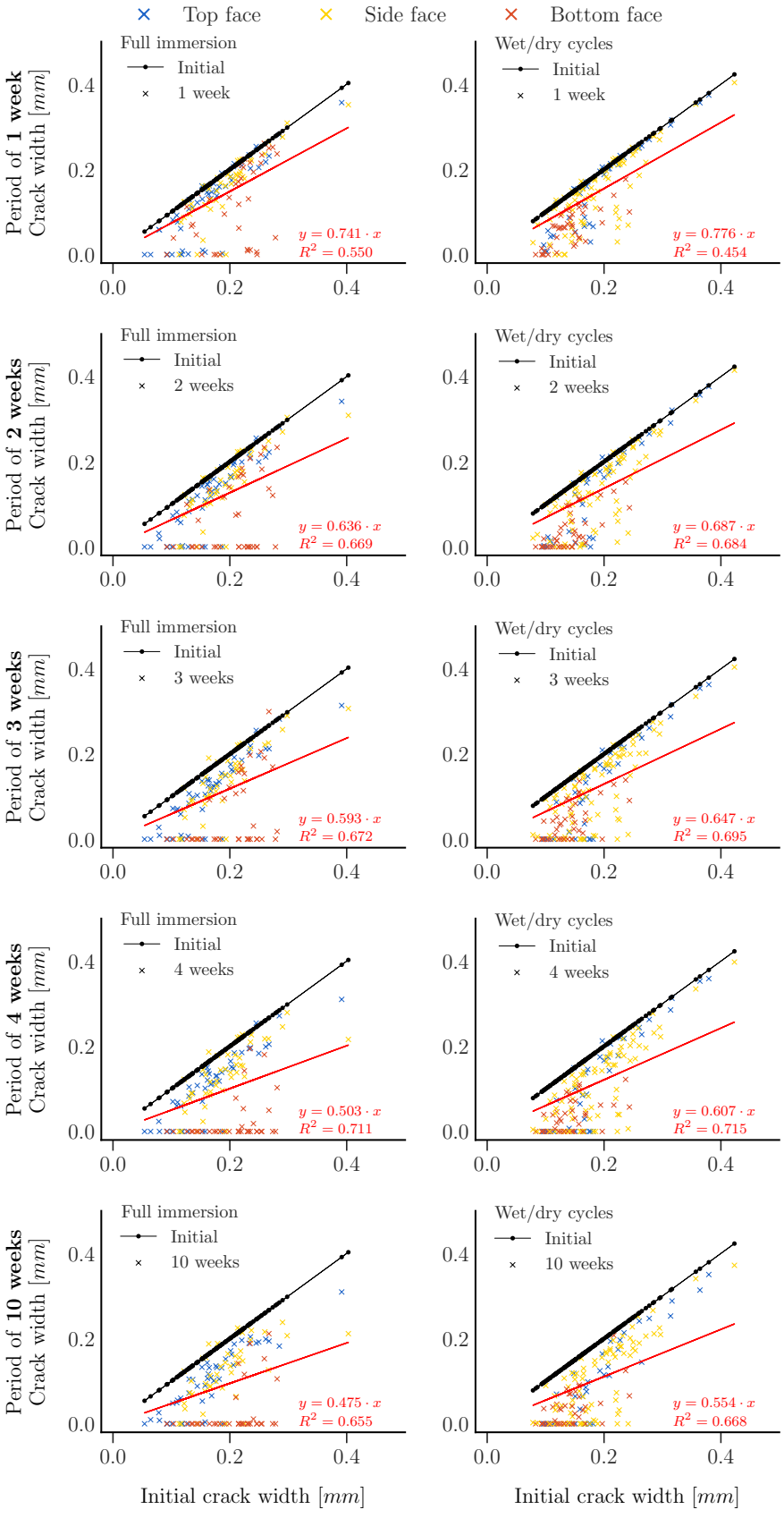

Figure D.12: Development of crack widths in specimens containing nutrients (N) under full immersion (left) and wet/dry cycles (right; 2 hours wet alternated by 4 hours dry) over a period of 1, 2, 3, 4 and 10 weeks

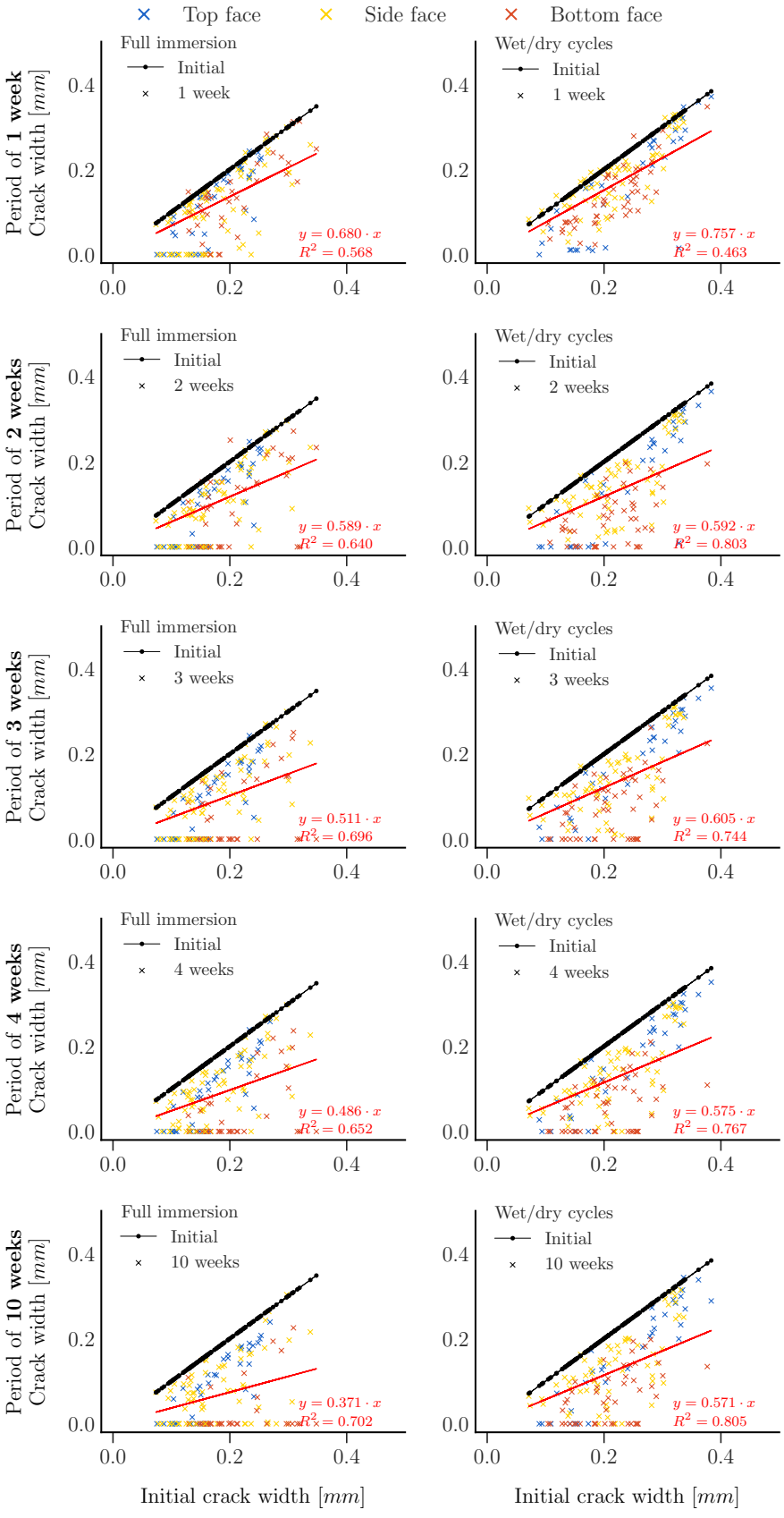

Figure D.13: Development of crack widths in specimens containing both nutrients and spores (NS) under full immersion (left) and wet/dry cycles (right; 2 hours wet alternated by 4 hours dry) over a period of 1, 2, 3, 4 and 10 weeks

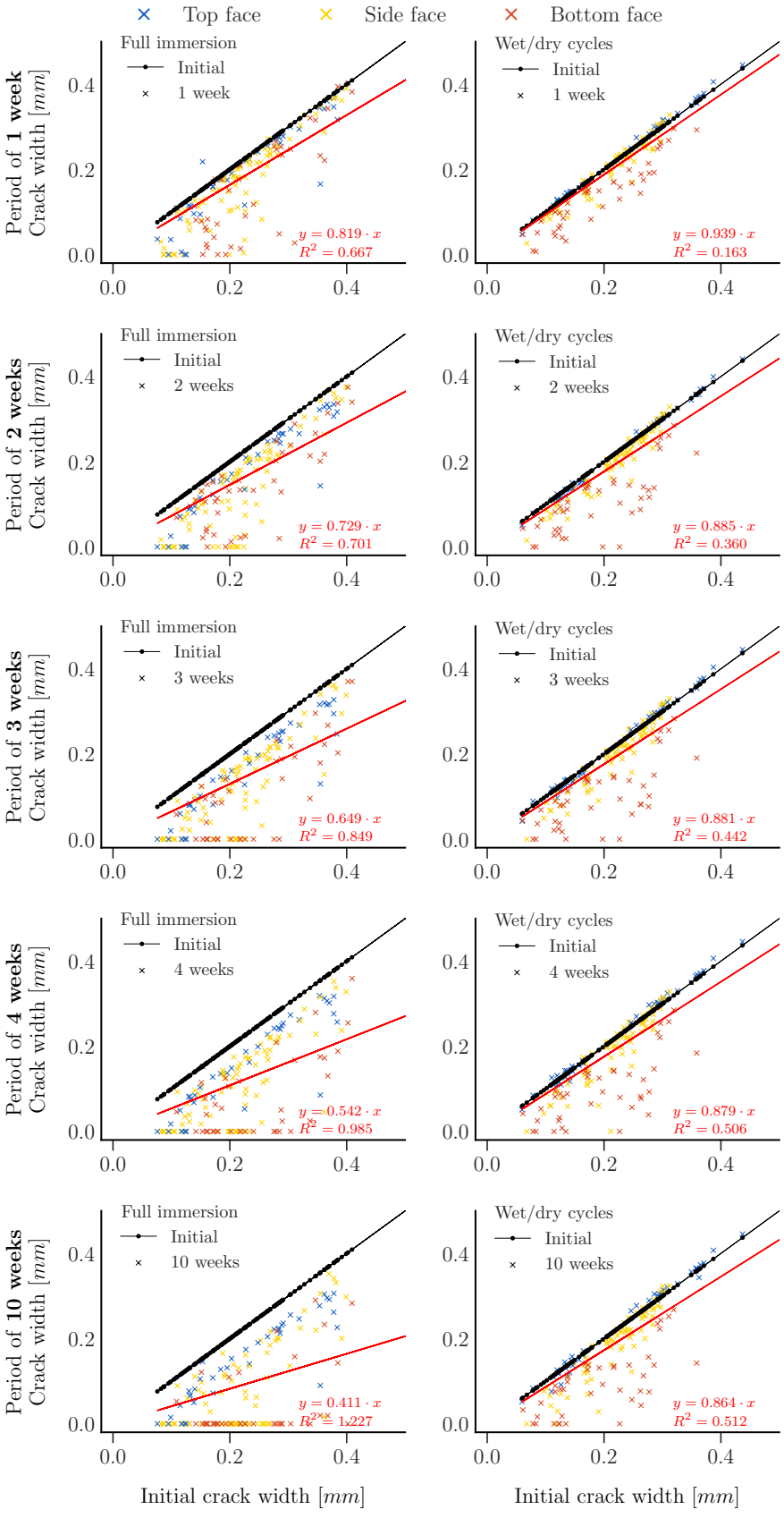

Figure D.14: Development of crack widths in specimens containing ChiMOD/DMAEMA (CD) under full immersion (left) and wet/dry cycles (right; 2 hours wet alternated by 4 hours dry) over a period of 1, 2, 3, 4 and 10 weeks

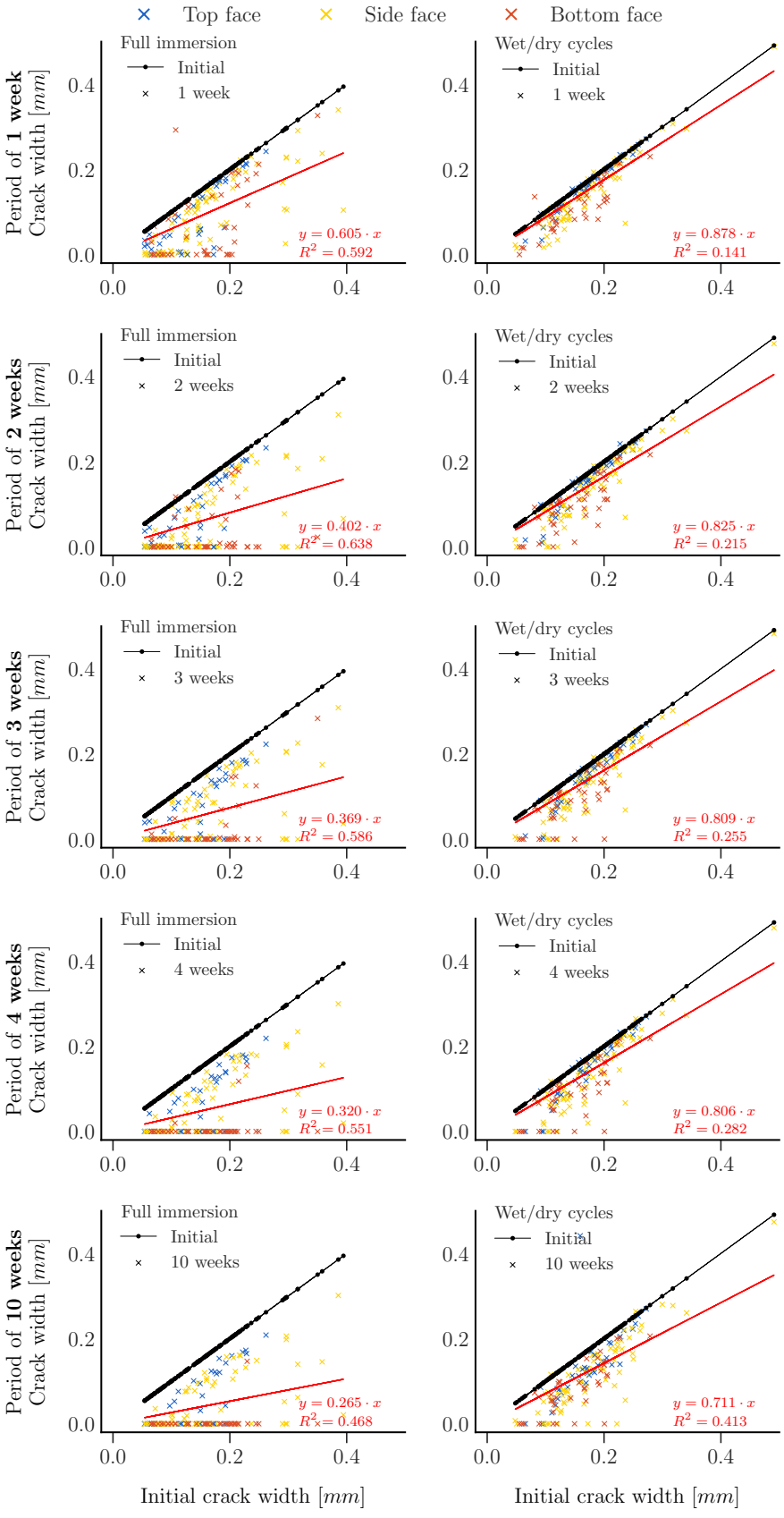

Figure D.15: Development of crack widths in specimens containing ChiMOD/DMAEMA and non-immobilised spores (CD+S) under full immersion (left) and wet/dry cycles (right; 2 hours wet alternated by 4 hours dry) over a period of 1, 2, 3, 4 and 10 weeks

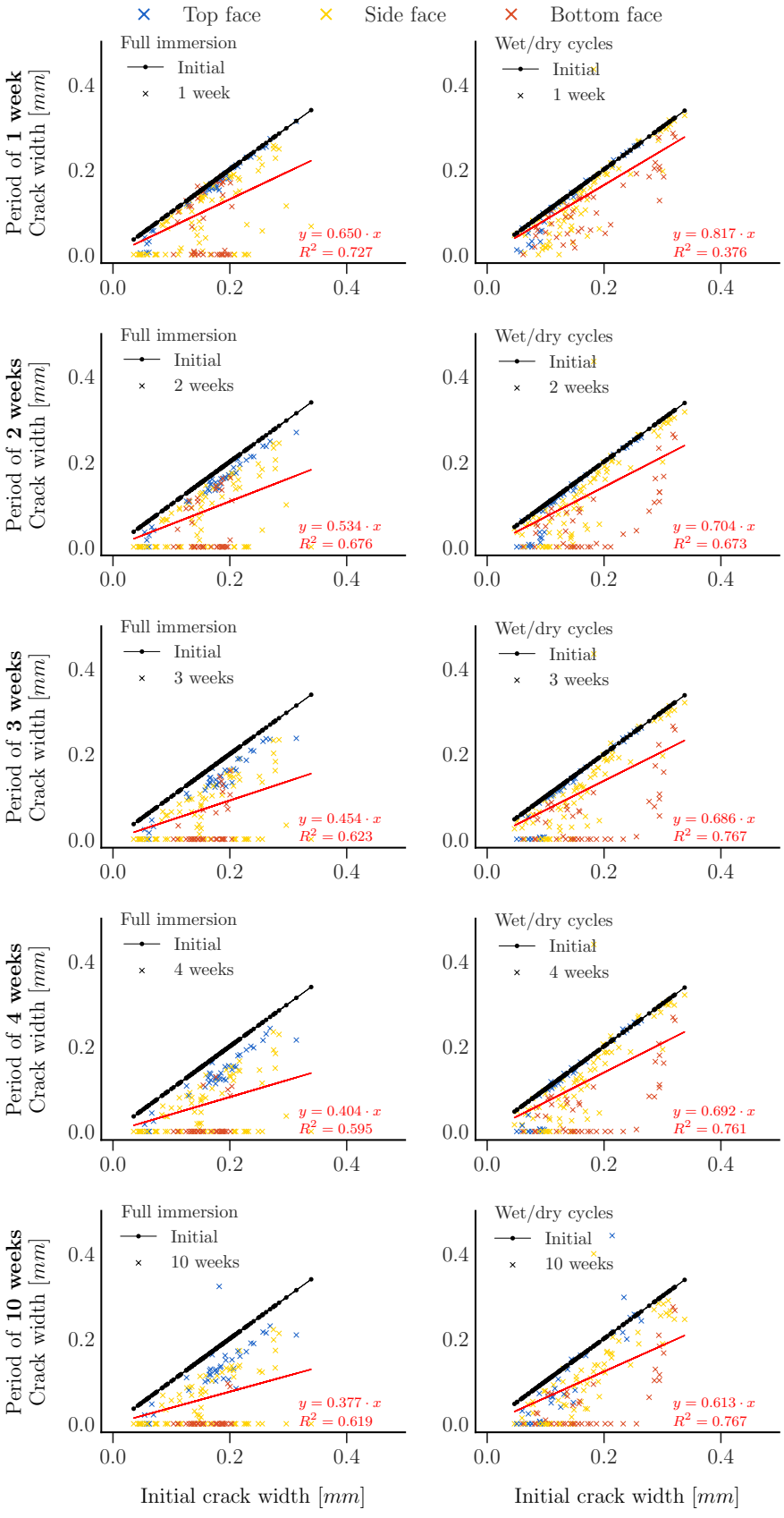

Figure D.16: Development of crack widths in specimens containing ChiMOD/DMAEMA immobolised spores (CDS) under full immersion (left) and wet/dry cycles (right; 2 hours wet alternated by 4 hours dry) over a period of 1, 2, 3, 4 and 10 weeks

List of Figures

List of Tables